CR-159710
PWA-5550-31

NASA

EXPERIMENTAL AERODYNAMIC AND ACOUSTIC MODEL TESTING OF THE VCE TESTBED COANNULAR EXHAUST NOZZLE SYSTEM

By
D.P Nelson and P.M. Morris

Commercial Products Division
Pratt & Whitney Aircraft Group
United Technologies Corporation

Prepared for

NATIONAL AERONAUTICS AND SPACE ADMINISTRATION
Lewis Research Center
Under
Contract NAS3-20061

TABLE OF CONTENTS

TABLE OF CONTENTS (Continued)

LIST OF ILLUSTRATIONS

LIST OF ILLUSTRATIONS (Continued)

LIST OF ILLUSTRATIONS (Continued)

LIST OF TABLES

SECTION 1.0

SUMMARY

The overall objective of the NASA-sponsored Coannular Nozzle Model Technology Program is to identify and develop the aerodynamic and acoustic nozzle technology for an advanced second-generation supersonic propulsion system such as the Variable Stream Control Engine (VSCE). The work reported here was directed towards: (1) acquisition of static aerodynamic and acoustic nozzle model data for comparison with large scale engine data to be obtained during the Variable Cycle Engine (VCE) Testbed Program, and (2) evaluation of the acoustic prediction procedure developed under a preceding effort.

In accomplishing these objectives, a one-sixth scale model of the VCE testbed exhaust system was designed, fabricated and experimentally investigated over a range of operating conditions. The model was designed to simulate the nozzle operating at a duct burner exit temperature of 1089 K (1960°R), and had a fan to primary nozzle area ratio of 0.65 and a fan nozzle radius ratio of 0.82. Tests were conducted both with and without the ejector portion of the nozzle system.

Acoustic testing was completed in the Pratt & Whitney Aircraft anechoic chamber (Stand X-206) at the Andrew Willgoos Turbine Laboratory. The test matrix consisted of a total of 39 sets of operating conditions. Data were acquired at operating conditions that will enable a direct comparison of model and testbed data to evaluate scaleability of inverted velocity profile (IVP) data. Noise characteristics at this match point were predicted using the procedure developed in an earlier program. Agreement between test data and noise predictions was generally within the scatter of the data from which the prediction method is derived. The standard deviations of these prediction curves vary from 1.0 to 2.4 dB, depending on the angle of radiation.

In another series of tests, fan stream and primary stream pressure and temperature levels were varied independently in order to establish acoustic sensitivity to these parameters, thereby ensuring the ability to interpolate data to match actual testbed demonstrator operating conditions. Data trends showed no deviation from earlier model test results. Also, the acoustic data responded to stream property variations in a way which was in general agreement with predictions.

Testing was accomplished with a hardwall ejector at four selected conditions. In general, noise levels with the ejector were slightly higher than without the ejector, but analyses indicate that a longer ejector could reduce the noise level.

Following the acoustic evaluation, the model was tested for aerodynamic performance in the Large Nozzle Thrust Facility at the United Technologies Research Laboratory. The test matrix consisted of a total of 30 cold flow performance points, and the model was evaluated over a range of fan and primary nozzle pressure ratios similar to that in the preceding acoustic tests. Again, agreement was demonstrated between measured and predicted performance. In all cases, agreement between predicted and measured thrust coefficients was within one percent.

Results of performance tests without the ejector showed thrust coefficients over the range of flow conditions tested from 0.972 to 0.983. Installation of the ejector increased performance 0.2 to 0.4 percent, with the greater increase tending to occur at the higher flow conditions. At the simulated testbed condition, the thrust coefficient was 0.977 without the ejector and 0.980 with the ejector.

At fan to primary pressure ratios greater than 1.0, variations in fan nozzle pressure ratio imparted a significant effect on the primary nozzle discharge coefficient. At a primary nozzle pressure ratio of 1.6, increasing the fan nozzle pressure ratio from 2.4 to 3.2 decreased the primary nozzle discharge coefficient from 0.93 to 0.86.

Overall, this work has contributed substantially to the data base for developing an acoustically and aerodynamically viable coannular exhaust nozzle system. In addition, it has provided valuable insight in anticipating the nozzle aero/acoustic performance and identifying possible refinements to the VCE testbed demonstrator.

SECTION 2.0

INTRODUCTION

The increasing importance of environmental considerations is expected to require substantial reductions in exhaust system noise levels for the next generation of supersonic commercial transport aircraft. Adequate noise reduction must be obtained with a high level of exhaust system efficiency.

In the past several years, numerous analytical and experimental propulsion system studies, conducted as part of the NASA-sponsored Supersonic Cruise Airplane Research (SCAR) effort, identified the Variable Stream Control Engine (VSCE) as a promising propulsion system concept for both high system performance and low noise generation. The engine is an advanced duct burning turbofan configuration that uses a low-noise, high performance coannular exhaust system. The VSCE cycle can be matched to provide a high velocity duct (fan) stream surrounding a low velocity core (primary) stream resulting in an inverted velocity profile (IVP) that offers an inherent jet noise benefit without mechanical noise suppressors.

Reference 1 documents the earliest results of scale model IVP jet nozzle noise tests and identifies the noise advantages of the IVP jet over conventional turbojet or turbofan cycles. Since this early work was based on static testing, the NASA-Lewis Research Center sponsored further studies to identify the effects of flight on noise characteristics of scale model IVP jets. Results of a flight simulation investigation (ref. 2) indicated that the IVP jet noise benefits observed under static conditions would be retained in flight.

Since no procedure was available to predict the IVP noise characteristics for a wide range of applications for an advanced supersonic transport (AST), additional experimental and analytical studies were undertaken to develop and verify a new IVP prediction method. This prediction procedure was developed during an earlier phase of the current NASA-sponsored Coannular Nozzle Model Technology Program (refs. 3 and 4).

Data obtained to date, although extensive, are based on scale model test results. Extrapolation of the data to noise predictions of a full scale engine are based on the application of scaling laws developed for conical nozzles. The assumption was made that these scaling laws are applicable to inverted velocity profile jet noise.

In this segment of the Coannular Nozzle Model Technology Program, work was directed towards obtaining model acoustic data that can be scaled to predict noise levels of the VCE testbed demonstrator. This will allow comparison of noise data at the same thermodynamic conditions to determine IVP scaling factors. In addition, data were obtained for comparison to the aerodynamic/acoustic prediction procedure developed in the earlier effort. Data were acquired using a one-sixth scale model of the VCE testbed exhaust system with a removable hardwall ejector. Major findings and results of the program are presented in this report. All of the basic data obtained in this program are reported separately in the companion Comprehensive Data Report (CDR) (ref. 5).

SECTION 3.0

TEST FACILITIES, MODEL CONFIGURATION, AND INSTRUMENTATION

3.1 INTRODUCTION

This section presents a brief description of the test facilities and model used in the program. All acoustic evaluations were conducted in the Anechoic Jet Noise facility at the Pratt & Whitney Aircraft Commercial Products Division, while performance tests were conducted in the Large Nozzle Thrust Facility at the United Technologies Research Center. Both facilities were used in conducting the aero/acoustic testing during the preceding phase of the program, and more detailed information about these facilities is contained in Reference 3.

The test model, as also described in this section, was designed to duplicate major features of the exhaust system in the VCE testbed. In addition to the model design, this section contains a discussion of the various acoustic and aerodynamic test instrumentation.

3.2 TEST FACILITIES

3.2.1 Anechoic Jet Noise Test Facility

The Pratt & Whitney Aircraft Anechoic Jet Noise Facility, stand X-206, was used to obtain both acoustic data and jet plume velocity and temperature profiles. The facility is located at the Andrew Willgoos Turbine Laboratory and is specially designed to provide an accurate simulation of pure jet noise characteristics using scale model nozzles.

The test chamber, as shown schematically in Figure 3.2-1, is lined with acoustic absorbant wedges to provide an anechoic environment at frequencies above 150 Hz. The volume of the chamber is approximately 340 cubic meters (12,000 cubic feet). The nozzle, which is oriented vertically in the test chamber, exhausts through a stack located atop the chamber. The stack is equipped with blowers and exhaust silencers. A slight inflow of cooling air passes through the perforated walls of the chamber to eliminate secondary air currents induced by the nozzle exhaust and to provide for a uniform propagating medium within the chamber.

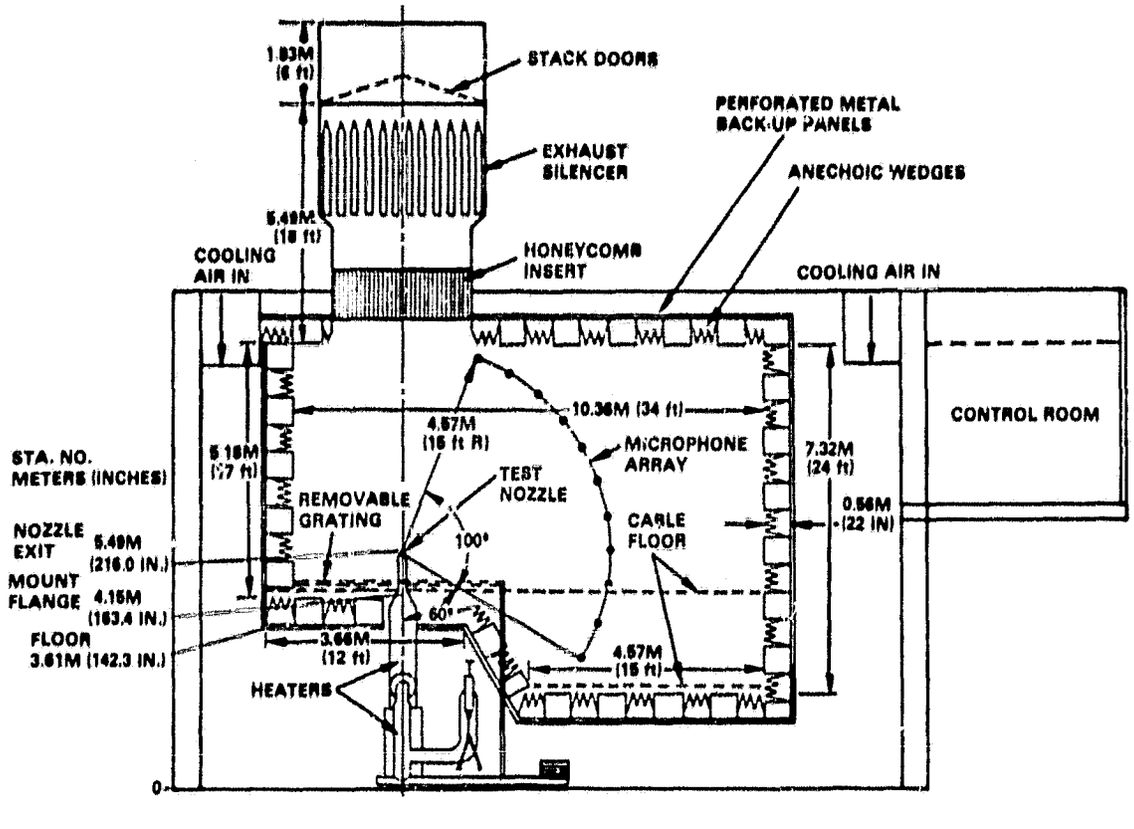

Figure 3.2-1 Pratt & Whitney Aircraft Anechoic Jet Noise Test Facility (Stand X-206)

The air supply to each of the two streams of the coannular nozzle is supplied by the laboratory compressed air system at a maximum flow rate of 14 kg/sec (31 lb/sec) at a maximum pressure of 4.14×10^5 N/m^2 (60 psia). The flow in each stream is independently controlled and measured by flow measuring venturis calibrated to within ±0.2 percent at the Colorado Engineering Experimentation Station, Inc. Air in each stream is heated by direct natural gas-fired burners. The maximum temperature in each stream is 1089 K (1960°R) and the maximum nozzle pressure ratio is 4.0. Fuel flow into the system is measured by calibrated fuel flow venturis. Airflow silencers capable of 25 dB noise suppression are installed in each stream to prevent duct noise from reaching the test nozzle.

3.2.2 Large Nozzle Thrust Facility

Aerodynamic performance tests were conducted in the Large Nozzle Thrust Facility shown schematically in Figure 3.2-2. This facility operates on the blowdown principle and consists of an air supply connected to an apparatus that measures thrust and airflow. Dried air enters the stand from the 2.7×10^6 N/m^2 (400 psia) blowdown system through a large

1.016 m (40 in) diameter plenum. The high pressure air system, when operated in the blowdown mode, can provide runs of at least a 200 second duration with airflow rates up to 34.05 kg/sec (75 lb/sec) and nozzle exit pressures of 10 atmospheres.

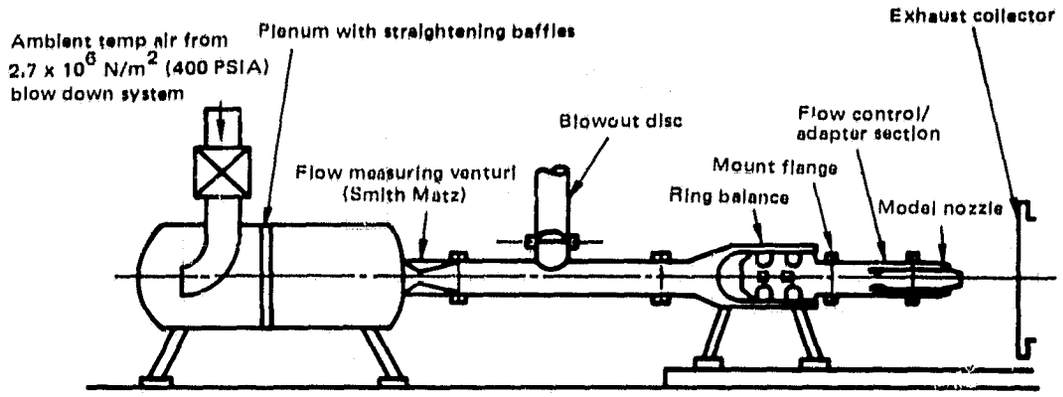

Figure 3.2-2 UTRC Large Nozzle Thrust Facility

During operation, ambient air, throttled from the $2.7 \times 10^6 N/m^2$ (400 psia) blowdown system, is supplied to the upstream plenum. The flow is straightened aerodynamically in the plenum chamber before passing through a Smith-Matz flow measurement venturi for a measurement of the total flow and into a balance section. The flow then passes through the mount flange into the adapter/flow control section of the model, which is indicated in Figure 3.2-3. At this point, the total flow is divided into fan and primary flow. Primary flow is measured by a second venturi. Both fan and primary flows are independently controlled by translating choke plates in each stream that simultaneously serve as flow straighteners and control valves.

Each of these throttle-choke plate assemblies consists of two disks with a series of drilled holes coincident with the full open position. Flow is regulated by translating one of the disks relative to the other to reduce the flow area. Flow quantity can be adjusted very precisely and with practically no flow distortion over the full range. The throttled flows then pass through the instrumentation section and exit from the model into the exhaust collector.

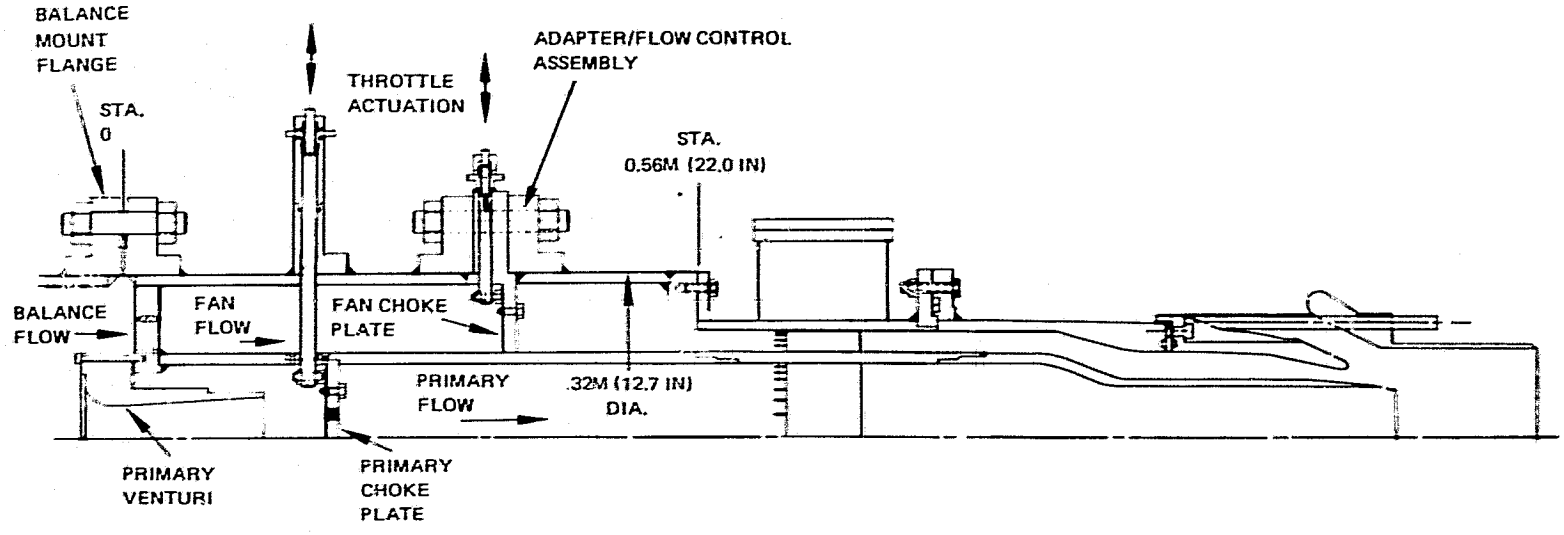

Figure 3.2-3 Installation of the Testbed Nozzle Model in the Large Nozzle Thrust Facility

3.3 TESTBED ENGINE EXHAUST SYSTEM CONFIGURATION

The coannular nozzle model designed and fabricated for this program is a one-sixth representation of the configuration in the VCE testbed. Basically, the VCE testbed has a fixed-geometry conical primary nozzle, a variable-geometry coannular fan duct nozzle and a removable ejector. The variable fan nozzle provides the area variation necessary to satisfy duct burner augmentation requirements.

A cross sectional view of the testbed exhaust system at the operating conditions that served as the basis for the model design definition is shown in Figure 3.3-1. These conditions are based on computer sumulation estimates of the testbed engine operating characteristics. Further description of the testbed demonstrator design and operation, including pertinent design details of the nozzle component, is contained in the VCE Testbed Final Design Report (ref. 6). Detailed design drawings of the model hardware are included in the CDR (ref. 5).

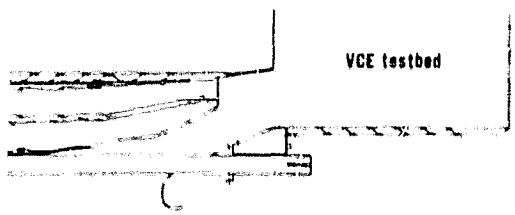

	Fan duct	Primary
• Nozzle pressure ratio P_t/P_a	2.4	1.6
• Total temperature K (°R)	1089 (1960)	802 (1443)
• Nozzle area meter^2 (in.^{2})	0.181 (280)	0.277 (430)
• Fan/primary area ratio	0.65	
• Fan/primary velocity ratio V_f/V_p	1.56	

Figure 3.3-1 VCE Testbed Demonstrator Exhaust System at Model Design Operating Conditions

A total nozzle jet area (primary area + fan area, or $A_8 + A_{18}$) equivalent to a 12.7 cm (5.0 in) diameter conical nozzle was selected for the model design for consistency with models previously tested (ref.

3). The selection of a model nozzle area of 0.0127 m^2 (19.64 in^2) established the scaling factor for defining the model configuration relative to the testbed exhaust system, as shown:

$$\text{Area Scale Factor (ASF)} = \frac{A_j \text{ total model}}{A_j \text{ (fan and primary) testbed demonstrator}}$$

$$\text{ASF} = \frac{0.0127 \text{ m}^2 \text{ (19.64 in}^2\text{)}}{0.181 \text{ m}^2 \text{ (280 in}^2\text{)} + 0.277 \text{ m}^2 \text{ (430 in}^2\text{)}}$$

$$\text{ASF} = 0.0277$$

$$\text{Linear Scale Factor (LSF)} = \sqrt{\text{ASF}}$$

$$\text{LSF} = \sqrt{0.0277}$$

$$\text{LSF} = 0.1664 \text{ (1/6 scale)}$$

The scale model fan and primary nozzle areas are defined as follows:

	Engine	X	ASF	=	Scale Model
A_j fan m^2 (in^2)	0.181 (280)	X	0.02766	=	0.00501 (7.745)
A_j primary m^2 (in^2)	0.277 (430)	X	0.02766	=	0.00767 (11.894)

The resulting scale factors were applied to the testbed exhaust system to dimensionally define the fan duct cowl, primary afterbody/nozzle, ejector and ejector support assembly. All model components were fabricated of AISI 304 heat resistent stainless steel. Photographs of the fan and primary nozzle assembly, ejector and support assembly and ejector/nozzle assembly are shown in Figures 3.3-2 through 3.3-4. A cross sectional view of the model and instrumentation sections installed on the X-206 stand is shown in Figure 3.3-5.

The comparison of the model and testbed nozzle flow paths in Figure 3.3-6 shows the duplication of major exhaust system features in the model. Detail drawings of the model hardware are included in the companion CDR (ref. 5). The comparison also indicates the duct burner cooling liners and associated cooling flows, approximately eight percent on the outer wall and four percent on the inner wall, that were not modeled. Neither the acoustic or nozzle performance test facilities had the capability of simulating the cooling flows nor was it possible to accurately characterize the properties of the flows exiting the liners. Although the cooling flow characteristics were not simulated, the total duct nozzle flow area of the model was comparable to the full-scale testbed engine. The small rear facing step, approximately 0.305 cm (0.120 in) between the testbed fan nozzle flap and flap fairing, was not simulated in the model. It was felt that without the simulation of low velocity cooling flow over the step, a smooth fan nozzle contour was preferable for analysis of the acoustic data and correlations with testbed data.

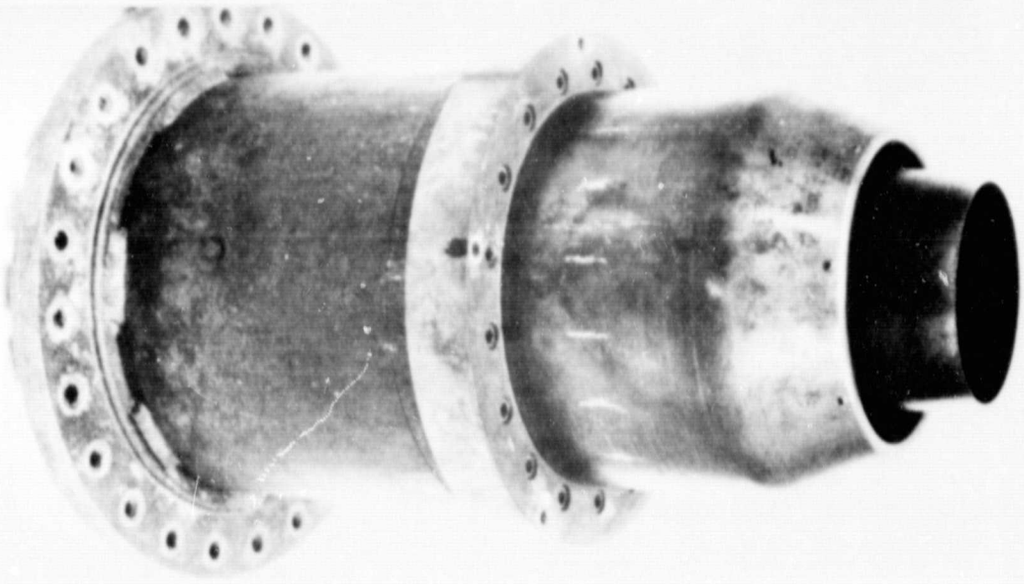

Figure 3.3-2 VCE Testbed Fan and Primary Nozzle Model Assembly

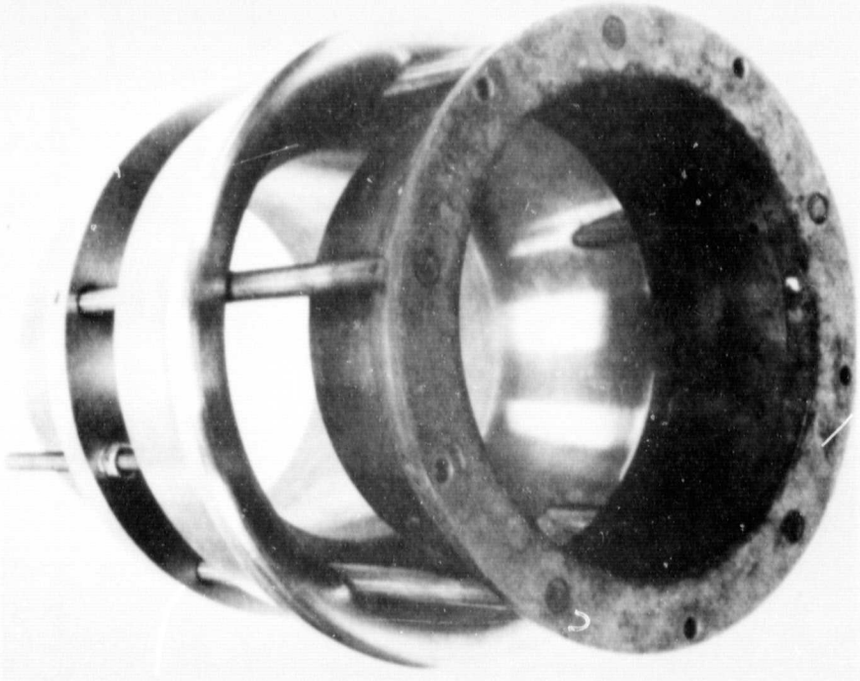

Figure 3.3-3 VCE Testbed Ejector and Fairing Model Assembly

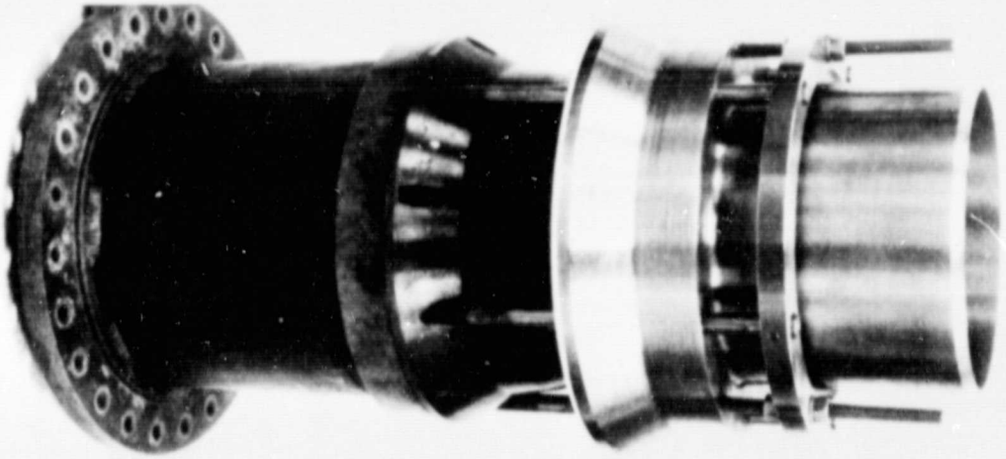

Figure 3.3-4 VCE Testbed Ejector Model Assembled on Nozzle

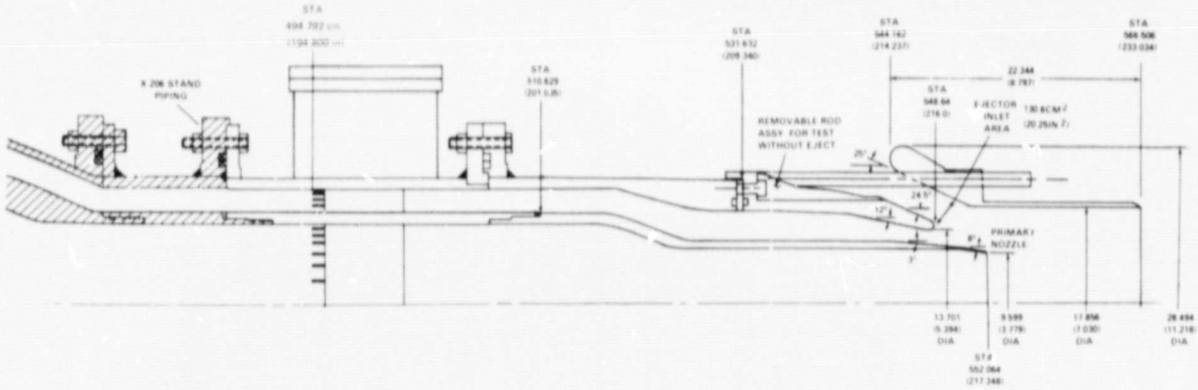

Figure 3.3-5 VCE Testbed Model Installed on X-206 Stand Piping

3.4. TEST INSTRUMENTATION

3.4.1 Acoustic Instrumentation

In the anechoic chamber, acoustic signals were detected by a polar array of 0.635 cm (0.250 in) diameter Bruel & Kjaer (B&K) microphones (model no. 4135) positioned at normal incidence (0 degree) from the center of the test nozzle exit plane at a distance of 4.57 m (15 ft). Microphones were located every 10 degrees from 60 to 160 degrees relative to the upstream jet axis, as depicted in Figure 3.2-1. All microphones were calibrated prior to testing by a procedure traceable to the National Bureau of Standards. Daily calibrations were performed with a B&K No. 4220 Pistonphone.

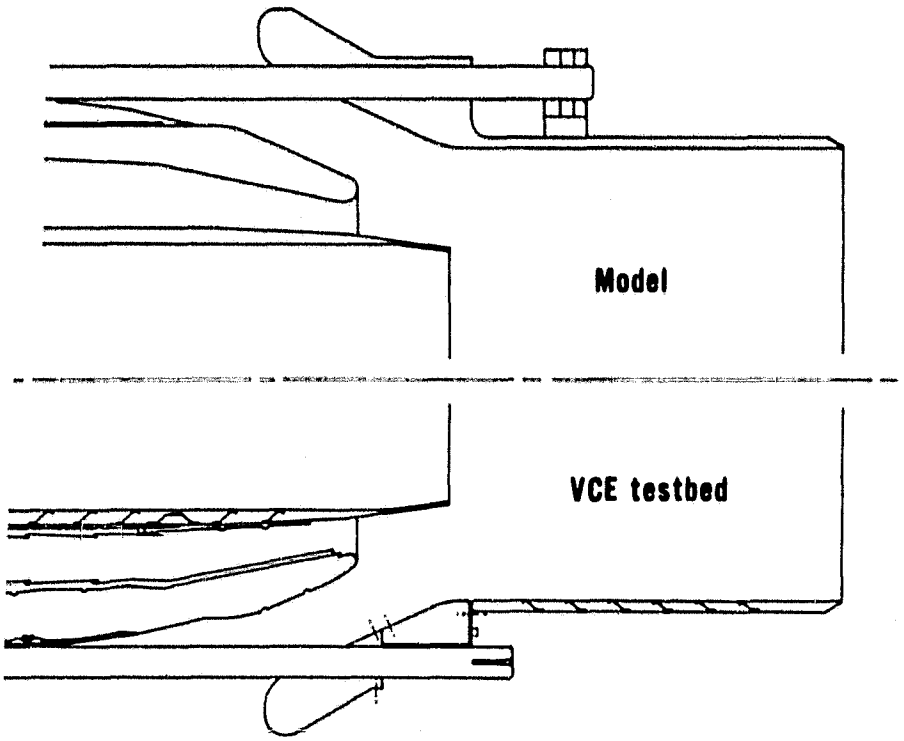

Figure 3.3-6 Comparison of Test Model and VCE Testbed Nozzle Flow Paths

3.4.2 Aerodynamic Instrumentation

3.4.2.1 Nozzle Operating Condition Instrumentation

The instrumentation and support section is located 0.533 m (21 in) upstream from the fan nozzle exit plane and serves a dual purpose. It maintains the concentricity of the coannular nozzle assembly and contains all necessary instrumentation to define the properties of flow entering the nozzle. The section was employed for both the acoustic and aerodynmanic portions of the test program, and thus used in both the anechoic and Large Nozzle Thrust facilities.

The major portions of the instrumentation duct are shown in Figure 3.4-1. The instrumentation in the primary passage consisted of six total pressure probes, six total temperature probes and four wall static pressure taps. The fan stream instrumentation consisted of two total pressure probes and two total temperature probes mounted in each of the two duct struts and four static taps in both the inner and outer wall. The total pressure and total temperature probes were installed protruding through the leading edge of the struts. The probes are made up of removable rakes which are held in place at the ends of the support struts.

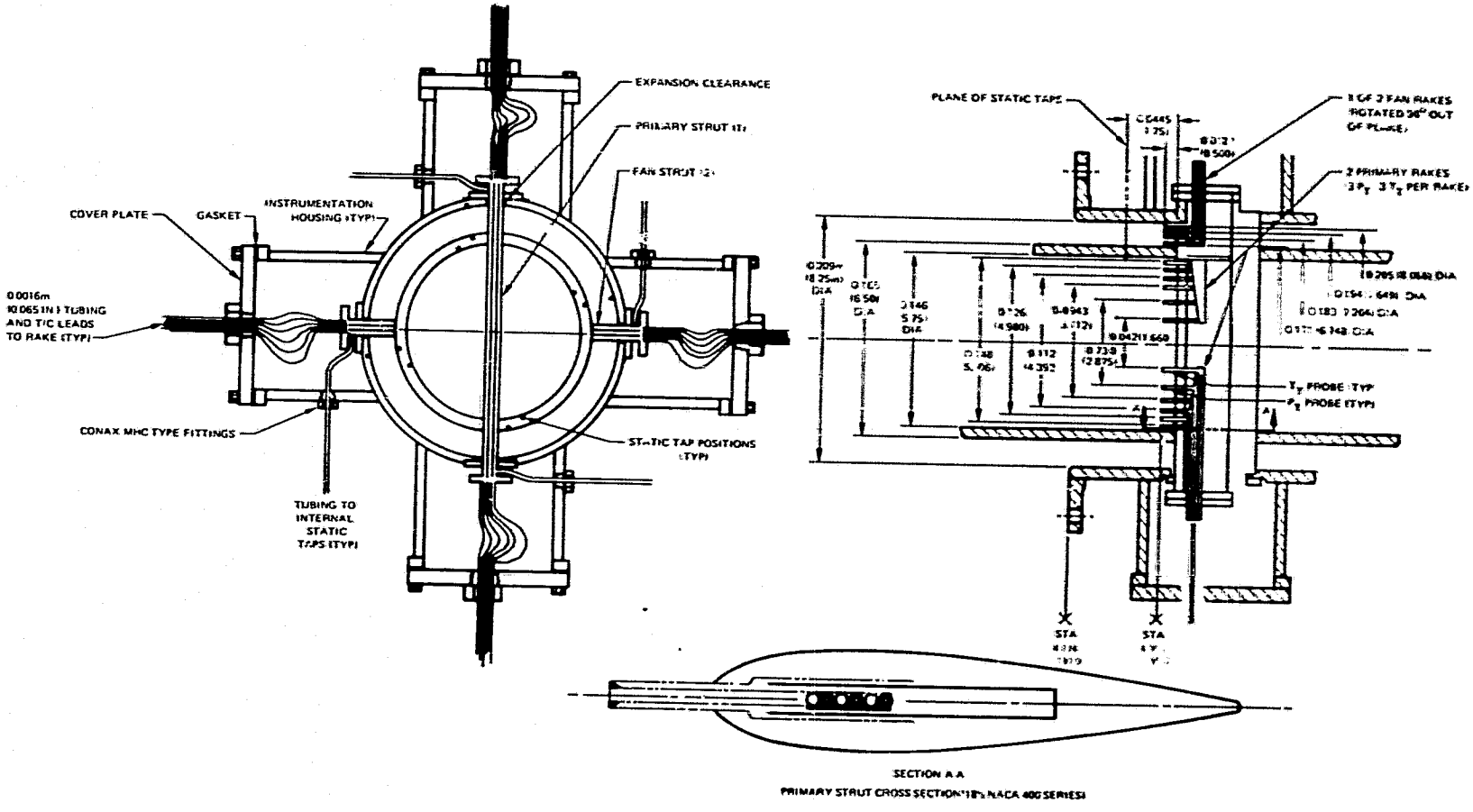

Figure 3.4-1 Details of Instrumentation and Support Section

3.4.2.2 Nozzle Exhaust Plume Traverse Instrumentation

Surveys of the jet exhaust plume were conducted in the anechoic chamber. These were made at several locations downstream of the model to determine the radial pressure and temperature profiles.

A combination wedge probe with total pressure, total temperature and static pressure measurement capability was used in this program. This type of probe has been used extensively in other NASA and Pratt & Whitney Aircraft sponsored programs during recent years. A schematic of the probe is shown in Figure 3.4-2. Static pressure is measured with two orifices (a and b), one on each side of the 20-degree wedge. Total temperature is determined by means of a thermocouple that is exposed to flow through ports at the rear of the wedge at points d and e. The flow exits at the base of the wedge through port f, which controls the flow past the thermocouple head. This port was sized to establish the best balance between conductive and convective heat transfer. The probe was extensively calibrated for pressure and temperature recovery up to Mach no 1.6 and yaw angle of $\pm$ 5 degrees at high and low Reynolds numbers. Strain gages were placed at high stress areas on the wedge so that probe stress could be monitored while traversing the jet plume.

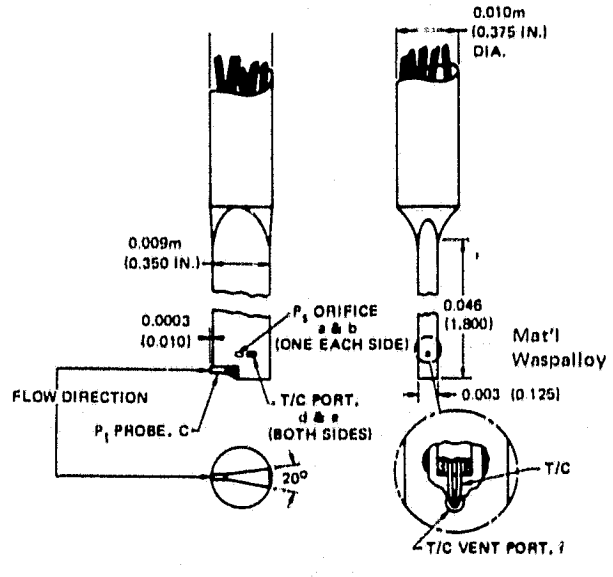

Figure 3.4-2 Details of Wedge Traverse Probe For Pressure and Temperature Measurement

SECTION 4.0

ACOUSTIC TEST RESULTS AND DISCUSSION

4.1 INTRODUCTION

This section contains a discussion of the acoustic portion of model testing and data analysis. The discussion includes a description of the test matrix, operating conditions at each point and procedures employed to establish the nozzle operating conditions. This is followed by a description of the acoustic data reduction methods, along with the method of data validation. Finally, results of the acoustic tests are presented and discussed.

4.2 ACOUSTIC TEST MATRIX AND TEST PROCEDURE

4.2.1 Acoustic Test Matrix

The model VCE nozzle was tested over the range of operating conditions listed in Table 4.2-I. This matrix was structured to provide sufficient data to perform the following:

(1) Validate the data by means of comparison of noise from the model nozzle with only primary flow to noise predictions from Reference 7.

(2) Define an envelope through which the operating line of the testbed is anticipated to pass. This envelope is expected to contain at least one point that will match conditions at which the testbed will operate at an area ratio 0.65.

(3) Provide acoustic data at sufficient operating conditions to determine the sensitivity of noise to variations in stream parameters.

(4) Compare noise characteristics of an IVP jet from a coannular nozzle with and without an ejector shroud at the same operating conditions.

The additional test matrix points listed in Table 4.2-I were defined to provide various diagnostic and comparative data.

4.2.2 Acoustic Test Procedure

The procedure for obtaining an acoustic data point consisted of setting the fan and primary pressures and temperatures to specified values. These values were then held constant with automatic controllers and operation of the model was allowed to stabilize for approximately five minutes before initiating data acquisition.

TABLE 4.2-I

ACOUSTIC TEST MATRIX
NOMINAL OPERATING CONDITIONS

Test Pt.	P_{tf}/P_a	T_{tf} K (^oR)	V_f m/sec(ft/sec)	P_{tp}/P_a	T_{tp} K (^oR)	V_p m/sec(ft/sec)
1	2.40	1089(1960)	702(2303)	1.60	800(1440)	451(1479)
2	2.40	1000(1800)	672(2206)	1.60	800(1440)	451(1479)
3	2.40	922(1660)	645(2116)	1.60	800(1440)	451(1479)
4	2.40	700(1260)	561(1839)	1.60	800(1440)	451(1479)
5	2.40	589(1060)	513(1684)	1.60	800(1440)	451(1479)
6	2.20	1089(1960)	670(2197)	1.60	800(1440)	451(1479)
7	2.80	1089(1960)	755(2476)	1.60	800(1440)	451(1479)
8	2.60	1089(1960)	730(2395)	1.60	800(1440)	451(1479)
9	2.80	700(1260)	602(1975)	1.60	800(1440)	451(1479)
10	2.60	922(1660)	671(2201)	1.60	800(1440)	451(1479)
11	2.20	922(1660)	615(2019)	1.60	800(1440)	451(1479)
12	2.00	1089(1960)	637(2091)	1.60	800(1440)	451(1479)
13	2.00	700(1260)	503(1650)	1.60	800(1440)	451(1479)
14	2.40	1089(1960)	702(2303)	1.60	1089(1960)	527(1728)
15	2.40	1089(1960)	702(2303)	1.60	922(1660)	484(1589)
16	2.40	1089(1960)	702(2303)	1.60	589(1060)	386(1267)
17	2.40	1089(1960)	702(2303)	2.00	589(1060)	462(1516)
18	2.40	1089(1960)	702(2303)	1.40	589(1060)	329(1081)
19	2.10	889(1600)	587(1927)	2.08	850(1530)	571(1873)
20	1.93	933(1679)	566(1858)	1.93	933(1679)	566(1858)
21	2.34	903(1625)	630(2067)	1.79	817(1471)	504(1652)
22	2.10	1072(1930)	649(2130)	1.37	718(1292)	353(1158)
23	2.25	1072(1930)	668(2190)	1.47	753(1356)	397(1301)
24	2.50	1089(1960)	717(2351)	1.53	811(1460)	433(1420)
25	3.20	1089(1960)	796(2612)	1.53	811(1460)	433(1420)
26	2.40	478(860)	434(1423)	1.60	800(1440)	451(1479)
27	3.20	1089(1960)	796(2611)	1.60	800(1440)	451(1479)
28	3.20	700(1260)	635(2082)	1.60	800(1440)	451(1479)
29	2.40	1089(1960)	702(2303)	2.40	800(1440)	600(1968)
30	2.00	857(1543)	563(1848)	2.00	857(1543)	563(1848)
38	2.40	1089(1960)	702(2303)	1.40	800(1440)	385(1262)
1E	2.40	1089(1960)	702(2303)	1.60	800(1440)	451(1479)
3E	2.40	922(1660)	645(2116)	1.60	800(1440)	451(1479)
4E	2.40	700(1260)	561(1839)	1.60	800(1440)	451(1479)
19E	2.10	889(1600)	587(1927)	2.08	850(1530)	571(1873)
1P	----------			1.60	800(1440)	451(1479)
14P	----------			1.60	1089(1960)	527(1728)
15P	----------			1.60	922(1660)	484(1589)
17P	----------			2.00	589(1060)	462(1516)

NOTES: 1) All values normalized to Federal Aviation Administration (FAA) standard day conditions (T_a = 298°K (537°R), relative humidity = 70 %)
E = Operation with the ejector installed
P = Operation with only primary flow

2) Actual nozzle and ambient test conditions are listed in Appendix C.

Both acoustic and nozzle operating condition data were acquired simultaneously. During data acquisition, nozzle operating conditions were closely monitored for fluctuations. If fluctuations were observed, data were not taken and operating conditions were stabilized again before initiating data acquisition.

4.3 ACOUSTIC DATA REDUCTION METHODS

The acoustic signals measured by the microphone array in the anechoic chamber were corrected, analyzed, scaled to testbed and VSCE-502B study engine size, and extrapolated from the measuring radius to several radii and sidelines. Figure 4.3-1 presents a flowchart of the data reduction sequence and indicates the available data outputs. The methods of calculating overall sound pressure level (OASPL), power level (PWL), overall power level (OAPWL) and perceived noise level (PNL) are given in Appendix A.

4.3.1 Correction Factors

The recorded acoustic data were reduced to one-third octave band sound pressure levels from 100 Hz to 80 kHz by analog/digital analysis performed with a General Radio No. 1921 Analyzer. The one-third octave band model scale sound pressure levels were then corrected for calibrated cable and microphone responses.

In order that all data be on the same basis, one-third octave band data were transformed into "theoretical day" or "lossless day" data by applying the values of atmospheric absorption, as defined in Reference 8. These corrections add sound pressure level (SPL) values to measured data thereby representing the noise that would be measured at the microphone if no noise was lost through atmospheric absorption. The model data that were scaled to represent the testbed and full size engines, as discussed in Section 4.3.2, were corrected to a Federal Aviation Administration (FAA) standard day (T_a = 298°K (537°R), relative humdity = 70 percent) by adding the corrections of Reference 8.

4.3.2 Scaling and Extrapolation Techniques

Model noise data were scaled to represent both testbed and full size engine data. The model, having a 0.127 m (5 in) equivalent diameter, was scaled up six times for the testbed demonstrator and twelve times for the study engine. The scaling method consisted of increasing model SPL values by the amount 20 log S and reducing the model size frequencies by the factor S, where S is the linear scale factor.

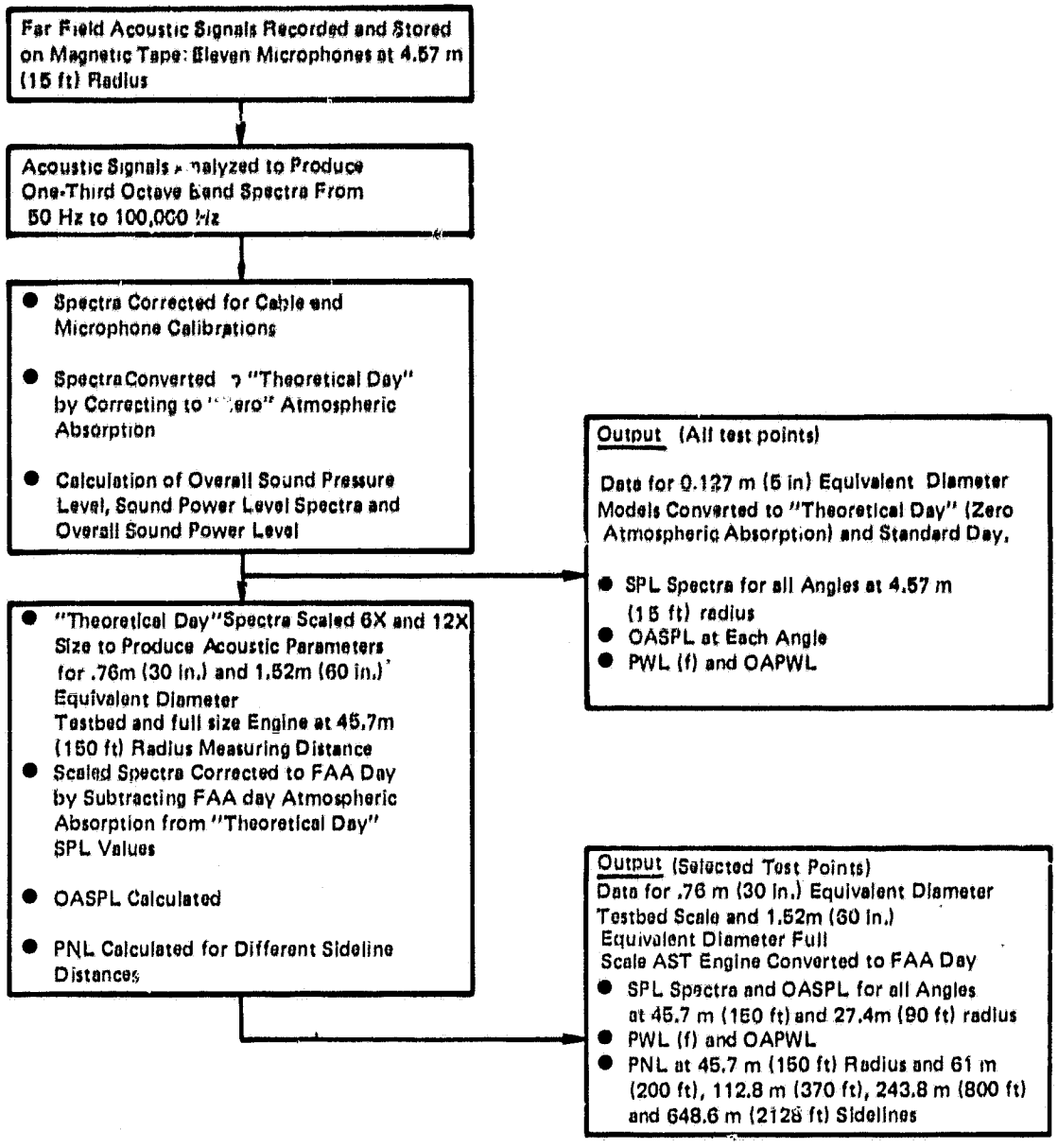

Figure 4.3-1 Flow Chart of Acoustic Data Reduction Sequence

Model data were extrapolated from the 4.57 m (15 ft) measuring radius to several radii and sidelines, by applying the spherical divergence law. Thus, data were adjusted by subtracting the correction 20 log d/dm, where d is the distance from the nozzle to the radius or sideline being extrapolated to and dm is the measuring radius from the nozzle. Both distances are for a particular angle. The atmospheric absorption corrections of Reference 8 were also applied to extrapolated data. Because the characteristics of the test facility ensured far field acoustic signals free from ground reflections, all acoustic values calculated from measured data were also free field. The extrapolated data do not include extra ground attenuation.

4.4 DATA VALIDITY

Testing was conducted at four operating conditions with only primary stream flow for the purpose of comparing measured levels with levels predicted using the SAE single jet method to evaluate data validity. The stream total temperature ranged from 800 K (1440°R) to 1089 K (1960°R), while the jet velocity was varied from 451 m/sec (1479 ft/sec) to 527 m/sec (1728 ft/sec). Acoustic data from the convergent primary nozzle, as recorded and processed by the data acquisition system, were compared to the SAE single jet prediction method of Reference 7. The stated accuracy of this prediction procedure is ± 3 dB. Spectra and OASPL directivity for typical model data are shown in Figures 4.4-1.through 4.4.3. The agreement of spectral shapes and directivity patterns, along with measured levels that are for the most part within the accuracy band of the SAE prediction method, provides the confidence that test data are valid and accurately represent the noise generated by the model nozzle.

4.5 DISCUSSION OF ACOUSTIC TEST RESULTS

Representative results obtained during acoustic testing are presented in this section. The following topics are discussed: effects of parametrically varying fan and primary stream properties on IVP jet noise, effects of a hardwall ejector on jet noise characteristics, and a testbed data comparison.

4.5.1 Parametric Variations

In this series of tests, the influence of primary and fan stream temperature and pressure ratio on noise was examined. The purpose of this type of testing was to determine a point of direct comparison of model and testbed data for assessing the applicability of scaling laws developed for other types of jets to IVP jets. Thus, a range of operating conditions was covered to allow interpolation of data at conditions closely duplicating those of the testbed.

Variations in stream temperature or pressure ratio affect jet mixing noise levels of conventional jets. To determine the effect of changes in stream properties on the acoustic characteristics of an IVP jet, total temperatures and pressures were varied independently in each stream. Figure 4.5-1 shows the test matrix variations in fan stream properties at constant primary conditions, and Figure 4.5-2 identifies those for the primary stream at constant fan conditions.

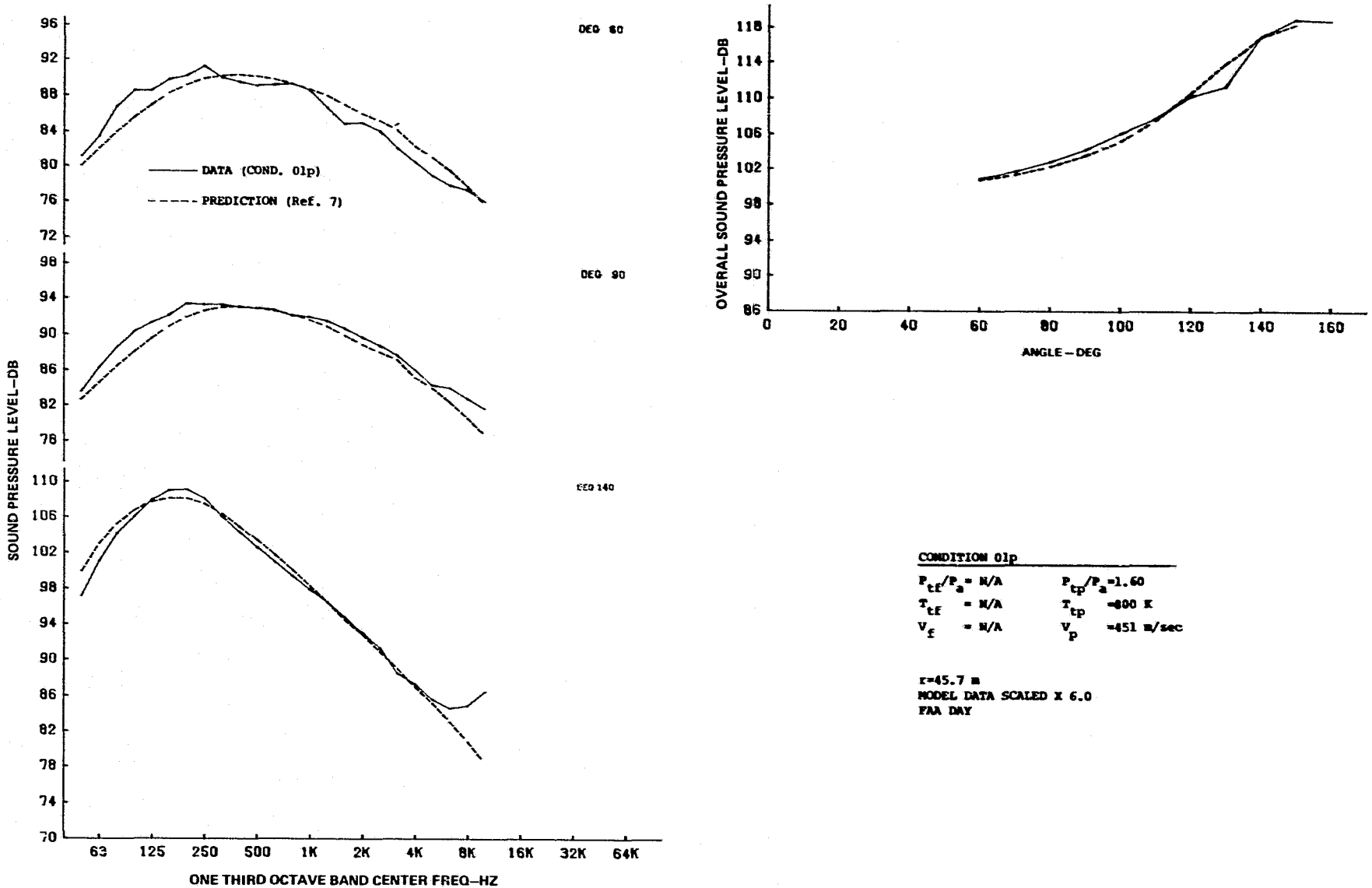

Figure 4.4-1 Comparison of Primary Jet Noise to SAE Predicted Jet Noise Test Point 1

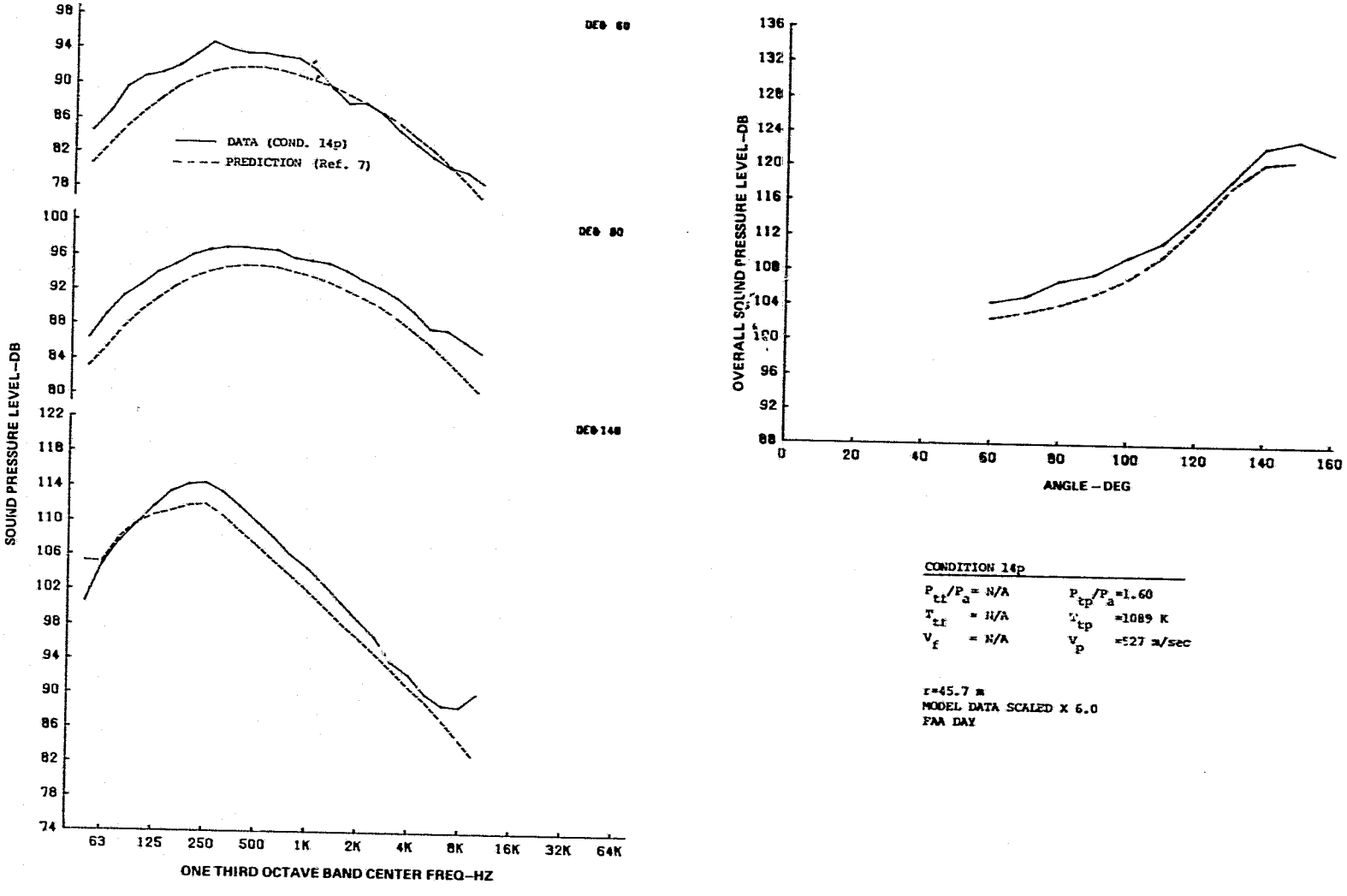

Figure 4.4-2 Comparison of Primary Jet Noise to SAE Predicted Jet Noise Test Point 14

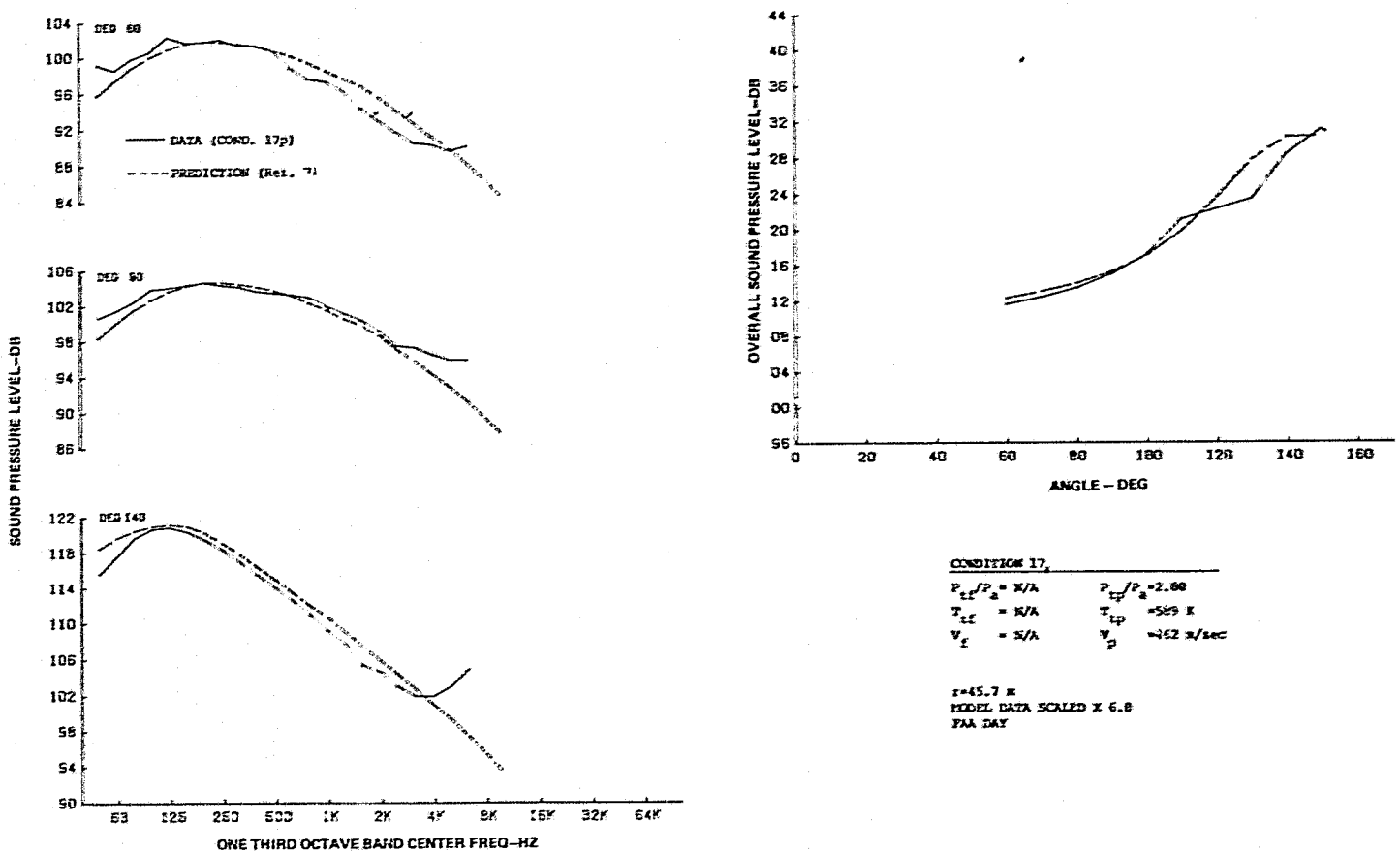

Figure 4.4-3 Comparison of Primary Jet Noise to SAE Predicted Jet Noise Test Point 17

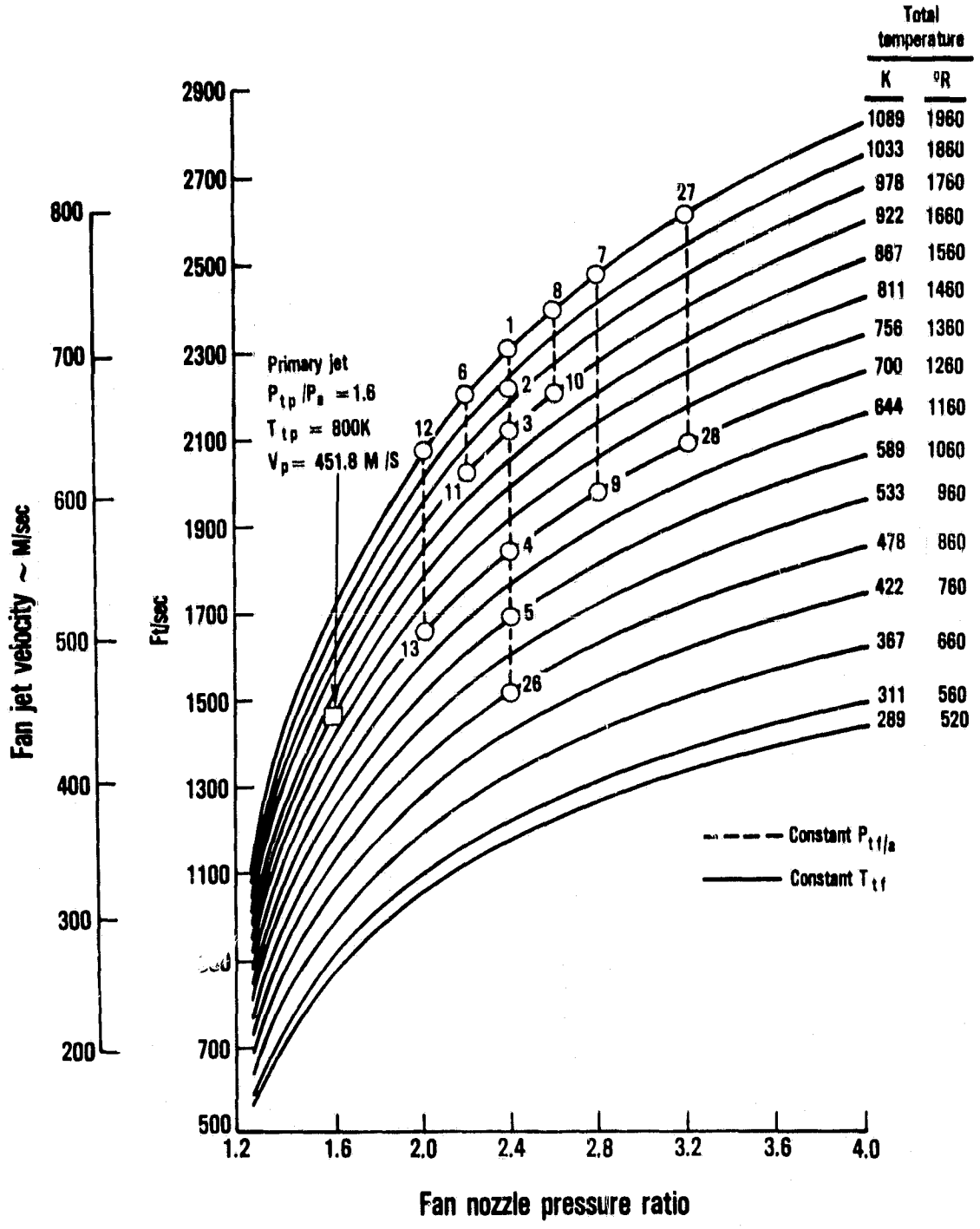

Figure 4.5-1 Parametric Variation of Fan Stream Properties at Constant Primary Operating Conditions

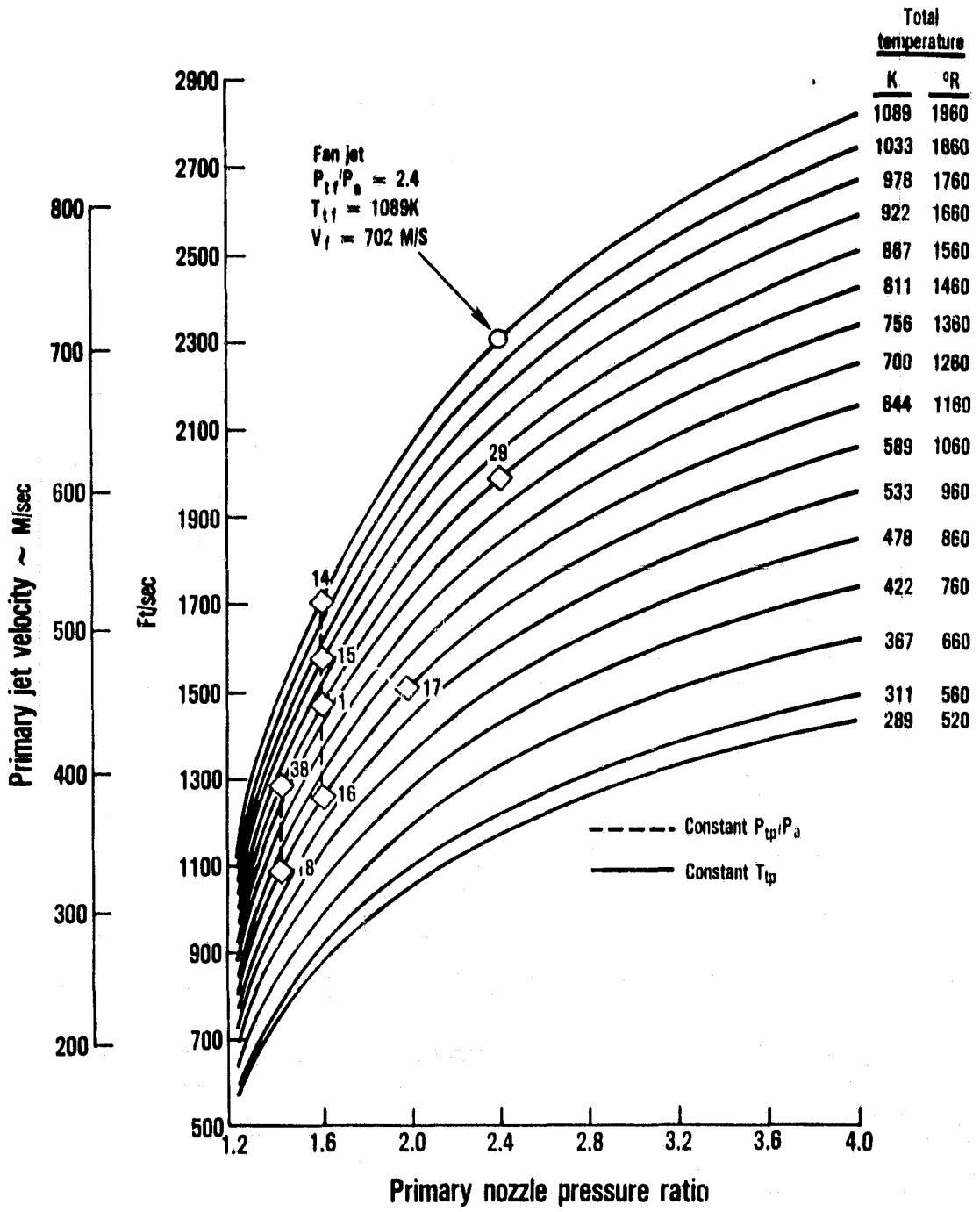

Figure 4.5-2 Parametric Variation of Primary Stream Properties at Constant Fan Operating Conditions

In each figure, properties of one stream were varied while the other was maintained constant. For all points shown in Figure 4.5-1, primary stream conditions were maintained constant and fan stream properties were varied systematically. Test points at constant fan pressure ratios are connected by dashed lines and points at constant fan temperature by solid ones. Fan stream temperature was varied from 422°K (760°R) to 1089°K (1960°R) at six pressure ratios. Correspondingly, fan pressure ratio was varied from 2.0 to 3.2 at six fan stream temperature levels. Figure 4.5-2 shows variations of primary stream properties in a manner similar to that of Figure 4.5-1. Primary stream temperature ranged from 589°K (1060°R) to 1089°K (1960 °R) at a pressure ratio of 1.6. Primary stream pressure ratio varied from 1.4 to 2.4 at primary temperature of 800 K (1440°R).

4.5.1.1 Noise Sensitivity to Variations in Fan Temperature

In Figure 4.5-3, overall sound pressure level directivity and spectra at 60, 90, 130 and 150 degrees are shown with the fan stream temperature varied from 478 K (860°R) to 1089 K (1960°R) at a fan pressure ratio of 2.4. The primary stream conditions were the same for all six points. Figure 4.5-3 indicates that SPL values increased with increasing fan temperature. The greatest effect of increasing fan temperature, and thus velocity, is in the high frequency premerged portions of the spectra. In this high frequency region, SPL increased with fan temperature at all angles while the low frequency merged region was relatively unaffected. In Figure 4.5-3, the increase in noise for low angles at 16 kHz is attributed to fan shock noise. The data indicate that this fan shock noise decreased with increasing fan temperature, as predicted by the procedure reported in Reference 3. The OASPL directivity indicated that the effect of fan temperature variations was greatest at 100 to 130 degrees from the upstream axis.

4.5.1.2 Noise Sensitivity to Variations in Fan Pressure Ratio

At constant primary stream conditions and constant fan temperature of 1089 K (1960°R), fan pressure ratio was varied from 2.0 to 3.2. Typical results at these conditions are presented in Figure 4.5-4. As indicated, noise levels increased with fan pressure ratio and, again, the greatest effect was in the high frequency, premerged part of the spectra. Over the range of operating conditions in this test, the low frequency IVP jet noise was more sensitive to fan velocity resulting from changes in fan pressure ratio than to those due to changes in fan temperature (refer to Figure 4.5-3). This was because, in the case of increasing fan temperature, the increased noise resulting from higher merged jet velocity was offset by reduced noise resulting from decreased merged jet density.

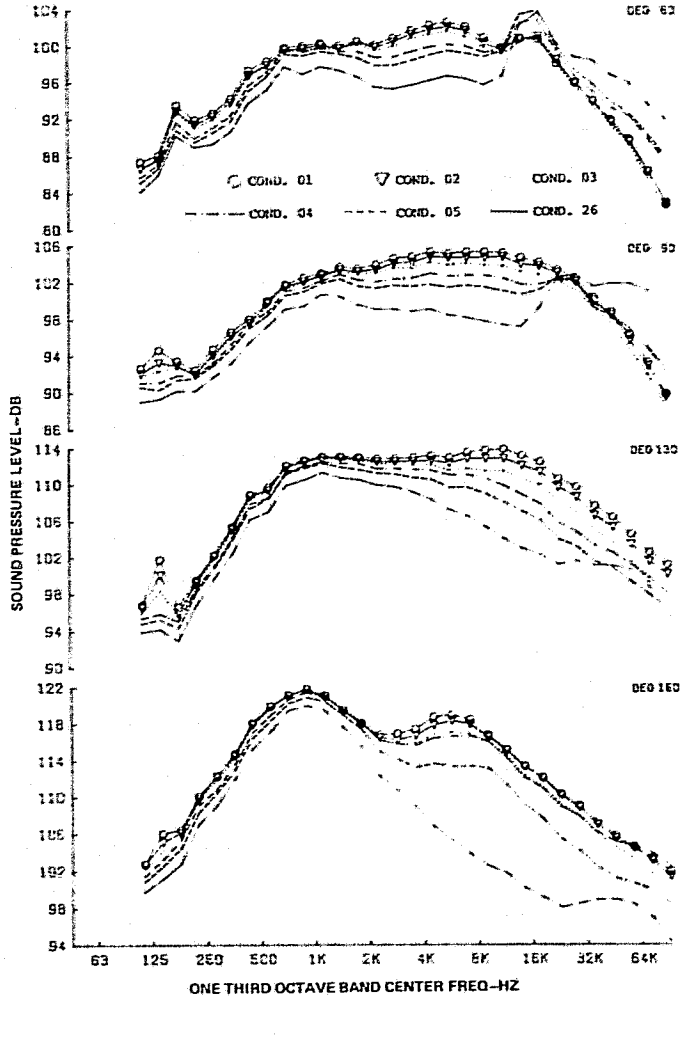

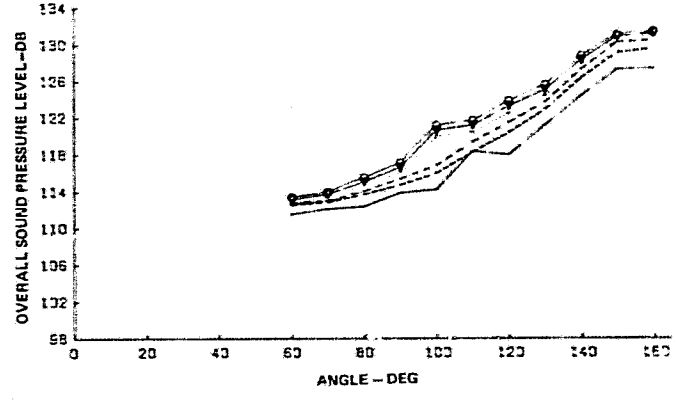

CONDITION 01

P_{tf}/P_a=2.40 P_{tp}/P_a=1.60
T_{tf} =1085 K T_{tp} =800 K
V_f =702 m/sec V_p =451 m/sec

CONDITION 02

P_{tf}/P_a=2.40 P_{tp}/P_a=1.60
T_{tf} =1000 K T_{tp} =800 K
V_f =672 m/sec V_p =451 m/sec

CONDITION 03

P_{tf}/P_a=2.40 P_{tp}/P_a=1.60
T_{tf} =922 K T_{tp} =800 K
V_f =645 m/sec V_p =451 m/sec

CONDITION 04

P_{tf}/P_a=2.40 P_{tp}/P_a=1.60
T_{tf} =760 K T_{tp} =800 K
V_f =561 m/sec V_p =451 m/sec

CONDITION 05

P_{tf}/P_a=2.40 P_{tp}/P_a=1.60
T_{tf} =589 K T_{tp} =800 K
V_f =513 m/sec V_p =451 m/sec

CONDITION 26

P_{tf}/P_a=2.40 P_{tp}/P_a=1.60
T_{tf} =478 K T_{tp} =800 K
V_f =434 m/sec V_p =451 m/sec

r=4.57 m
MODEL SCALE
FAR DAY

Figure 4.5-3 Effect of Varying Fan Temperature on Jet Noise

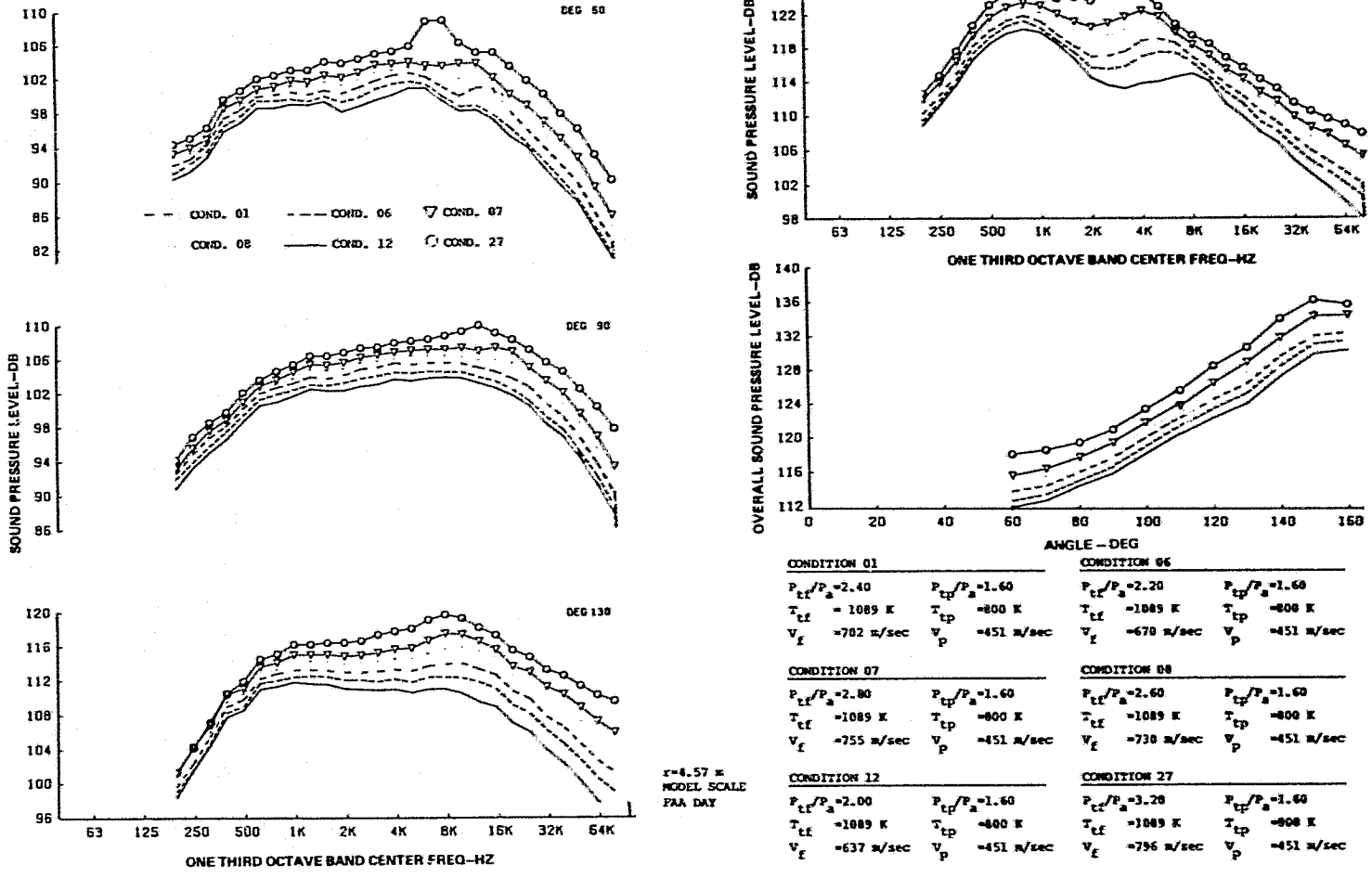

Figure 4.5-4 Effect of Varying Fan Pressure Ratio on Jet Noise

In contrast, as fan pressure ratio increased at constant fan temperature, the noise increased with rising fan stream velocity, while there was little change in noise resulting from density changes. Fan shock noise is evident at pressure ratios of 2.4, 2.6 and 3.2. The OASPL directivity indicates that the effects of fan pressure ratio variations are nondirectional.

4.5.1.3 Noise Sensitivity to Variations in Primary Temperature

Primary stream temperature was varied from 589 K ($1060^{\circ}R$) to 1089 K ($1960^{\circ}R$) at a constant primary pressure ratio of 1.6 and constant fan conditions. Figure 4.5-5 shows the acoustic results. At 60 degrees, fan shock noise in the region of 16 kHz was evident in all cases. Noise levels increased with primary temperature at all angles. The effect of increasing primary temperature was to increase the level of the low frequency merged jet noise while high frequency levels were unchanged. Variations in primary stream temperature produced the greatest changes in jet noise at aft angles.

4.5.1.4 Noise Sensitivity to Variations in Primary Pressure Ratio

Spectra and OASPL directivity for three points with varying primary stream pressure ratio are shown in Figure 4.5-6. The primary total temperature was the same for all three points, along with the fan stream conditions. The effects of variations in primary pressure ratio were in the low frequency merged regions of the spectra. In this region, SPL values increased with primary pressure ratio. Premerged parts of the spectra were nearly unaffected by pressure ratio variations in the primary stream. The OASPL directivity indicated that noise changes due to varying primary pressure ratio were most pronounced at aft angles.

4.5.1.5 Summary of Parametric Investigations

Results of these parametric evaluations show noise levels varied smoothly with each of the parameters. Variation of primary stream parameters produced the greatest effect at low frequencies and angles near the downstream jet axis. In contrast, variation of fan stream properties had the greatest influence in the high frequency region of the spectrum, and these effects were nondirectional over the angles measured.

4.5.2 Ejector Effects on Noise

In the related VCE Testbed Program, the nozzle will be tested both with and without an ejector. The ejector will be a hardwall configuration with provisions for acoustic treatment. For the model testing conducted in this program, however, only a hardwall ejector that simulated the geometry of the testbed configuration was tested. Details of the ejector design are in Section 3.3. The ejector differs from a flight design in that it has a bellmouth inlet. This feature was incorporated in the model and testbed designs to more accurately simulate the flowpath of the entrained air into an ejector during takeoff.

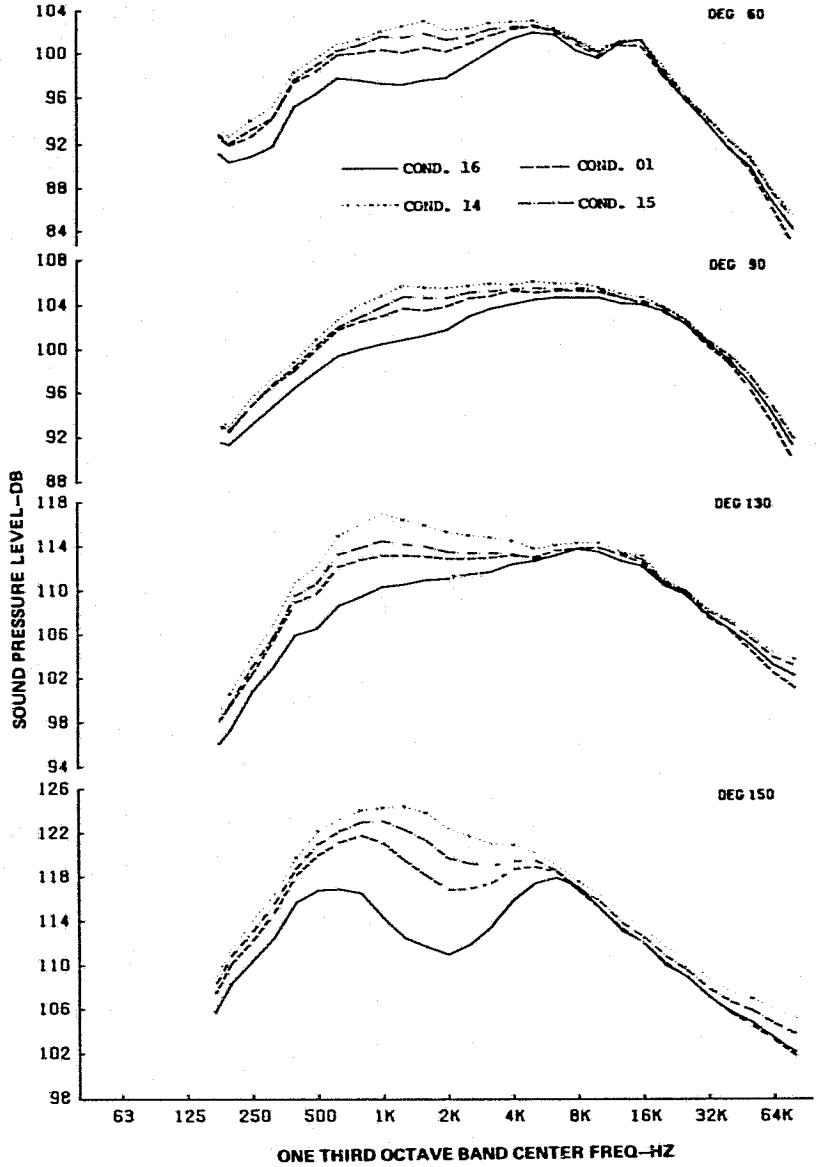

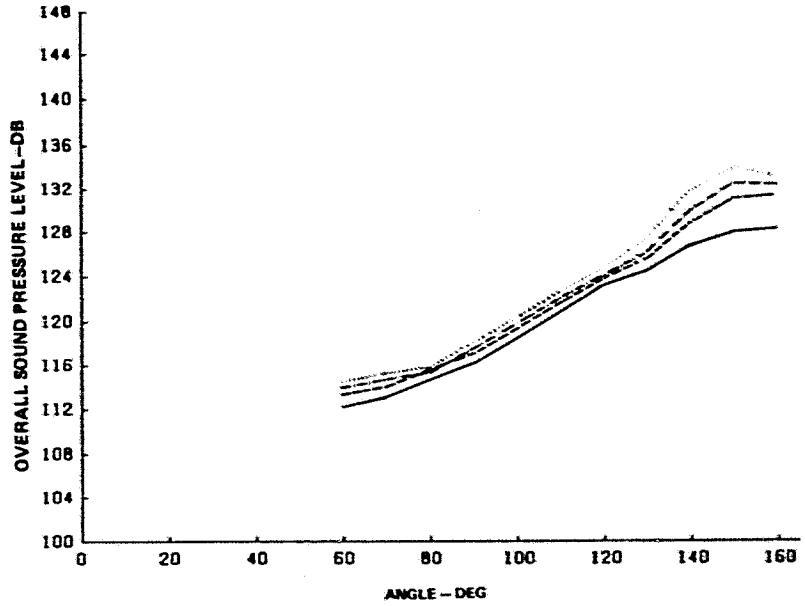

CONDITION 01

P_{tf}/P_a=2.40 P_{tp}/P_a=1.60
T_{tf} =1089 K T_{tp} =800 K
V_f =702 m/sec V_p =451 m/sec

CONDITION 14

P_{tf}/P_a=2.40 P_{tp}/P_a=1.60
T_{tf} =1089 K T_{tp} =1089 K
V_f =702 m/sec V_p =527 m/sec

CONDITION 15

P_{tf}/P_a=2.40 P_{tp}/P_a=1.60
T_{tf} =1089 K T_{tp} =922 K
V_f =702 m/sec V_p =484 m/sec

CONDITION 16

P_{tf}/P_a=2.40 P_{tp}/P_a=1.60
T_{tf} =1089 K T_{tp} =589 K
V_f =702 m/sec V_p =386 m/sec

r=4.57 m
MODEL SCALE
FAA DAY

Figure 4.5-5 Effect of Varying Primary Stream Temperature on Jet Noise

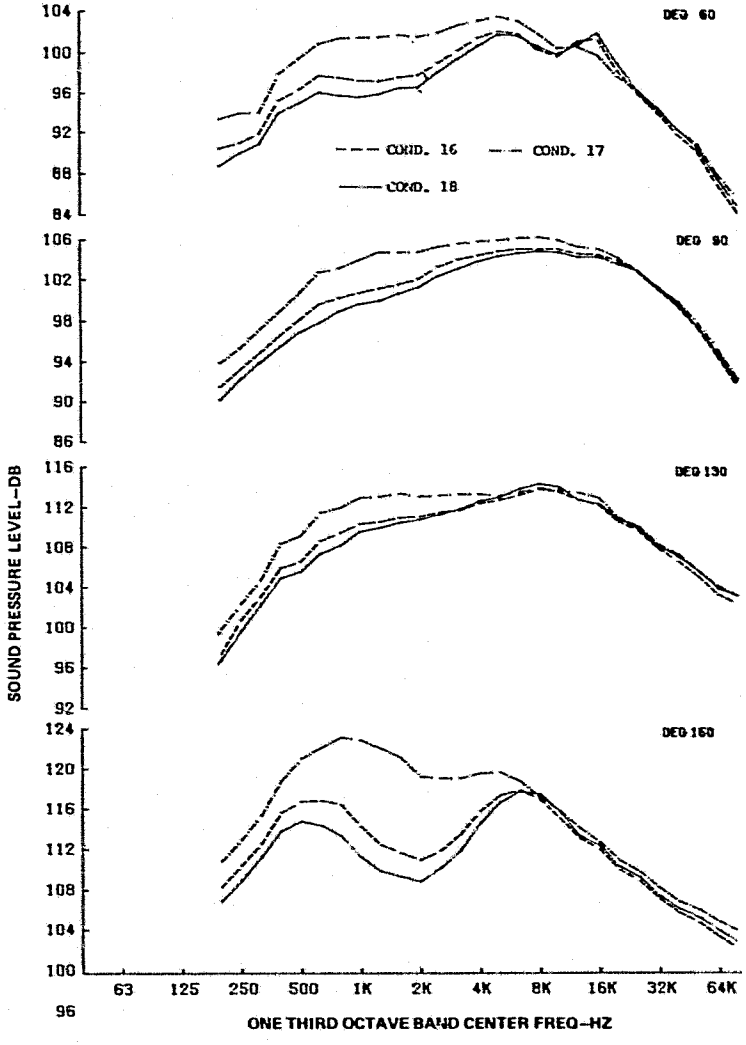

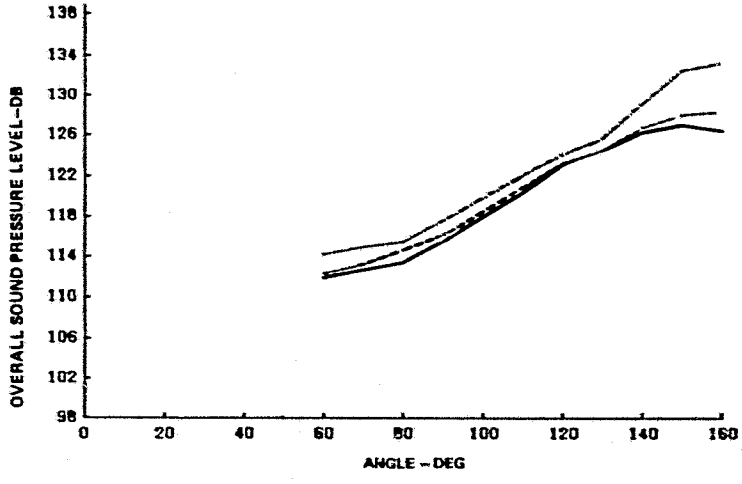

CONDITION 16

P_{tf}/P_a=2.40	P_{tp}/P_a=1.60
T_{tf} =1089 K	T_{tp} =589 K
V_f =702 m/sec	V_p =386 m/sec

CONDITION 17

P_{tf}/P_a=2.40	P_{tp}/P_a=2.00
T_{tf} =1089 K	T_{tp} =589 K
V_f =702 m/sec	V_p =467 m/sec

CONDITION 18

P_{tf}/P_a=2.40	P_{tp}/P_a=1.40
T_{tf} =1089 K	T_{tp} =589 K
V_f =702 m/sec	V_p =329 m/sec

r=4.57 m
MODEL SCALE
FAA DAY

Figure 4.5-6 Effect of Varying Primary Stream Pressure Ratio on Jet Noise

In this portion of the program, a total of four points was evaluated, both with and without the ejector, to isolate its effects on the acoustic characteristics of an IVP jet. Fan stream velocity ranged from 561 m/sec (1839 ft/sec) to 702 m/sec (2303 ft/sec), while fan stream temperatures varied from 700 K (1260°R) to 1089 K (1960°R). The primary stream conditions for three of the four points were held at a total temperature of 800 K (1440°R) and a velocity of 451 m/sec (1479 ft/sec). The fourth point, having a fan velocity of 587 m/sec (1927 ft/sec), had a primary stream total temperature of 850 K (1530°R) and a primary stream velocity of 571 m/sec (1873 ft/sec).

When initially tested, installation of the ejector resulted in the generation of large amplitude tones at 500 Hz with a harmonic of 1000 Hz, at every test condition. The mechanism precipitating this result was suspected to be a feedback loop between the fan nozzle lip and the inner surface of the ejector. Since this condition was postulated to be a consequence of a very symmetrical and aerodynamically smooth configuration not typical of a flight engine, the model was modified to eliminate the smoothness. This was accomplished by inserting 0.318 cm (0.125 in) diameter screws through the lip of the fan nozzle into the fan stream, as shown in Figure 4.5-7. These "tone suppressors" were equally spaced at eight locations around the nozzle lip, and the depth of intrusion in the fan stream was varied incrementally until at 0.127 cm (0.050 in) the tone was not observed in the spectra. On the basis of these results it was thought that the suppressors disrupted the fan stream flow sufficiently at the nozzle lip to eliminate the feedback loop between the nozzle and ejector.

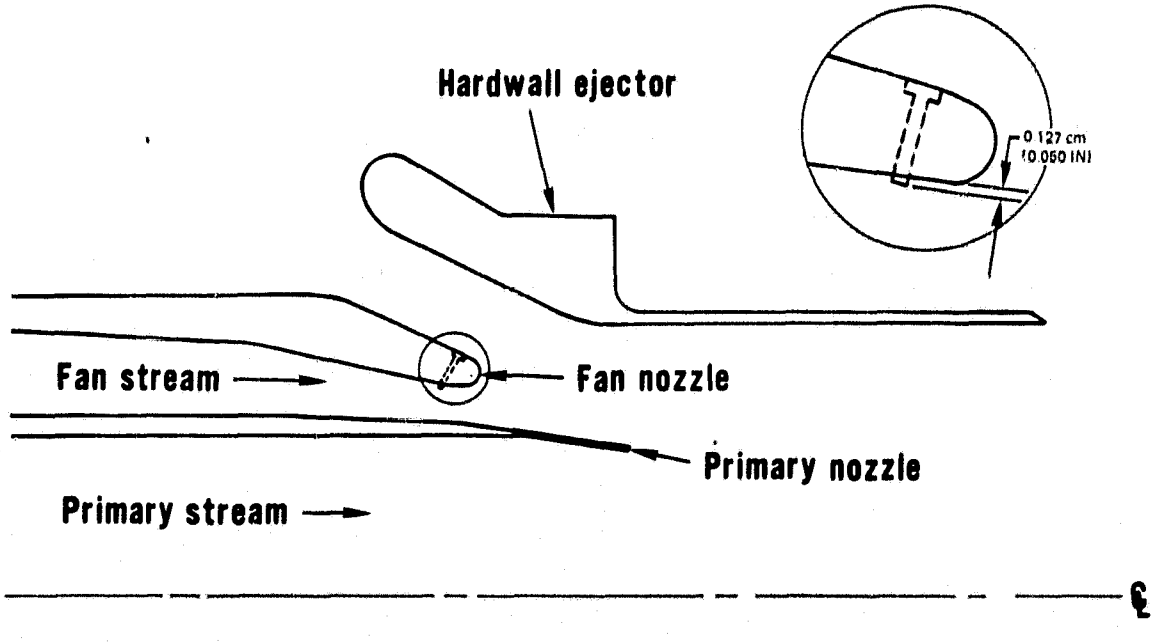

Figure 4.5-7 Tone Suppressors Installed on Fan Nozzle

Figure 4.5-8 shows the positive effects of the tone suppressors on model jet noise. Spectra for the same operating condition and at the same angle are shown both with and without tone suppression. As indicated, the tone was reduced greatly, although there appears to be some increase in high frequency broadband noise.

Comparisons of acoustic data with and without the ejector were accomplished by taking the high frequency portion ($f \geq 16$ kHz) of the ejector spectra from data without tone suppressors and the portion of the spectra at $f < 16$ kHz from the data with suppressors. This procedure provides the most accurate assessment of acoustic changes since high frequency broadband noise produced by the "tone suppressors" was not present in the spectra of nonejector jet noise.

Figure 4.5-9 shows spectra and directivity at a low fan velocity point. At these operating conditions, the ejector produced a small reduction in peak PNL. The directivity (Figure 4.5-9a) shows that a reduction in SPL was produced at the aft angles, while a slight increase was produced at mid angles. The spectra (Figures 4.5-9b through e) indicate that the ejector was effective in reducing high frequency noise at the aft angles.

In Figure 4.5-10, there is another point of comparison for evaluating the effects of an ejector. Overall sound pressure level directivity and spectra at 60, 90, 120 and 150 degrees are shown. This was the operating condition that the ejector was least effective in reducing jet noise. In this series of curves, Figure 4.5-10a illustrates that at all angles forward of 140 degrees from the upstream axis, the ejector increased SPL values, while at other angles the ejector had little effect. The spectra, Figures 4.5-10b through 10e, indicate that at low frequencies (i.e. $f < 4000$ Hz) the ejector also produced little effect. This is because the region of the jet generating low frequencies is downstream of the ejector and, therefore, not influenced by it. This result is typical and had been observed during a previous program (ref. 1). Also, the high frequency ($f > 20$ kHz) portions of the spectra were relatively unaffected by the ejector. However, this is not consistent with the data of reference 1. This lack of agreement with earlier findings provided the impetus to conduct a more comprehensive examination of the design of the ejector model.

Figure 4.5-11 presents a comparison of the ejector designed for this study with the configuration evaluated in the earlier NASA-sponsored coannular model test program, Reference 1. This figure clearly indicates two major configurational differences. The first is the ejector inlet. The inlet of the model used in this test is a bellmouth geometry, as stated previously, but the Reference 1 configuration was a high Mach number, flight-type inlet design.

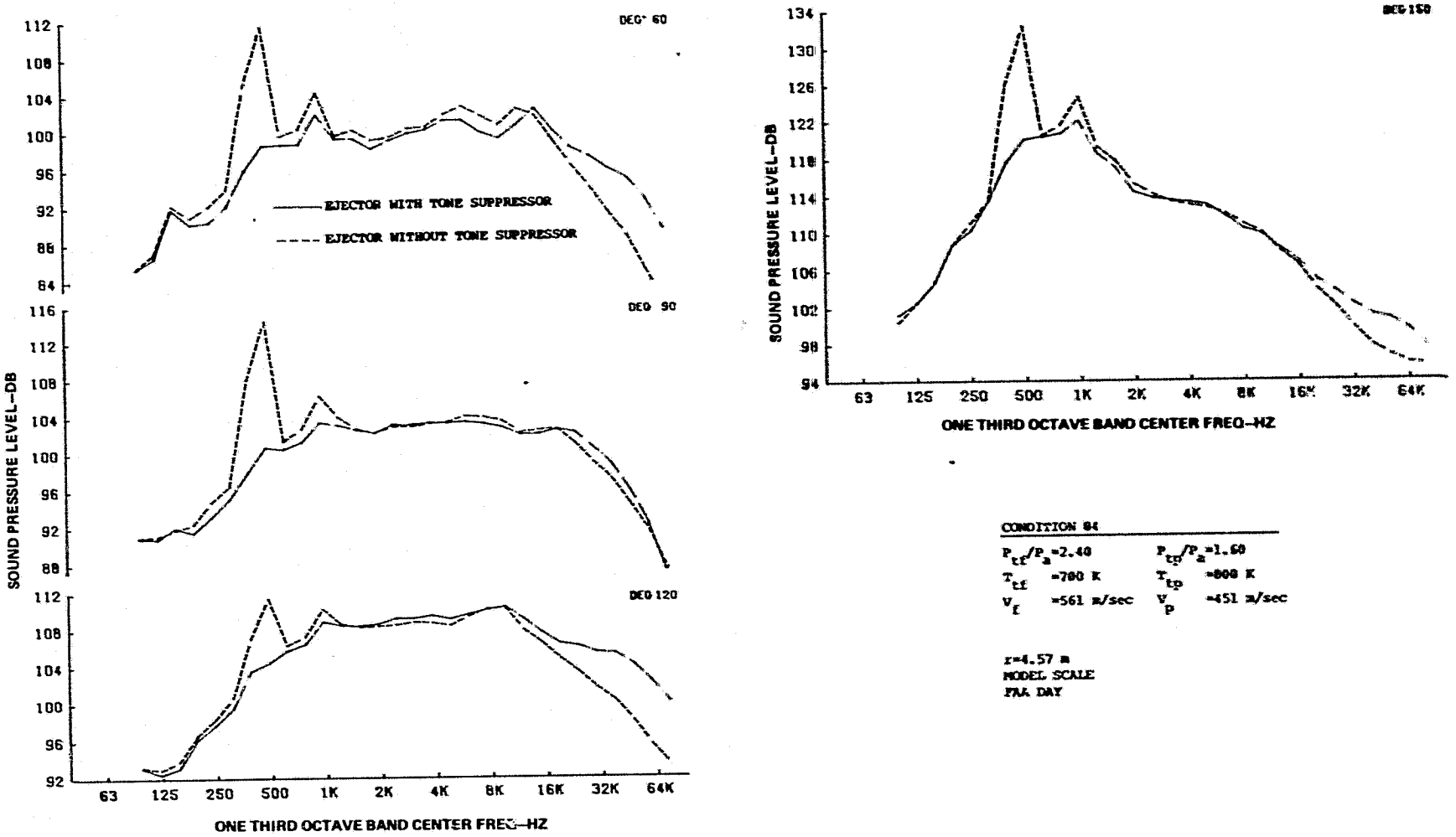

Figure 4.5-8 Effect of Tone Suppressors on Discrete Tones Associated with Ejector

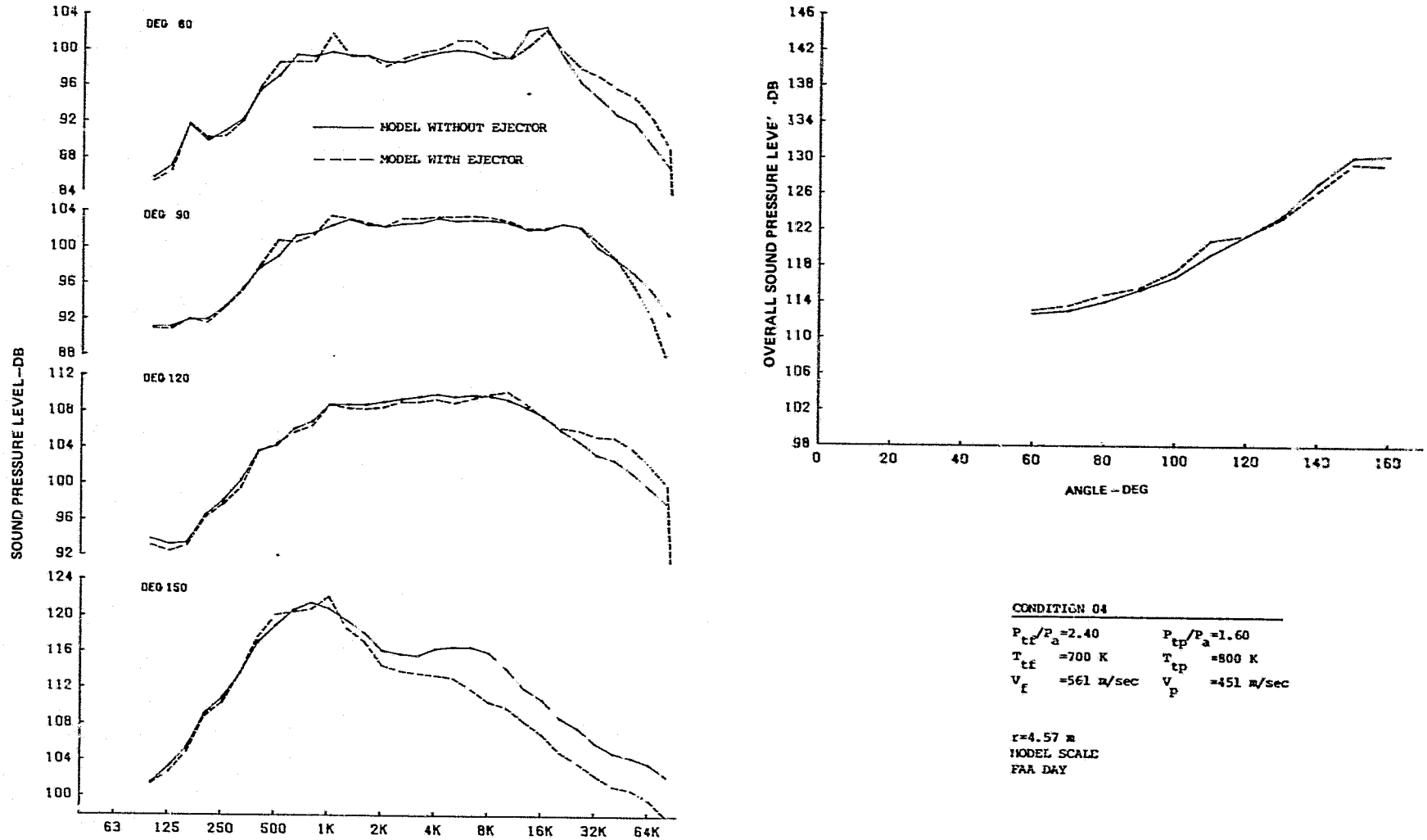

Figure 4.5-9 Effect of Ejector with Tone Suppressor on Jet Noise

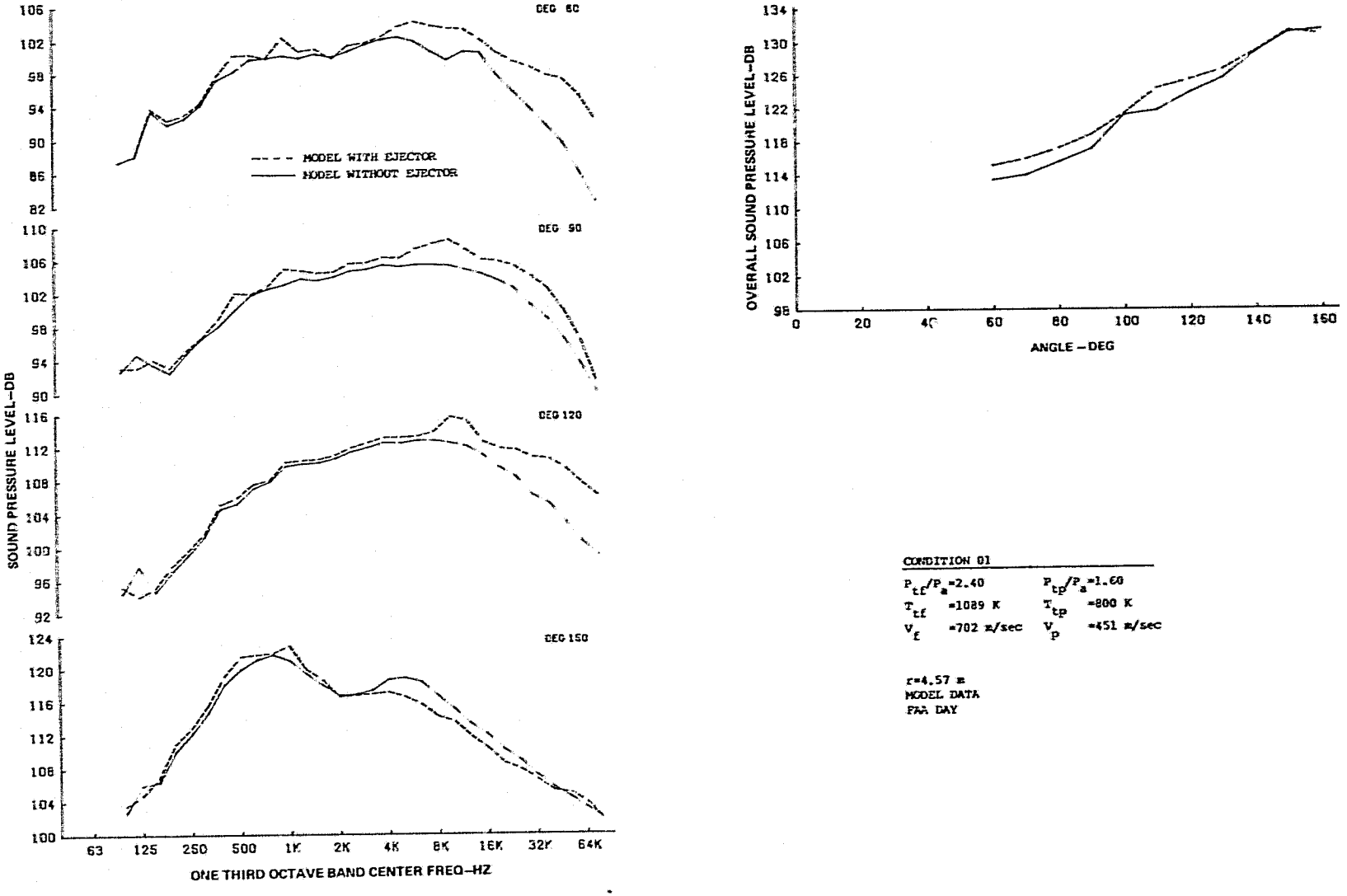

Figure 4.5-10 Effect of Ejector with Tone Suppressor on Jet Noise

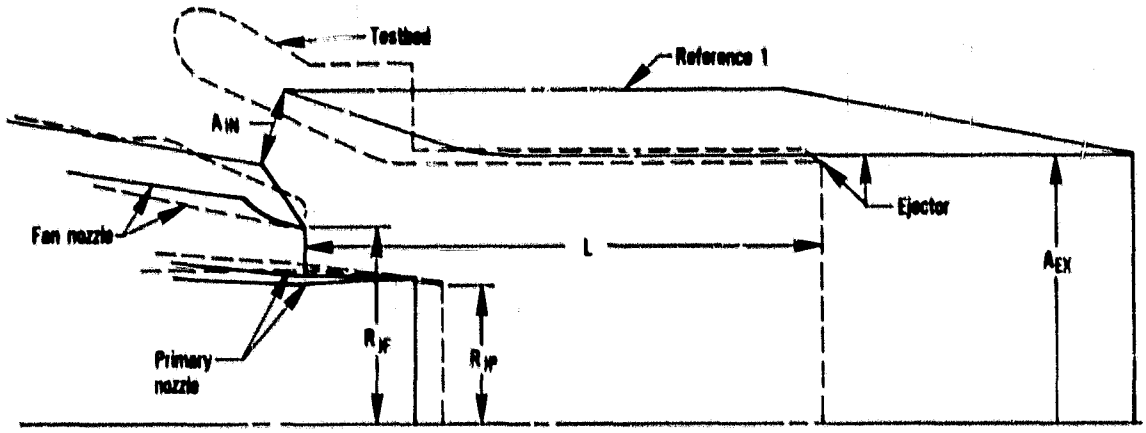

	Testbed	Reference 1
A_{IF}/A_{IP}	0.65	0.75
A_{EX}/A_{IF+P}	1.98	2.07
A_{IN}/A_{IF+P}	1.03	1.15
L/R_{IF}	2.63	4.22

Figure 4.5-11 Comparison of Testbed Model Ejector to Previously Tested Ejector Configuration

The second major difference is the ejector length. The earlier configuration is more than 50 percent longer than the current design relative to the equivalent diameters of the two models. In view of the test results, this would suggest that the region of the jet generating very high frequency noise was not contained within the short ejector, whereas it was contained by the longer ejector.

In an IVP jet, very high frequency noise is generated near the fan nozzle lip and the noise sources generating lower frequencies are distributed further downstream along the jet axis (ref. 9). Because of this spatial distribution of the noise source, a difference in length between the two ejectors could result in spectral differences since a long ejector would influence more of the high and intermediate noise generating sources.

In Figure 4.5-12, differences in one-third octave band SPL between test points both with and without the ejector are shown for the long and short ejector configurations. The fan pressure ratios for the long and short ejectors are 2.50 and 2.40 respectively. The fan stream temperatures are 1089 K (1960°R) for both configurations. Primary stream conditions are also quite similar, as seen from the figure. Data for several angles are presented. The data suggest several conclusions, as follows:

(1) Low frequency noise is relatively unaffected by either ejector.

(2) At the aft angles and high frequencies, a large difference existed between the acoustic effects of the two ejectors. The long ejector exhibits a much larger reduction in high frequency noise than the short ejector. This may indicate that high frequency noise sources are far enough upstream to be strongly influenced by the long ejector, but not far enough to be affected significantly by the short ejector. If this is the case for the short ejector, high frequency noise would radiate to the aft angles as if the ejector was not present. In contrast, high frequency noise with the long ejector would be influenced by it. A source inside an ejector shroud was modeled analytically (ref. 10), and results showed that noise would be redirected from the aft angles to mid angles. Figures 4.5-12b through 12f present data supporting this premise.

(3) The directivity of fan stream shock noise (fan pressure ratio 2.4) was altered by both ejectors and the effect was more pronounced than that of the ejectors on mixing noise. Figure 4.5-12 shows that at angles forward of 120 degrees shock noise levels in the 10 kHz and 12.5 kHz one-third octave bands are greater with the ejector installed. At 130 degrees, the long ejector reduced shock noise by a small amount, while no reduction was evident with the short ejector. At 140 degrees, both ejectors reduced fan shock noise; the longer configuration having a greater effect. Redirection of shock noise by both ejectors is similar to the redirection of high frequency mixing noise by the long ejector. That is, shock noise is being redirected from the aft angles to the side and forward ones by both ejectors. This could indicate that the source location of the fan shock noise is further upstream than the high frequency mixing noise. Therefore, shock noise is influenced by the short ejector, whereas mixing noise is not. In addition, the effect of both ejectors on shock noise is distinct from and greater than their effect on mixing noise. This might also result from the shock noise source being located further upstream than high frequency mixing noise sources.

In summary, the testbed ejector did not affect the acoustic characteristics of the model nozzle to the degree expected on the basis of data obtained from previous testing. The absence of peak PNL reductions by the later ejector was postulated to be due to the ejector design, specifically, the shorter length.

4.5.3 Testbed Comparison

One objective of this study was to obtain scale model IVP jet noise data for comparison with the testbed results when available. In this manner, the ability to scale the model IVP jet data may be evaluated. To provide this comparison, acoustic data were obtained at several points in the model test matrix in order to bracket the expected testbed demonstrator operating line. Data have been scaled to the testbed size and extrapolated to the measuring radius of the planned testbed aero/acoustic evaluation.

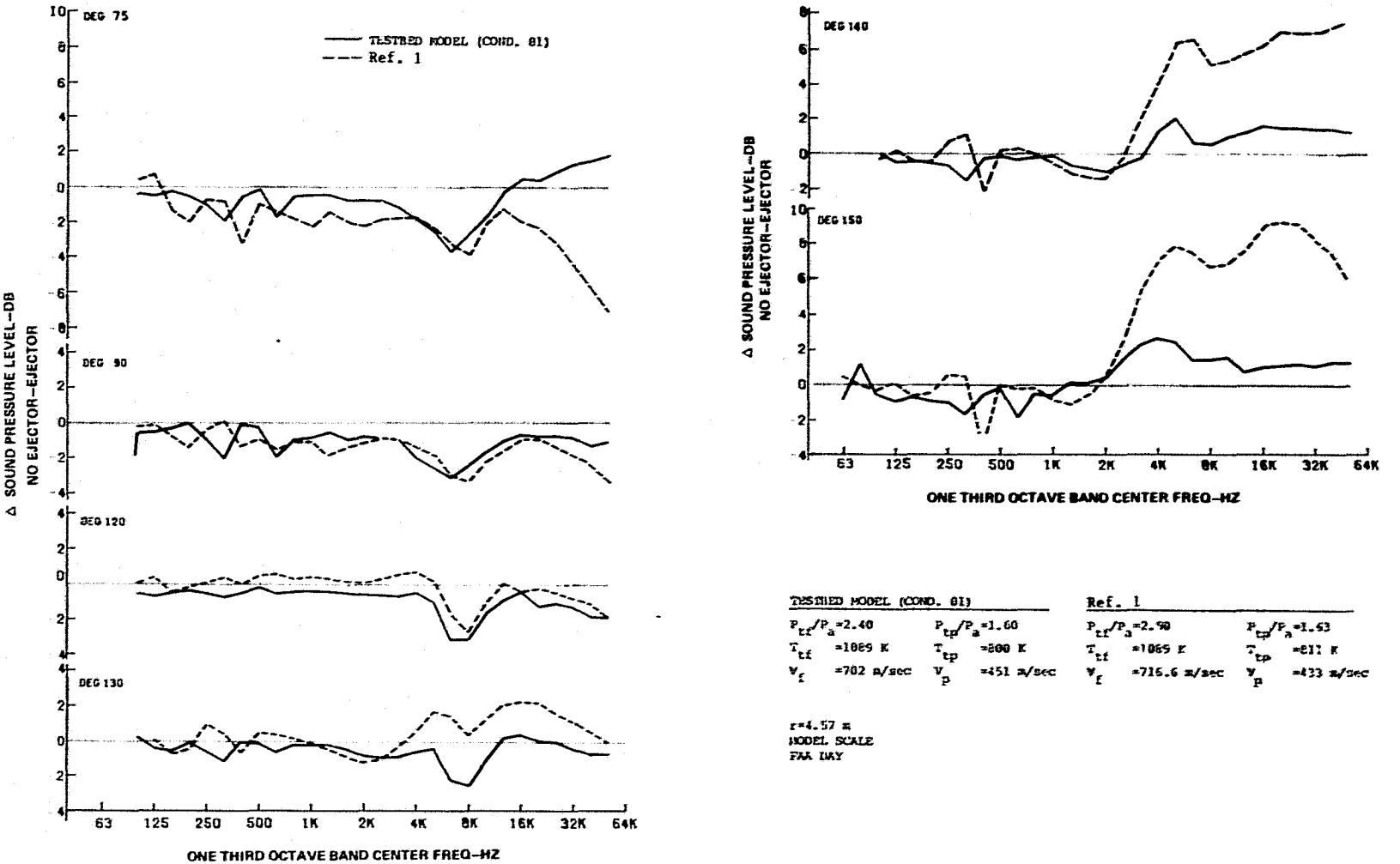

Figure 4.5-12 Comparison of Testbed Model Ejector Effect on Jet Noise to Effect of Previously Tested Ejector Configuration

Prior to the model test, a detailed knowledge of the operating characteristics of the testbed vehicle was not available. Preliminary cycle simulations were developed in order to provide a set of operating conditions for model-to-testbed noise comparisons. The model-to-testbed comparison was intended to correspond to a testbed fan stream temperature equal to the maximum flow temperature that the scale model jet noise facility could provide. At this temperature and the anticipated testbed fan nozzle pressure ratio, the ratio of the variable fan nozzle area to the primary nozzle area was expected to be approximately 0.65. Accordingly, the fixed model nozzle area ratio was designed to be 0.65. Subsequent to the completion of the model test program, preliminary testing and additional computer simulations of the testbed were obtained for a better definition of its operating characteristics. In Table 4.5-I it may be seen that the results of the simulation at one point and model test data provide a reasonably accurate comparison. These results indicate that a direct evaluation of scale model and testbed acoustic results should be possible. Note that the fan stream thermodynamic conditions are matched exactly. Primary stream pressure ratios and temperatures in the model and testbed vary by less than 2%, and the area ratios differ by less than 8%. The scale model and anticipated testbed operating conditions and geometries are sufficiently similar to achieve the objective of assessing the ability to scale IVP jet noise data. Because Table 4.5-I is based on a testbed simulation, the model was run at a variety of conditions to permit a good comparison if the actual engine points are not truly simulated. Additional data are provided in Appendix B for the anticipated engine match point and points near the anticipated engine match point. A complete presentation of test data is contained in the companion Comprehensive Data Report (ref. 5).

TABLE 4.5-I

OPERATING CONDITIONS AT POINT OF COMPARISON FOR MODEL AND TESTBED

	V_P (m/sec)	V_F (m/sec)	T_{TP} (K)	T_{TF} (K)	$P_{tp/Pa}$	$P_{tf/Pa}$	A_F/A_P	V_F/V_P
Model Data	450.8	702.0	800	1089	1.60	2.40	0.65	1.56
Testbed Simulation	441.4	702.0	801	1089	1.57	2.40	0.60	1.59

Microphones in the anechoic chamber are located on a 4.57 m (15 ft) polar arc. Therefore, the ratio of measuring distance to the model nozzle equivalent diameter is 36. To avoid complications arising from the spatial distribution of noise sources in the jet plume, it is desirable to make acoustic measurements at this same measuring distance/nozzle diameter ratio in the VCE Testbed Program. Accordingly, five ground plane microphones are planned on a 27.43 m (90 ft) polar arc centered on the testbed nozzle at the test facility.

The series of curves in Figures 4.5-13 and 4.5-14 show the model test point of the comparison scaled to testbed size and extrapolated to a 27.43 m radius. Spectra at 60, 90, 110, 120, 130, 140, and 150 degrees are shown in Figure 4.5-13. Overall sound pressure level directivity and perceived noise level directivity are shown in Figure 4.5-14.

4.5.4 Data Comparison With Prediction

Also shown in Figure 4.5-13 are results of jet noise predictions for the testbed without the ejector at the match point, using the procedure reported in Reference 3. Examination of the spectra shows that predictions are most accurate at 90 degrees, where agreement between predicted and model data is within 2dB. At this angle, both level and spectral shape are very close. Conversely, at 60 degrees, the prediction and data spectral shape differ, even though the overall level agrees. Aft of 90 degrees spectral shapes are well approximated by the prediction method and levels are generally within the data scatter of the prediction method given in Table 4.5-II.

PNL directivity, calculated from data scaled to testbed size and extrapolated to a 648.6 m. (2128 ft.) sideline is compared to predictions in Figure 4.5-14. Data and prediction agree to within 2 dB at all angles. The greatest difference between data and prediction occurs at 150° where the predicted levels were 2 dB higher than the measurements. Additional comparisons of predictions and data are contained in the CDR, Reference 5.

TABLE 4.5-II

STANDARD DEVIATIONS OF IVP JET NOISE PREDICTION CURVES
(from Ref. 3)

Low Frequency Jet Mixing Noise		High Frequency Jet Mixing Noise	
Θ	σ	Θ	σ
60	1.0	70	2.4
90	1.5	90	1.6
120	1.0	110	1.5
150	1.4	130	1.7
		150	1.7

Θ = Degrees from upstream jet axis

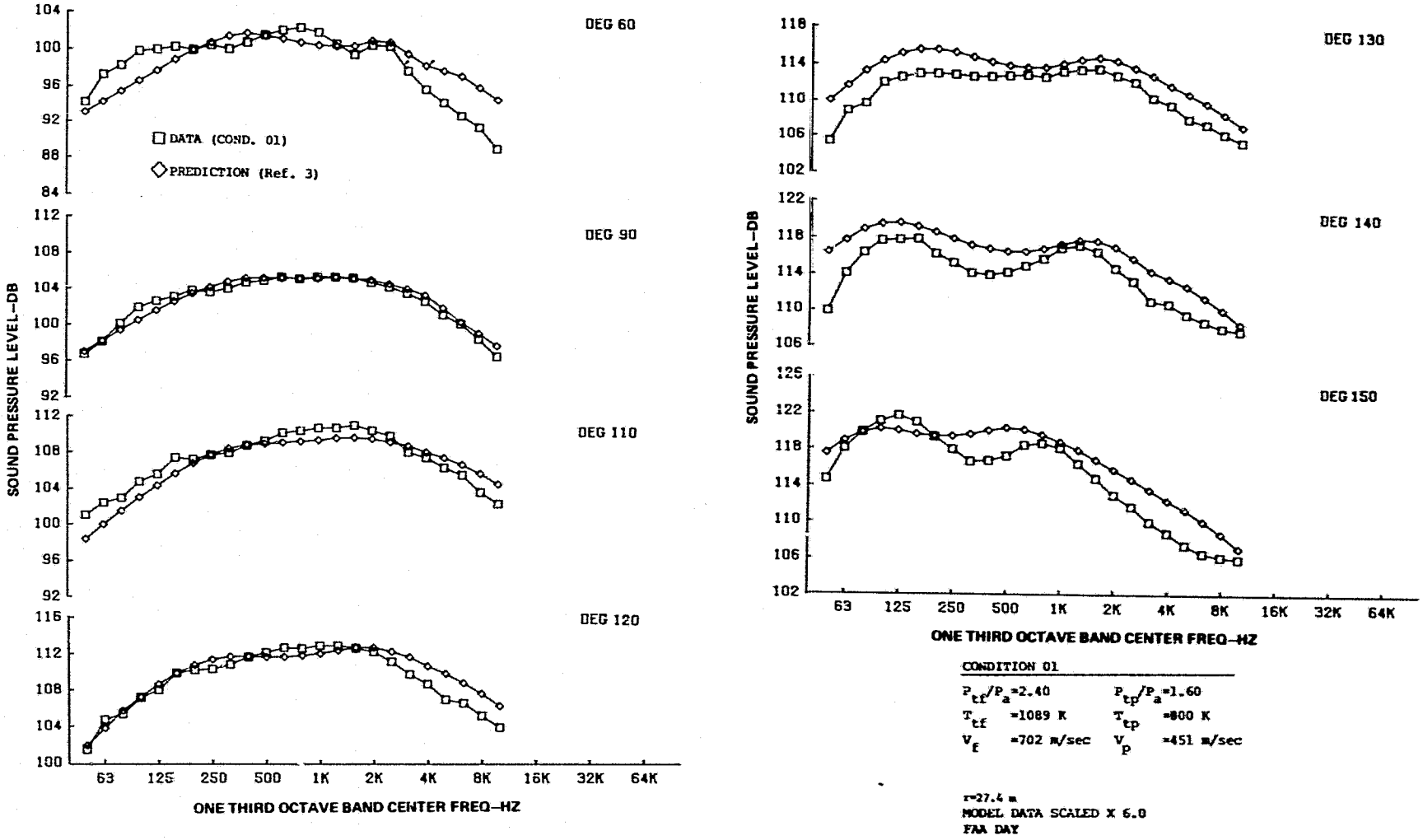

Figure 4.5-13 Comparison of Model Data to Predicted Jet Noise at Simulated Testbed Engine Operating Conditions - SPL

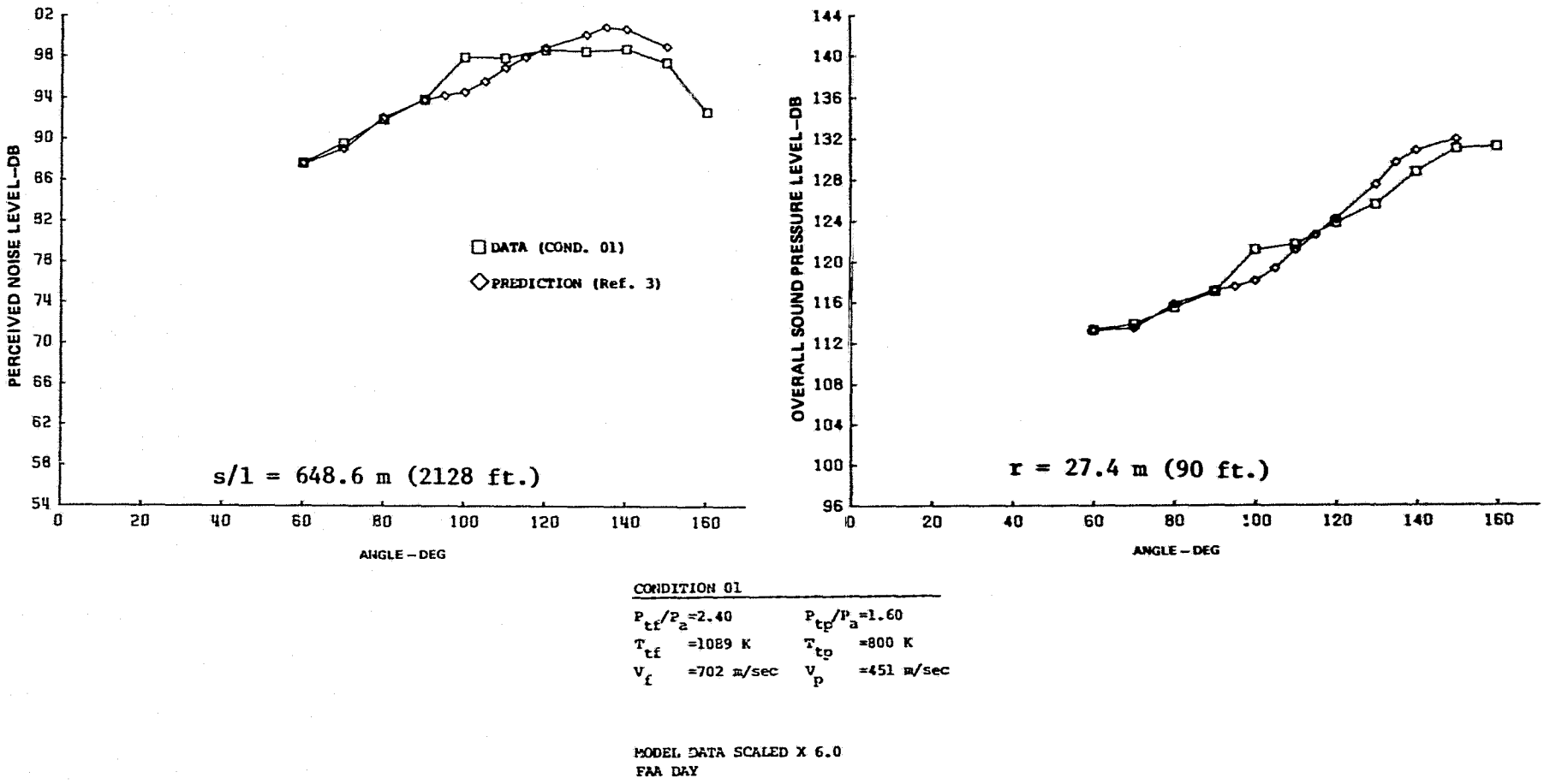

Figure 4.5-14 Comparison of Model Data to Predicted Jet Noise at Simulated Testbed Engine Operating Conditions – OASPL and PNL

SECTION 5.0

AERODYNAMIC TEST RESULTS AND DISCUSSION

5.1 INTRODUCTION

Aerodynamic data obtained from the performance test phase of the program are described in this section, along with the test procedure and test matrix. Included is a discussion of nozzle performance data and exhaust plume velocity profiles obtained from the plume survey data. Comparisons of predicted and measured nozzle thrust coefficients are also presented.

5.2 AERODYNAMIC TEST PROCEDURE AND TEST MATRIX

5.2.1 Exhaust Plume Surveys

Jet exhaust plume pressure and temperature surveys were conducted in X-206 stand in conjunction with the acoustic tests. Data were acquired with the traversing probe system described earlier in Section 4.2.2.

The procedure used in this series of tests consisted of making traverse measurements along one radial line from the nozzle centerline to the extremity of the jet plume at various axial positions downstream of the nozzle exit. A detailed description of the traverse procedure is contained in reference 3.

Two exhaust plume surveys were conducted: one without an ejector and one with the ejector installed on the model. Each survey was conducted at the nozzle operating conditions corresponding to point 1 of the acoustic test matrix shown in Table 4.2-I. Each set of plume survey data consisted of 45 individual measurements obtained by radial traverses at five axial locations. The number of data points and axial location, relative to the fan nozzle exit plane, for each traverse is shown in Table 5.2-I. The axial locations are defined both in terms of linear dimensions and equivalent nozzle diameters, L/D_{eq}, based on the fan and primary total jet area, 0.0127 m^2 (19.63 in^2).

5.2.2 Nozzle Performance Tests

Static nozzle aerodynamic performance tests were conducted in the Large Nozzle Thrust Facility at the United Technologies Research Center with an unheated air flow. Data were acquired over a range of fan nozzle pressure ratios for one primary operating condition and also over a range of primary nozzle pressure ratios for one fan operating condition. Nozzle thrust and discharge coefficients were determined from measurements of pressure, temperature, thrust and airflow data over a range of conditions. Tests were also conducted over a range of primary pressure ratio without fan flow. ASME reference nozzle tests were conducted before and after the nozzle performance tests to verify the operation of the Thrust Facility nozzle balance.

TABLE 5.2-I

PLUME SURVEY TRAVERSE MATRIX

	Nozzle Operating Conditions	
	Fan	Primary
P_t/P_a	2.4	1.6
T_tK (^oR)	1089 (1960)	800 (1440)
V_{id} m/sec (ft/sec)	702 (2303)	451 (1479)

Station Number	Axial Location Relative to Fan Nozzle Exit Plane			Number of Data Points
	m	(in)	L/D_{eq}	
1(1)	0.114	4.50	0.90	10
1A(2)	0.185	7.28	1.46	10
2	0.292	11.50	2.30	10
3	0.445	17.5	3.50	9
4	0.589	23.2	4.64	8
5	0.881	34.7	6.94	8

(1) without ejector
(2) with ejector

The test procedure employed during testing consisted of varying the fan or primary nozzle pressure ratio to cover the defined operating range, while maintaining the other stream at a fixed operating condition. At each test point, the output of the force balance and flow metering systems were recorded, along with charging station pressure and temperature values. Ambient conditions in the test facility were also recorded.

The aerodynamic performance test matrix is presented in Table 5.2-II. This matrix includes a total of 30 operating points and covers a range of operating conditions at constant fan and primary pressure ratio with and without the ejector. An ASME reference nozzle was also tested over a range of pressure ratios (1.8 to 4.2) prior to, and upon completion of the model performance test program.

5.3 AERODYNAMIC DATA REDUCTION

Aerodynamic data are discussed in two categories: (1) nozzle exhaust profiles, and (2) thrust and flow coefficients.

5.3.1 Traverse Data Reduction

Nozzle exit velocity and temperature distributions were determined from the traverse data obtained in the anechoic chamber. The probe simultaneously measured a static pressure (P_s), a total pressure (P_t) and a total temperature (T_t) at a given radial location. The velocity (V) and Mach Number (M) were then calculated by equations 5-1 and 5-2.

TABLE 5.2-II

AERODYNAMIC PERFORMANCE TEST MATRIX

Configuration	Fan Nozzle Pressure Ratio	Primary Pressure Ratio
ASME Nozzle		1.8 to 4.2
Testbed Model Without Ejector	1.8, 2.0, 2.2, 2.4, 2.8, 3.2	1.6
	2.4	1.4, 1.6, 1.8, 2.0, 2.2, 2.4
	Fan Flow Off	1.4, 1.7, 2.0, 2.4, 2.7, 3.2
With Ejector	1.8, 2.0, 2.2, 2.4, 2.8, 3.2	1.6
	2.4	1.4, 1.6, 1.8, 2.0, 2.2, 2.4

$$V = \sqrt{\left(\frac{\gamma g_c R T_t M^2}{1 + \frac{\gamma - 1}{2} M^2}\right)} \text{ m/sec (ft/sec)} \qquad \text{Eq. (5-1)}$$

where:

$$M = \sqrt{\frac{2}{\gamma - 1}\left((P_t/P_s)^{\frac{\gamma - 1}{\gamma}} - 1\right)} \qquad \text{Eq. (5-2)}$$

γ = Specific heat ratio
R = Gas constant = 88.51 Nm/kg ^{o}K (53.3 lbf ft/lbm ^{o}R)
g_c = Conversion factor = 1.0 kg m/N sec^2 (32.174 lbm ft/lbf sec^2)

5.3.2 Nozzle Thrust and Discharge Coefficient Data Reduction

Nozzle thrust and discharge coefficient were determined from the performance tests. By definition, the thrust coefficient (C_T) of a nozzle is the ratio of the actual nozzle thrust (as measured by the test stand balance) to the ideal thrust (which is based on the thermodynamic properties of the flow entering the nozzle).

$$C_T = \frac{F_t}{F_{id_t}}$$ where F_t = measured thrust — Eq. (5-3)

F_{id_t} = total ideal thrust

= F_{id} primary + F_{id} fan

The ideal thrust (F_{id}) of each stream is calculated by the equation:

$$F_{id} = P_t A^* \sqrt{\frac{2\gamma^2}{\gamma-1}\left(\frac{2}{\gamma+1}\right)^{\frac{\gamma+1}{\gamma-1}}\left(1-\left(\frac{P_a}{P_t}\right)^{\frac{\gamma-1}{\gamma}}\right)}$$ Eq. (5-4)

where:

P_t = area weighted average total pressure at instrumentation station (N/m^2 (psia))

P_a = ambient pressure (N/m^2 (psia))

$$A^* = \frac{W_t}{P_t}\sqrt{\frac{T_t R}{g_c \gamma}}\left(1+\frac{\gamma-1}{2}\right)^{\frac{\gamma+1}{2(\gamma-1)}}$$ Eq. (5-5)

A^* = Nozzle throat area

and W_t = Total measured air flow rate (kg/sec, (lbm/sec))

T_t = Total temperature at instrumentation station (K (^oK))

The nozzle discharge coefficient for each stream is calculated by the equation:

$$C_D = \frac{W_t}{W_{id}}$$ Eq. (5-6)

where:

$$W_{id} = \frac{P_t A}{\sqrt{T_t}} M \sqrt{\frac{\gamma g_c}{R}}\left(1+\frac{\gamma-1}{2}M^2\right)^{-\frac{(\gamma+1)}{2(\gamma-1)}}$$ Eq. (5-7)

(kg/sec (lbm/sec))

A = Nozzle exit area in each stream (m^2 (ft^2))

M = 1.0 if $P_t/P_a > 1.8929$

$$M = \sqrt{\frac{2}{\gamma-1}\left((P_t/P_a)^{\frac{\gamma-1}{\gamma}} - 1\right)}$$ (Eq. (5-8)

if $P_t/P_a \leq 1.8929$

5.4 DISCUSSION OF AERODYNAMIC TEST RESULTS

A discussion of the aerodynamic test results is presented in this section. The effect of the ejector on exhaust plume velocity profile is discussed in Section 5.4.1. Tests verifying the nozzle balance operation are discussed in Section 5.4.2. Nozzle performance, thrust and flow coefficients, both with and without the ejector, are described in Sections 5.4.3 and 5.4.4, respectively. A comparison of predicted and measured thrust coefficients without the ejector is contained in Section 5.4.5.

5.4.1 Nozzle Exhaust Velocity Profiles

Radial exhaust velocity profiles from plume traverse measurements were normalized relative to the fan stream ideal velocity (V_{id_f}) 700 m/sec (2300 ft/sec) and fan nozzle outer radius (R_{of}) 0.0683 m (2.69 in). A comparison of normalized profiles with and without the ejector indicates that the ejector had little effect on the decay of the inverted velocity exhaust plume, as shown in Figure 5.4-1. Both in the initial premixed region and merged region of the plume (stations 2 and 5, respectively), the peak velocity measured with or without the ejector is similar. Although the shape of the profiles are similar, presence of the ejector tends to displace the fan stream flow inward towards the centerline. This effect is more pronounced in the premixed regions of the plume.

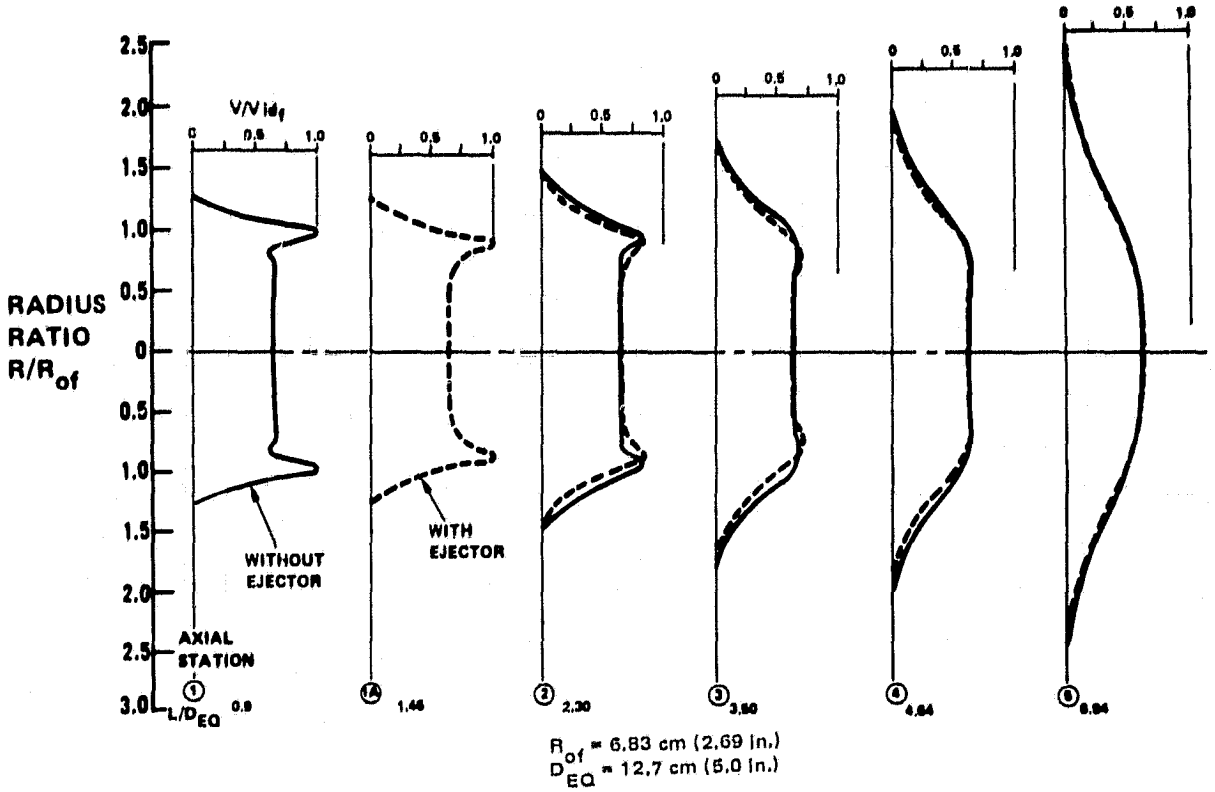

Figure 5.4-1 Comparison of Exhaust Plume Velocity Profiles With and Without Ejector

In close proximity to the nozzle exit plane, 0.9 L/D_{eq}, the flow deficit due to boundary layer growth on the flow splitter is apparent in the mixing region. However, the deficit dissipates rapidly, as evidenced by downstream profiles.

5.4.2 Verification of Nozzle Balance Operation

To ensure validity of performance results, a 0.102 m (4.0 in) ASME reference nozzle was tested before and after testing of the testbed model to verify balance operation. These verification tests were conducted over a range of pressure ratios similar to the model test program. The ASME reference nozzle is schematically illustrated in Figure 5.4-2.

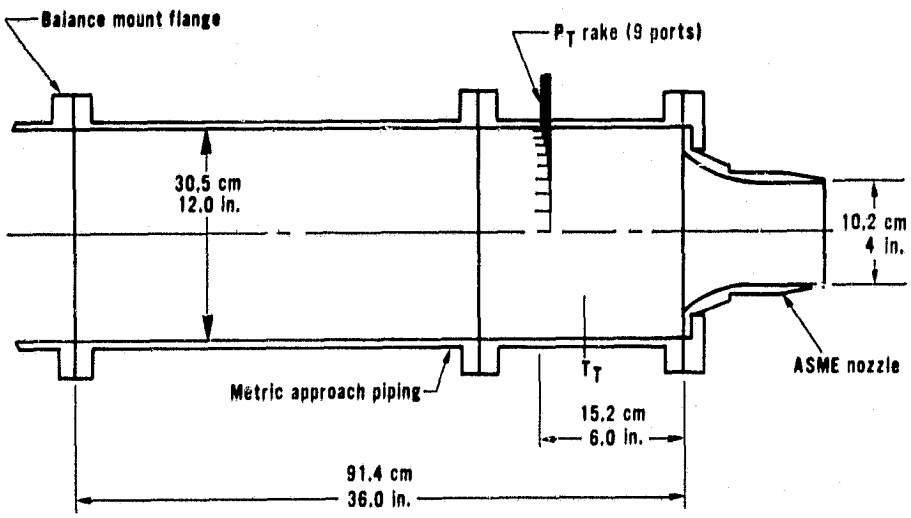

Figure 5.4-2 ASME Reference Nozzle

Pretest and post test thrust coefficients and discharge coefficients were compared to levels previously established for the Large Nozzle Thrust Facility and also levels obtained at Fluidyne. As illustrated in Figure 5.4-3, the comparison shows that repeatability of the nozzle balance is very good. The level of thrust coefficient data compares well with the established balance performance. The level of discharge coefficient measured was 0.1 to 0.2 percent higher than previous experience with the Large Nozzle Thrust Facility and tended to be more in agreement with Fluidyne's findings. However, this slight difference did not affect the level or repeatability of measured thrust coefficient data. Therefore, it is not believed to influence the thrust coefficient results of this program.

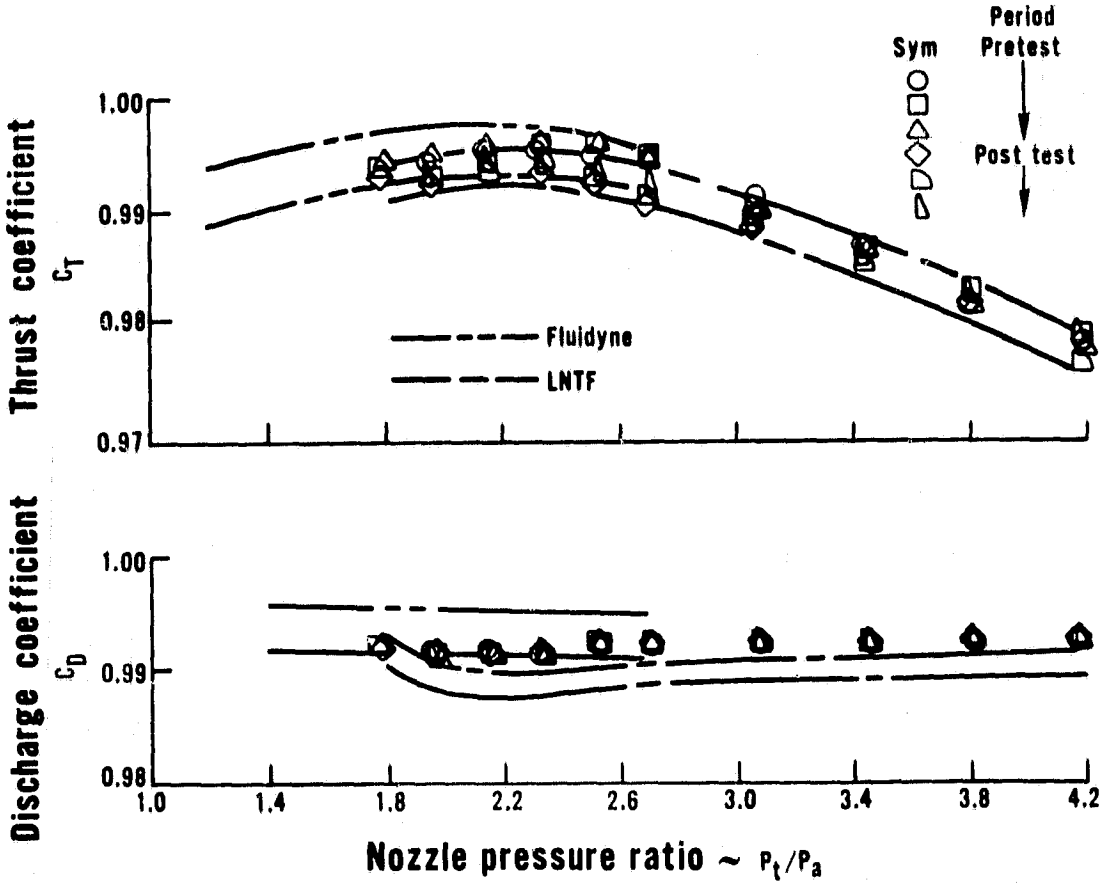

Figure 5.4-3 Comparison of Pretest and Post Test ASME Nozzle Results with Established Performance Levels

5.4.3 Nozzle Thrust Performance

Thrust coefficient data are presented in two parts. First, results obtained without the ejector are discussed, and then the effects of the ejector on thrust coefficient are described.

Data trends for nozzle operating conditions at constant primary pressure ratio of 1.6 and varying fan pressure ratio from 1.8 to 3.2 without the ejector are presented in Figure 5.4-4. As shown, the thrust coefficient increases with increasing fan pressure ratio to a maximum value of 0.983 at a fan pressure ratio of 2.8, then decreases to a level of 0.978 at a fan pressure ratio of 3.2. The reduced level of thrust coefficient of 0.974 at the lower fan nozzle pressure ratios (1.8 to 2.2) is characteristic of a convergent-divergent (C-D) nozzle overexpansion thrust loss, which occurs when operating at less than design pressure ratio, where the flow has separated from the divergent wall. Although the model is configured with a convergent primary nozzle, the expansion area ratio (A19/A18) of the coannular plug-type fan nozzle is 1.4 with a design pressure ratio of 5.6.

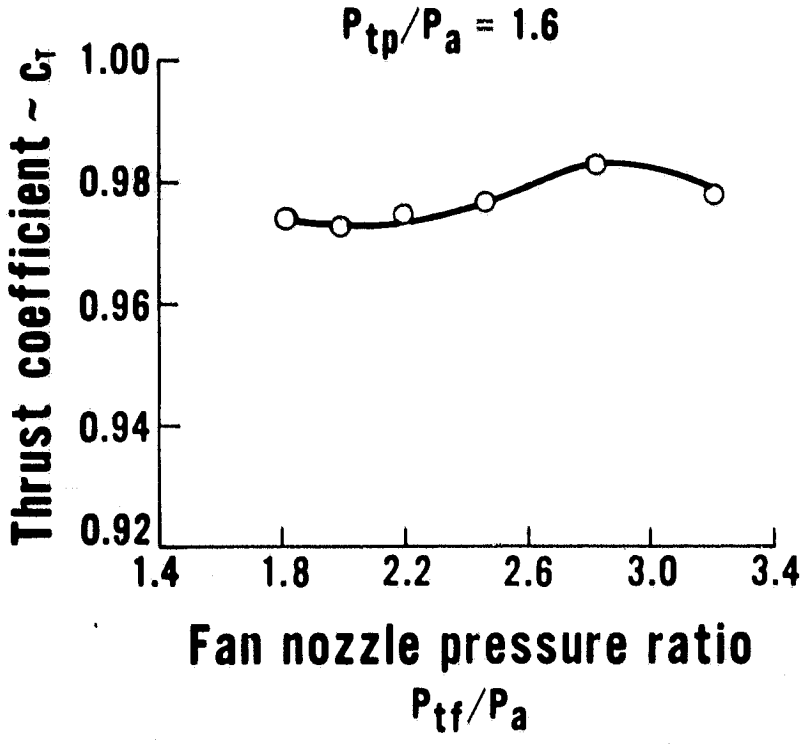

Figure 5.4-4 Thrust Coefficient at Constant Primary Nozzle Operating Conditions Without the Ejector

A feature of a plug-type nozzle is that exhaust flow aerodynamically adjusts to minimize overexpansion losses when operating below design in the overexpanded flow regime. Alignment of the nozzle throat flow with the downstream plug surface is critical to minimize overexpansion losses. The testbed model is configured with a 3-degree inner body in the region of the fan nozzle throat, followed by an 8-degree downstream surface that could result in an overexpansion loss. Experimental determination of the static pressure distributions on the afterbody was not possible because of a lack of instrumentation.

A curve of thrust coefficient versus primary nozzle pressure ratio from 1.4 to 2.4 at constant fan flow conditions is shown in Figure 5.4-5. Thrust coefficient is relatively constant, approximately 0.976, to a choking nozzle pressure ratio of 1.89. Then it subsides gradually to a level of 0.972 at a nozzle pressure ratio of 2.4. The trend is typical of a convergent nozzle with peak performance occurring near critical operating conditions and then falling off in the underexpanded flow regime at higher pressure ratios.

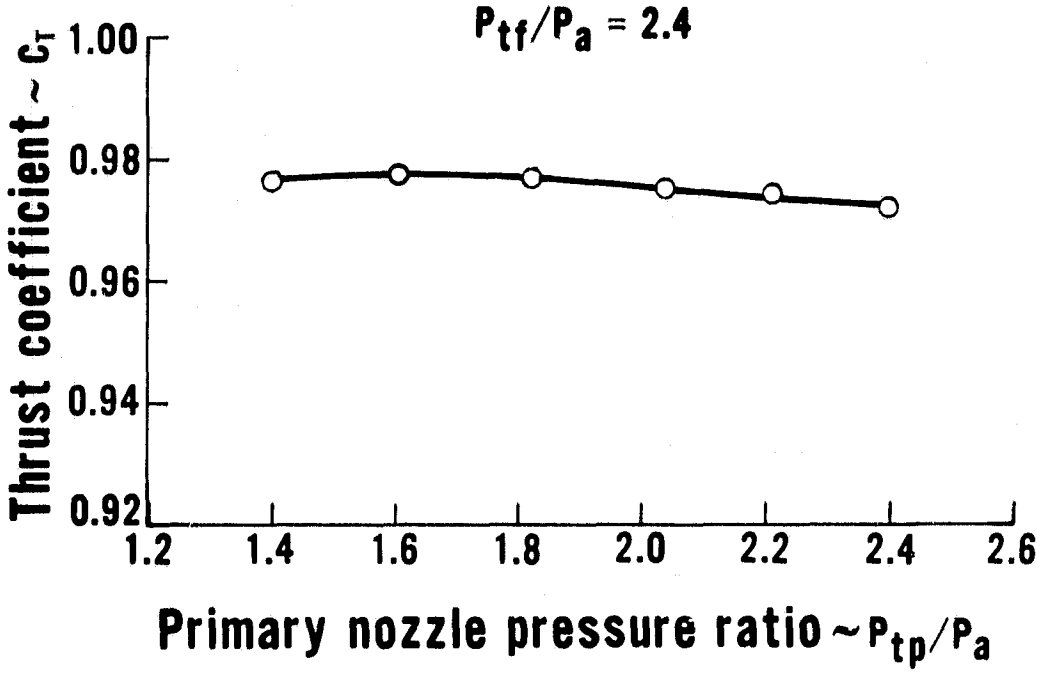

Figure 5.4-5 Thrust Coefficient at Constant Fan Nozzle Operating Conditions Without the Ejector

A comparison of results with and without the ejector shows that presence of the ejector increases nozzle performance for both constant primary and constant fan nozzle operating conditions, as illustrated in Figures 5.4-6 and 5.4-7. As shown for both sets of conditions, the ejector does not change the basic data trends, but increases the thrust coefficient level from 0.1 percent at low flow conditions to 0.4 percent at higher nozzle pressure ratios. The incremental increase in thrust coefficient is attributed to thrust augmentation of the ejector brought about by jet flow entrainment of ambient air induced through the inlet and the associated momentum increase of flow exiting the ejector. Thrust augmentation tended to increase with increasing nozzle pressure ratio over the ranges tested. Higher levels of thrust augmentation can be achieved with ejectors of sufficient length to obtain 100 percent mixing but are not practical for flight configurations. In addition, the ejector thrust augmentation observed at static conditions decays readily as flight speed increases due to increasing inlet ram drag. Overall, results with the ejector show that the testbed configuration should produce a 0.980 thrust coefficient at design operating conditions.

These model test results define a range of thrust coefficients with and without the ejector applicable to the full scale testbed nozzle system when the engine is operated under a combination of conditions that produce a 0.65 fan-to-primary area ratio and similar nozzle pressure ratios.

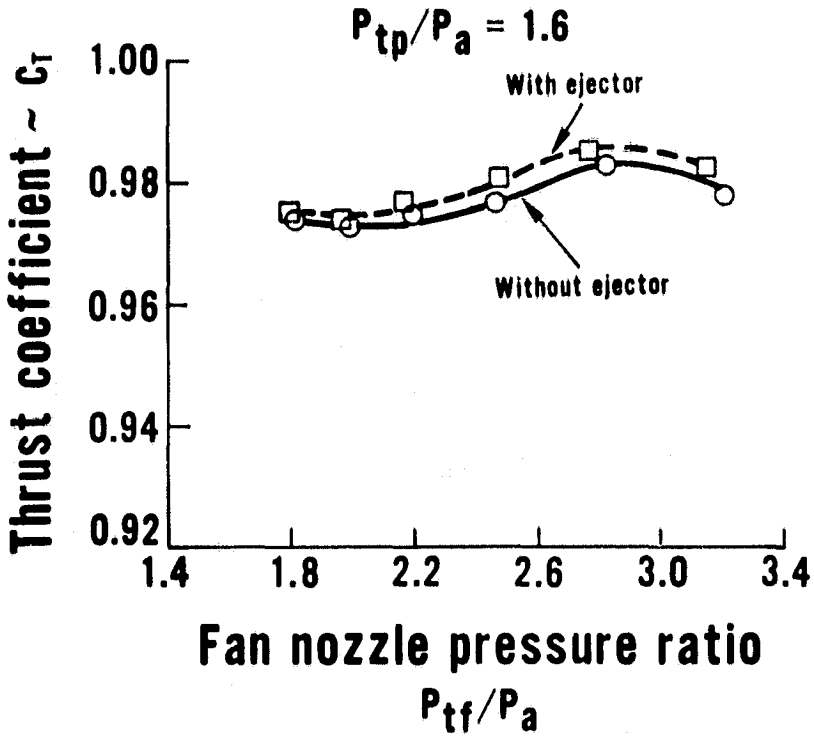

Figure 5.4-6 Effect of Ejector on Nozzle Thrust Coefficient at Constant Primary Operating Conditions

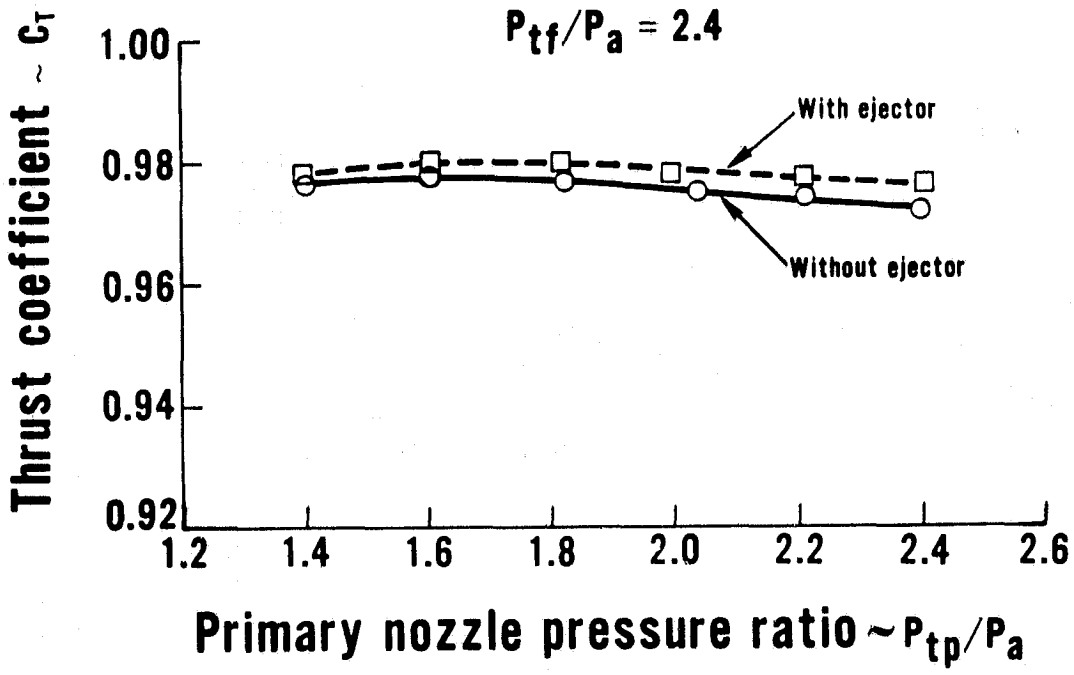

Figure 5.4-7 Effect of Ejector on Nozzle Thrust Coefficient at Constant Fan Operating Conditions

5.4.4 Nozzle Discharge Coefficients

Measured fan and primary nozzle discharge coefficients, both with and without the ejector, are discussed in this section. Fan and primary discharge coefficients without the ejector are presented in Sections 5.4.4.1 and 5.4.4.2, respectively. In Section 5.4.4.3, effects of the ejector on fan and primary discharge coefficients are discussed.

5.4.4.1 Fan Nozzle Discharge Coefficients

Fan nozzle discharge coefficients for test conditions of varying fan flow and constant primary flow (Figure 5.4-8) show that the fan discharge coefficient is constant at a level of 0.979 over the range tested, fan pressure ratio of 1.8 to 3.2. In the near sonic to supersonic flow regime, the fan discharge coefficient trend is characteristic of an annular plug type nozzle with shallow convergence to the nozzle throat and no abrupt changes in flowpath contour in the throat region.

Also shown in Figure 5.4-8 is the band of flow coefficients at conditions of varying primary flow, constant fan flow and fan pressure ratio of 2.4. The band indicates that the data are essentially consistent and compare favorably with the level of fan discharge coefficient at variable fan operating conditions. As expected, variations in primary flow (primary nozzle pressure ratios of 1.4 to 2.4) had no effect on the fan discharge coefficient. A constant level of discharge coefficient is desirable to maintain a constant engine flow match. However, the exhaust system in the testbed demonstrator has a variable-geometry fan nozzle that could accommodate variations in fan discharge coefficient, if required.

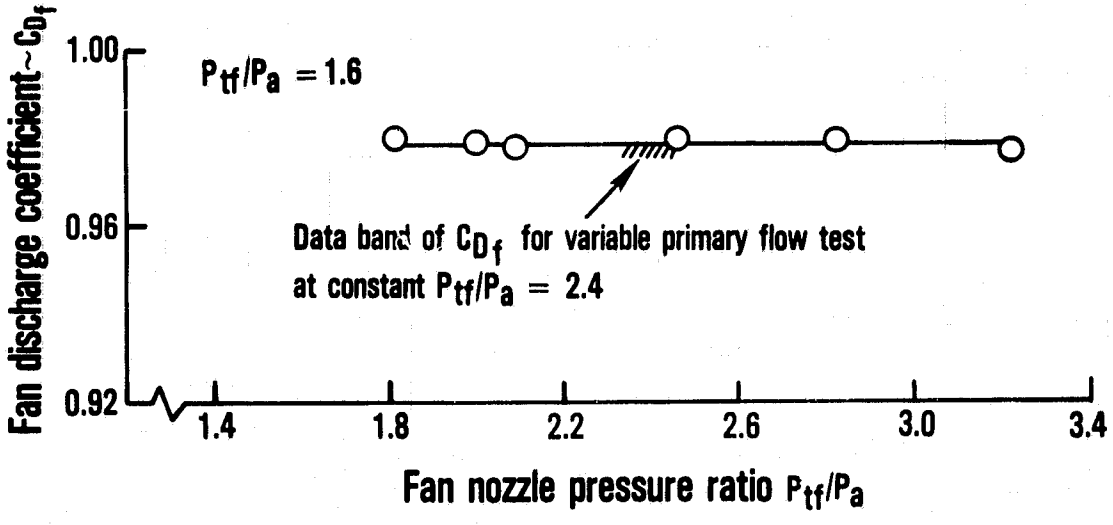

Figure 5.4-8 Fan Discharge Coefficient at Constant Primary Operating Conditions

5.4.4.2 Primary Nozzle Discharge Coefficients

A comparison of primary nozzle discharge coefficient, measured both with and without the fan stream at a pressure ratio of 1.6, is presented in Figure 5.4-9. The primary nozzle discharge coefficient did not exhibit the same characteristics observed for the fan stream. The trend of primary nozzle discharge coefficient for test conditions of varying fan pressure ratio and a constant primary nozzle pressure ratio of 1.6 indicates the fan stream has a restrictive effect on the primary flow, with primary nozzle discharge coefficient decreasing with increasing fan pressure ratio. The data show that in the dual flow case the primary nozzle discharge coefficient dropped from 4 to 11 percent relative to the level observed without fan flow (0.96).

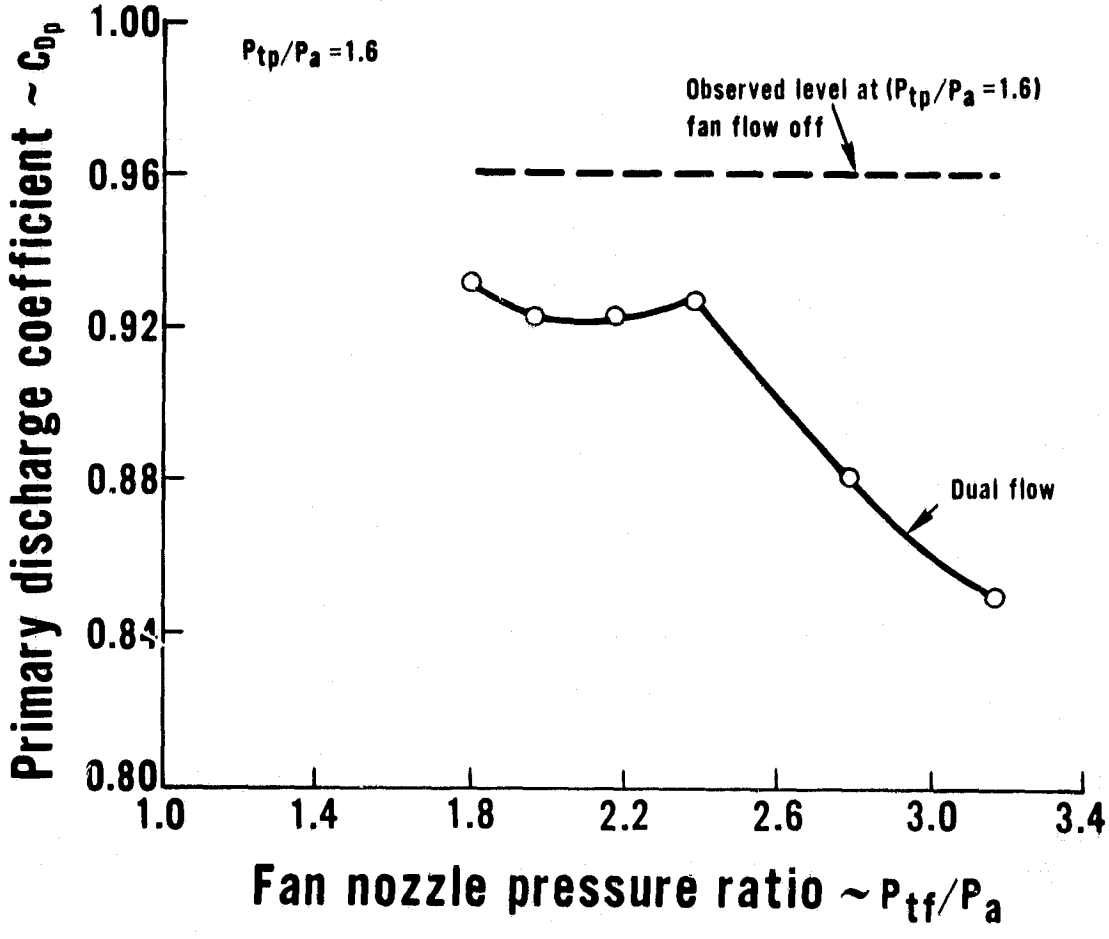

Figure 5.4-9 Effect of Fan Flow on Primary Nozzle Discharge Coefficient at Constant Primary Operating Conditions

The restrictive effect of the fan stream impinging on the primary flow is more pronounced at subcritical ($P_{tp}/P_a < 1.89$) primary nozzle operating conditions, where downstream pressure disturbances are communicated upstream of the nozzle throat. This trend is apparent from a comparison of primary nozzle discharge coefficient, measured with and without fan flow for varying primary pressure ratio from 1.4 to 2.4 and constant fan pressure ratio of 2.4 in the dual flow case (Figure 5.4-10).

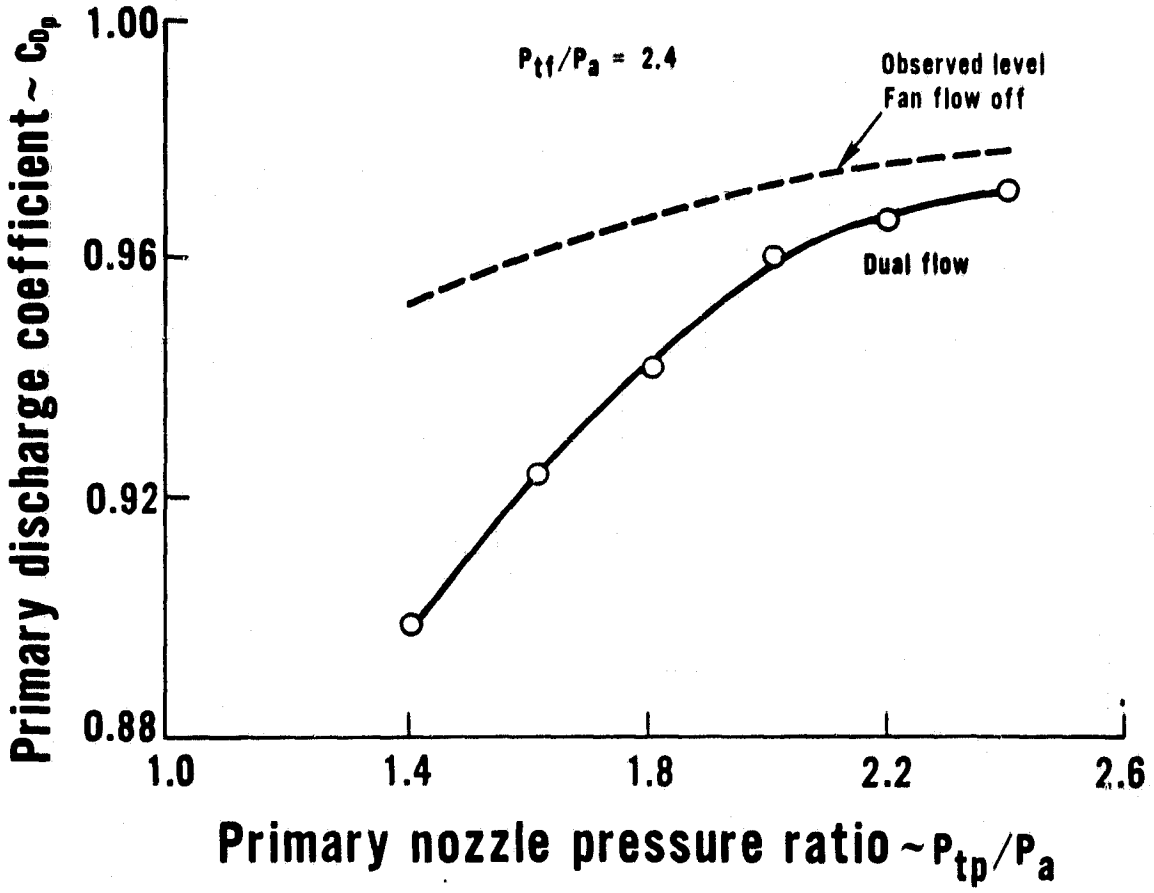

Figure 5.4-10 Effect of Fan Flow on Primary Discharge Coefficient at Constant Fan Operating Conditions

The data in Figure 5.4-10 also indicate that as the primary nozzle pressure ratio increases above 1.89, the primary discharge coefficient with dual flow approaches the primary nozzle discharge coefficient level observed without fan flow. Similar restrictive effects of the fan stream on primary flow were observed during the testing of Reference 3. During those tests it was observed that primary discharge coefficient trends were a function of nozzle geometry as well as operating conditions.

Data trends of the primary nozzle discharge coefficient suggest that the core flow of the testbed, operating with fixed area primary nozzle, will be influenced by nozzle operating conditions. However, conical primary nozzles in the exhaust system are designed to be trimmed to the required flow area which alleviates the restrictive effect of the fan stream on the primary flow. Also, the data in Figure 5.4-9 show that at testbed nozzle operating conditions up to the design limit (fan pressure ratio of 2.4) the level of primary nozzle discharge coefficient is relatively constant, varying from 0.92 to 0.93. At higher fan pressure ratios, the implication of these data trends is of significance to the VCE propulsion systems currently being considered for AST applications. At takeoff operating conditions, the fan nozzle pressure ratio for these cycles may range from 2.4 to 3.2 at core nozzle pressure ratios of 1.7 to 1.85. At these conditions, the restriction of core flow will become more pronounced and will influence the nozzle design requirements.

5.4.4.3 Ejector Effects on Discharge Coeffieients

Comparison of fan and primary discharge coefficients measured with and without the ejector showed that the ejector had a negligible effect on flow characteristics of either stream.

A comparison of fan discharge coefficient for conditions of varying fan pressure ratio and constant primary nozzle pressure ratio indicates that the ejector decreased fan discharge coefficient 0.2 percent over the range tested, as illustrated in Figure 5.4-11. A comparison of individual data points shows that this is within the accuracy of the flow measuring system, but the trend of data with the ejector, as shown, falls slightly below the level of that measured without the ejector.

Comparisons of primary discharge coefficients with and without the ejector for dual flow nozzle condition of constant primary pressure ratio and constant fan pressure ratio are shown in Figures 5.4-12 and 5.4-13, respectively. These comparisons also indicate that the ejector had a negligible effect on the primary nozzle discharge coefficient.

5.4.5 Data Comparison With Thrust Performance Prediction

Comparisons of measured nozzle thrust coefficients to performance predicted by the coannular nozzle aerodynamic prediction procedure (ref. 3) are presented in this section. This procedure is an empirical technique based on a combination of analytical estimates of internal and external viscous losses and empirical shock loss correlations as a function of nozzle geometry. The procedure does not consider the presence of an ejector and the shock loss correlations are limited to a primary nozzle pressure ratios of 1.6 and 2.0.

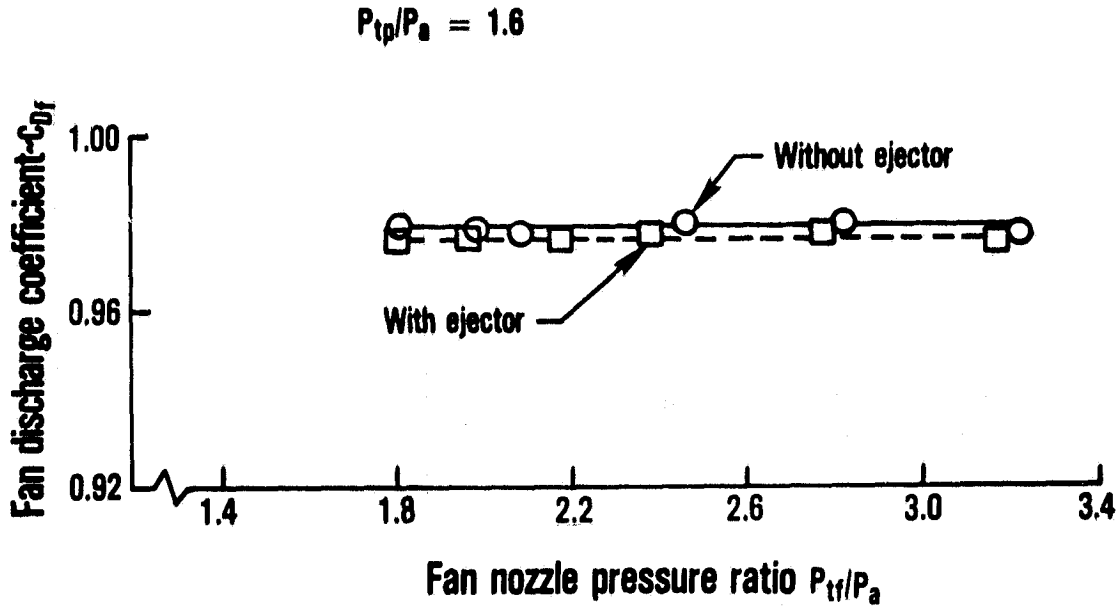

Figure 5.4-11 Effect of Ejector on Fan Discharge Coefficient at Constant Primary Operating Conditions

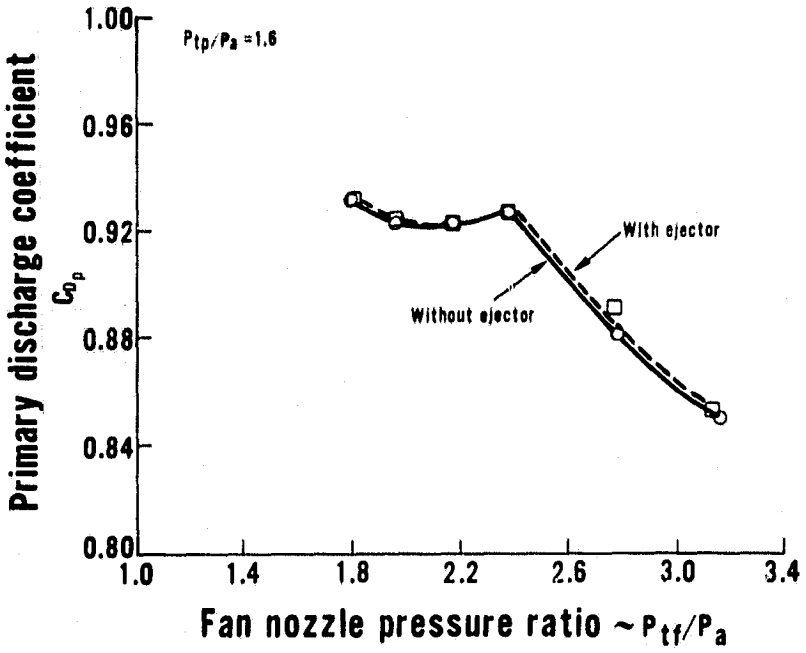

Figure 5.4-12 Effect of Ejector on Primary Nozzle Discharge Coefficient at Constant Primary Operating Conditions

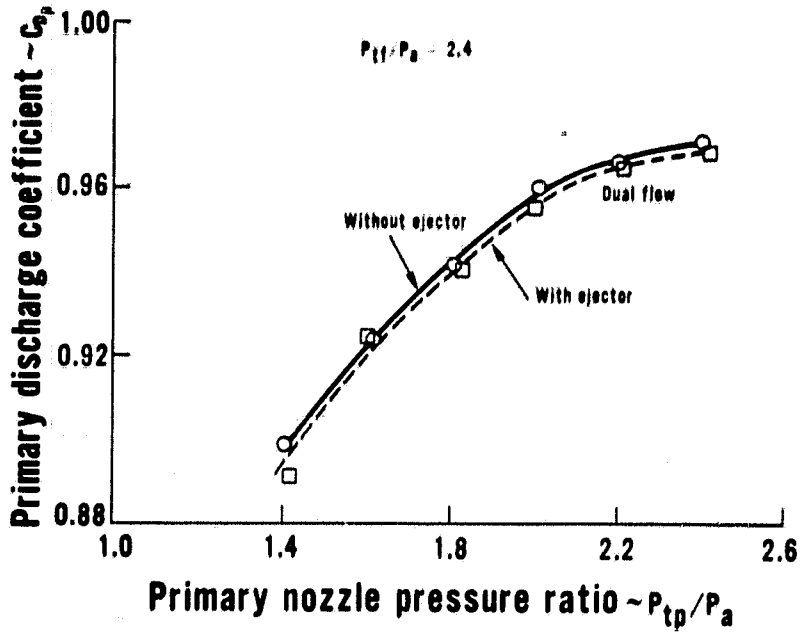

Figure 5.4-13 Effect of Ejector on Primary Discharge Coefficient at Constant Fan Operating Conditions

Predictions were made for fan nozzle pressure ratios of 1.8, 2.4, 2.8, and 3.2 at a primary pressure ratio of 1.6. Also, predictions were made at a fan nozzle pressure ratio of 2.4 and a primary nozzle pressure ratio of 2.0. A comparison of predictions shown in Figure 5.4-14 with measured performance at a primary nozzle pressure ratio of 1.6 shows agreement within 0.2 percent at the lower fan pressure ratio. The largest disparity is 0.6 percent at a fan pressure ratio of 2.8. In this case, the prediction tends to correlate well at the lower fan pressure ratios, but is low at the higher pressure ratios.

The predicted performance at a primary pressure ratio of 2.0 did not correlate as well as at a pressure ratio of 1.6, as depicted in Figure 5.4-15. The predicted performance was 0.7 percent higher than the measured data. The higher predicted performance is a result of an underestimation of the shock losses. The shock loss correlations indicate that the loss is minimal at these flow conditions and geometry. As noted previously in the discussion, the alignment of the fan nozzle flow with the downstream afterbody may have introduced a shock loss.

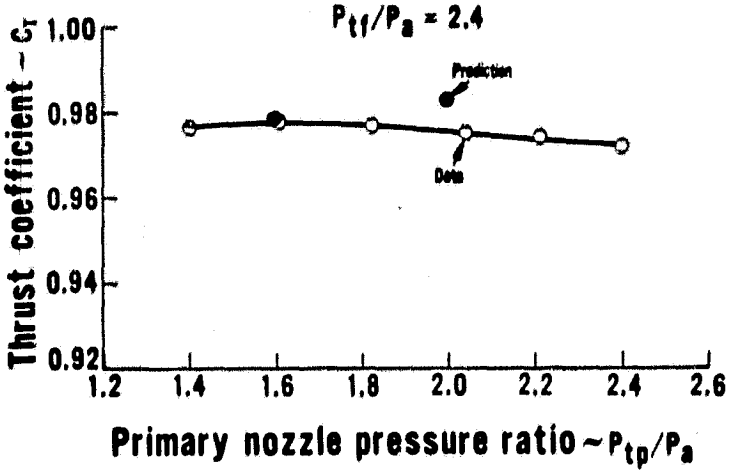

Figure 5.4-14 Comparison of Predicted and Measured Performance at Constant Primary Operating Conditions

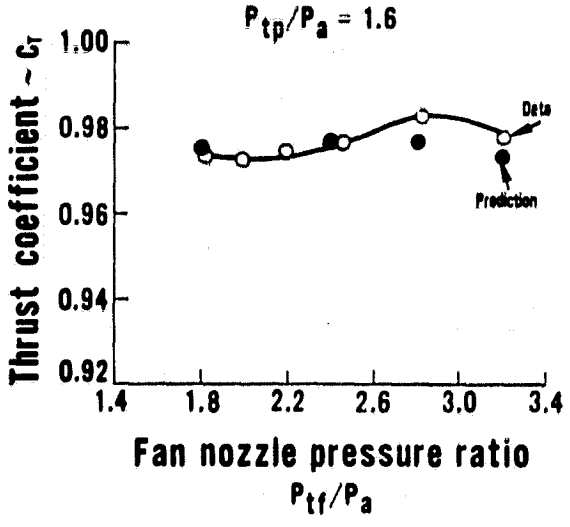

Figure 5.4-15 Comparison of Predicted and Measured Performance at Constant Fan Operating Conditions

SECTION 6.0

SUMMARY OF RESULTS AND CONCLUSIONS

6.1 ACOUSTIC RESULTS

Independent variations of fan and primary stream properties affected the acoustic characteristics of an IVP jet in a manner that is in general agreement with the earlier data. Overall, changes in fan stream properties affected both high frequency and low frequency jet noise, while changes in primary stream properties produced changes only in the low frequency jet noise. This result is in agreement with earlier tests.

The hardwall ejector model tested did not produce the expected noise attenuation. It is believed this was due to the shortness of the ejector, relative to the nozzle diameter. Fan stream shock noise was influenced by the ejector even though most high frequency jet mixing noise was not.

When test results from the VCE testbed are available, a direct comparison of a scaled model test point and measured testbed data will be possible. This, along with additional points lying near the testbed operating line, will permit an evaluation of the ability to scale the model IVP jet acoustic data. Jet noise predictions using the procedure previously developed compared favorably with model data. Predicted spectral shapes and levels are generally within the stated accuracy of the method.

6.2 AERODYNAMIC RESULTS

Results of performance tests without the ejector showed that, in general, reasonable levels of thrust coefficient were achieved over the range of flow conditions tested. The lowest level observed was 0.972, while the highest was 0.983. Installation of the ejector increased performance 0.2 to 0.4 percent, with the greater increase tending to occur at the higher pressure ratio conditions. Thrust coefficients wereldefined for a range of pressure ratios applicable to the testbed engine exhaust system when operated at conditions which simulate the model geometry.

At fan to primary pressure ratios greater than 1.0, variations in fan nozzle pressure ratio imparted a significant effect on the primary nozzle discharge coefficient. At a primary nozzle pressure ratio of 1.6, increasing the fan nozzle pressure ratio from 2.4 to 3.2 decreased the primary nozzle discharge coefficient from 0.93 to 0.86. Addition of the ejector had minimal effect on nozzle discharge coeffieients.

A comparison of measured and predicted nozzle thrust coefficients showed good agreement. In all cases evaluated, this agreement was better than one percent.

APPENDIX A - CALCULATION OF ACOUSTIC PARAMETERS

Several noise parameters were calculated directly from the measured data and from the data after it had been scaled. Following are the methods of calculation for these parameters.

1) Calculation of Overall Sound Pressure Level (OASPL)

$$OASPL = 10 \log \left[\sum_{f=20}^{K} 10^{.1(SPL_f)} \right]$$

where

f = one-third octave band number at a particular angle.

K = highest one-third octave band number for which calculation is performed. K=49 for model scale data and K=40 for testbed and full-size engine data.

SPL_f = SPL value for the f^{th} one-third octave band.

2) Calculation of Power Level (PWL) and Overall Power Level (OAPWL)

Sound power level spectra and overall power level were determined for the model data and scaled data by spatial integration over the eleven microphone positions from the listed SPL values assuming symmetry about the jet axis of noise generation. Since the theoretical day model scale data represent the noise that would be measured if no atmospheric absorption was present, the power levels represent noise generation at the source. The model size data adjusted to a standard FAA day and the scaled data, likewise adjusted, produce power levels which represent an integration of the far field noise levels on a standard day at a particular radius. The actual power level calculations employed were:

$$PWL = 10 \log \left(\frac{W}{W_{ref}} \right) = \text{sound power level, in decibels}$$

where:

$$W = \sum_{i=1}^{n} \frac{p_i^2}{\rho_o C} \Delta A_i = \text{the acoustic power, in watts}$$

$$W_{ref} = 10^{-12} \text{ watts} = \text{the reference power level}$$

$$p_i^2 = \left(\frac{SPL}{10} \right) p_{ref}^2 = \text{mean square sound pressure}$$

P_{ref} = 20×10^{-6} N/M^2 = reference acoustic pressure

ρ_o = atmospheric density

C = atmospheric speed of sound

n = number of microphones

ΔA_1 = surface area of spherical segment associated with i^{th} microphone

- for the first microphone

$$\Delta A_1 = 2\pi r^2 \left[\cos\theta_1 - \cos\left(\frac{\theta_1 + \theta_2}{2}\right)\right]$$

- for intermediate microphones

$$\Delta A_i = 2\pi r^2 \left[\cos\left(\frac{\theta_{i-1} + \theta_i}{2}\right) - \cos\left(\frac{\theta_i + \theta_{i-1}}{2}\right)\right]$$

- for the last microphone

$$\Delta A_n = 2\pi r^2 \left[\cos\left(\frac{\theta_{n-1} + \theta_n}{2}\right) - \cos\theta_n\right]$$

- where: r = distance of microphone from nozzle

Calculation of Overall Power Level (OAPWL)

$$OAPWL = 10 \log\left[\sum_{f=20}^{K} 10^{.1\ PWL_f}\right]$$

3) Calculation of Perceived Noise Level (PNL)

Perceived noise levels were computed from the SPL spectra at several radii and sidelines. The method of calculation is given in Reference 11.

APPENDIX B - ACOUSTIC DATA FOR TEST POINTS ADJACENT TO MODEL-TESTBED MATCH POINT

The following tables provide one third octave band sound pressure levels, overall sound pressure levels and perceived noise levels for model test conditions at and near the testbed engine match point. See Figure 4.5-1 for identification of operating conditions at point noted. The model data are scaled 6X to 0.76 m (2.5 ft) equivalent diameter size, and representative of testbed demonstrator engine noise data at anticipated measuring radius of 27.4 m (90 ft.)

20188F Q1364 VCE PRI./FAN NOZ. NO EJECTOR 15.2049 (match point)

STAND X206 RIG ID 70530 TEST DATE 10/04/78 SCALE RATIO 6.0/1 RUN NUMBER 20188 CONDITION 31

TEST DAY CONDITIONS				PRIMARY	FAN		PRIMARY	FAN		PRIMARY	FAN		PRIMARY	FAN
TEMP	88.0(F)	31.1(C)	AREA SQFT	2.97	1.93	SQM	0.276	0.180	MASS FLOW LB/S	128.2	114.1	KG/S	58.1	51.8
PRES	30.10IN	1.02BAR	P.R.	1.59	2.39		1.59	2.39	THRUST,IDL LB	5909.2	8249.8	N	26285	36697
REL H	37.0%		TEMP (R)	1464.0	2003.	(K)	813.3	1115.6	THRUST,MEA LB		0.0	N		0.0
SDSPD	1147FPS	349M/S	RHO LB/FT3	0.031	0.025	KG/M3	0.493	0.393	AREA (NOD) SQFT	0.08	0.05	SQM	0.008	0.005
			VEL FPS	1484.7	2327.7	M/S	452.5	709.5	W (MODEL) LB/S	3.6	3.2	KG/S	1.6	1.4

FAA DAY 1/3 OCTAVE BAND ENGINE JET NOISE DATA 27.4 M (90 FT) RADIUS (SCALED ENGINE)

BAND CENTER FREQ (KHZ)	MICROPHONE ANGLES IN DEGREES 60	70	80	90	100	110	120	130	140	150	160	POWER 1E-12W
.050	94.2	93.2	94.9	96.7	98.8	101.0	101.4	105.4	109.9	114.7	118.8	145.2
.063	97.3	96.6	97.5	98.1	101.0	102.4	104.7	108.9	114.1	118.1	119.9	148.0
.080	93.3	97.6	98.8	100.1	102.3	102.9	105.3	109.7	116.4	119.9	120.9	149.6
.100	99.8	99.3	100.5	101.9	104.3	104.7	107.1	112.1	117.7	121.1	121.7	150.9
.125	100.0	100.4	101.5	102.6	105.8	105.5	107.9	112.7	117.8	121.7	121.2	151.3
.160	100.3	101.1	102.1	103.1	107.1	107.3	109.8	113.1	117.9	121.0	120.9	151.1
.200	100.0	102.0	103.0	103.8	107.5	107.1	110.1	113.1	116.3	119.4	120.4	150.2
.250	100.5	101.3	102.8	103.6	107.6	107.6	110.2	113.0	115.3	118.0	119.3	149.4
.315	100.1	101.3	103.0	104.0	107.8	107.8	110.7	112.8	114.2	116.7	118.1	148.7
.400	100.8	101.5	103.2	104.7	108.7	108.6	111.5	112.8	114.0	116.8	118.0	148.9
.500	101.6	102.0	103.4	104.9	109.1	109.1	112.0	112.9	114.3	117.3	118.2	149.3
.630	102.1	102.2	103.8	105.3	109.4	110.0	112.5	113.0	115.0	118.5	118.2	150.0
.800	102.4	101.9	103.4	105.1	109.6	110.2	112.4	112.8	115.8	118.7	117.3	150.1
1.00	101.9	101.8	103.2	105.3	109.7	110.5	112.7	113.4	117.0	118.2	115.6	150.2
1.25	100.7	101.6	103.2	105.5	110.0	110.5	112.7	115.6	117.3	116.5	115.6	149.9
1.60	99.6	101.5	103.5	105.2	109.9	110.8	112.4	113.7	116.6	114.9	113.1	149.3
2.00	100.6	100.7	102.8	104.7	109.4	110.2	112.0	113.0	114.8	113.1	11 1	148.3
2.50	100.5	101.1	102.4	104.2	108.9	109.6	110.9	112.3	113.4	111.8	108.9	147.4
3.15	97.9	99.6	101.5	103.5	107.1	107.8	109.5	110.5	111.2	110.1	105.5	145.6
4.00	95.9	98.1	100.8	102.6	106.2	107.2	108.4	109.7	110.9	108.9	105.4	144.8
5.00	94.4	96.2	98.8	101.1	105.4	106.1	106.7	108.1	109.7	107.6	103.8	143.4
6.30	92.9	95.1	97.6	100.1	104.4	105.3	106.3	107.5	108.9	106.7	102.6	142.7
8.00	91.6	92.9	96.1	98.4	102.8	103.4	104.9	106.4	108.2	105.3	102.2	141.5
10.0	89.2	91.0	94.6	96.5	101.0	102.1	103.6	105.5	107.9	105.1	101.1	140.6
											OAPWL =	162.5
OASPL	113.3	113.9	115.5	117.0	121.1	121.6	123.8	125.5	128.7	131.0	131.2	
PNL	124.6	125.4	127.1	128.9	133.1	133.7	135.4	137.0	139.0	139.0	137.4	
61.0 M (200 FT) SIDELINE												
PNL	115.8	117.4	119.5	121.4	125.5	125.7	126.6	127.0	127.3	125.0	119.9	
112.8 M (370 FT) SIDELINE												
PNL	109.7	111.3	113.4	115.3	119.4	119.6	120.5	120.7	121.0	118.5	113.6	
243.8 M (800 FT) SIDELINE												
PNL	101.0	102.8	104.9	106.8	110.9	111.0	111.8	111.9	112.2	109.8	104.9	
648.6 M (2128 FT) SIDELINE												
PNL	87.5	89.4	91.8	93.7	97.8	97.7	98.5	98.4	98.7	97.4	92.7	

20188F Q1364 VCE PRI./FAN NOZ. NO EJECTOR 15.2049

STAND X206 RIG ID 70530 TEST DATE 10/04/78 SCALE RATIO 6.0/1 RUN NUMBER 20188 CONDITION 03

				PRIMARY	FAN		PRIMARY	FAN			PRIMARY	FAN		PRIMARY	FAN
TEST DAY CONDITIONS															
TEMP	85.0(F)	29.4(C)	AREA SQFT	2.97	1.93	SQM	0.276	0.180	MASS FLOW	LB/S	126.5	123.8	KG/S	58.3	56.2
PRES	30.10IN	1.02BAR	P.R.	1.61	2.38		1.61	2.38	THRUST,IDL	LB	5981.6	8169.2	N	26607	36338
REL H	39.0%		TEMP (R)	1467.0	1683.	(K)	815.0	935.0	THRUST,MEA	LB		0.0	N		0.0
SDSPD	1144FPS	348M/S	RHO LB/FT3	0.031	0.029	KG/M3	0.493	0.472	AREA (MOD)	SQFT	0.08	0.05	SQM	0.008	0.005
			VEL FPS	1498.6	2124.1	M/S	456.8	647.4	W (MODEL)	LB/S	3.6	3.4	KG/S	1.6	1.6

FAA DAY 1/3 OCTAVE BAND ENGINE JET NOISE DATA 27.4 M (90 FT) RADIUS (SCALED ENGINE)

BAND CENTER FREQ (KHZ)	MICROPHONE ANGLES IN DEGREES 60	70	80	90	100	110	120	130	140	150	160	POWER 1E-12W
.050	93.4	92.7	94.5	96.1	98.3	100.4	100.9	105.0	109.5	114.3	118.5	144.9
.063	96.8	96.1	97.2	97.7	100.7	102.4	104.3	108.5	113.7	117.8	119.4	147.7
.080	97.7	97.3	98.5	99.6	101.9	102.6	105.1	109.3	116.0	119.8	120.6	149.4
.100	99.6	98.8	99.9	101.4	104.0	104.5	106.8	111.9	117.7	121.1	121.6	150.9
.125	99.5	99.9	101.1	102.1	105.5	105.0	107.5	112.5	117.9	121.6	121.0	151.1
.160	99.9	100.7	101.7	102.9	106.8	106.8	109.3	113.0	118.0	121.0	120.9	151.1
.200	99.7	101.5	102.8	103.3	106.9	106.7	109.6	112.8	116.6	119.5	120.2	150.1
.250	100.2	100.9	102.1	103.1	106.9	107.1	109.7	112.6	115.5	118.2	119.0	149.3
.315	99.5	100.7	102.3	103.2	107.2	107.1	110.0	112.3	114.1	116.2	117.5	148.2
.400	99.9	100.7	102.4	103.7	107.6	107.9	110.4	112.3	113.5	115.7	116.9	148.1
.500	100.8	101.3	102.5	103.7	108.1	108.3	110.8	112.1	113.2	115.7	117.0	148.1
.630	101.1	101.3	102.7	104.2	108.3	108.7	111.2	112.0	113.2	116.6	116.9	148.5
.800	101.4	101.0	102.4	103.9	108.3	108.9	110.8	111.4	113.3	116.8	116.2	148.4
1.00	100.8	100.9	102.2	104.1	108.3	109.0	111.1	111.6	114.2	116.6	115.2	148.4
1.25	99.6	100.6	102.1	103.9	108.7	109.0	111.1	111.3	114.6	115.8	113.2	148.2
1.60	98.9	100.5	102.0	103.8	108.3	109.0	110.6	111.3	114.6	114.2	111.8	147.7
2.00	100.2	100.1	101.4	103.2	107.6	108.4	110.1	110.4	113.0	112.0	109.6	146.5
2.50	100.7	101.2	101.3	102.9	107.1	107.8	109.1	109.8	111.5	110.8	108.1	145.6
3.15	97.9	99.7	100.9	102.4	105.4	106.2	107.6	108.0	109.3	108.9	105.9	143.9
4.00	95.4	97.5	99.9	101.4	104.5	105.4	106.2	107.0	108.8	107.8	104.8	143.0
5.00	93.8	95.6	97.7	100.0	103.7	104.2	104.6	105.5	107.5	106.3	103.2	141.6
6.30	92.3	94.7	96.6	98.8	102.8	103.2	104.0	104.7	106.4	105.4	101.9	140.7
8.00	91.0	92.3	94.7	96.9	101.2	101.4	102.4	103.3	105.5	104.9	101.4	139.3
10.0	88.5	90.5	93.4	95.1	99.3	100.1	101.1	102.2	105.2	104.5	100.5	138.3
											OAPWL =	161.6
OASPL	112.7	113.3	114.6	116.0	120.0	120.4	122.5	124.3	127.8	130.5	130.8	
PNL	124.3	125.0	126.3	127.8	131.6	132.2	133.8	135.0	137.4	138.1	136.8	
61.0 M (200 FT) SIDELINE												
PNL	115.5	117.0	118.7	120.4	124.1	124.2	125.0	125.1	125.7	124.1	119.3	
112.8 M (370 FT) SIDELINE												
PNL	109.3	110.9	112.5	114.2	118.0	118.1	118.9	118.8	119.4	117.7	113.0	
243.8 M (800 FT) SIDELINE												
PNL	100.7	102.4	104.0	105.7	109.5	109.5	110.2	110.1	110.7	108.9	104.5	
643.6 M (2128 FT) SIDELINE												
PNL	87.0	89.0	90.8	92.6	96.5	96.3	97.1	97.1	97.7	96.9	92.2	

20188F Q1364 VCE PRI./FAN NOZ. NO EJECTOR 15.2049

STAND X206 RIG ID 70530 TEST DATE 10/04/78 SCALE RATIO 6.0/1 RUN NUMBER 20188 CONDITION 06

					PRIMARY	FAN		PRIMARY	FAN				PRIMARY	FAN		PRIMARY	FAN
TEST DAY CONDITIONS																	
TEMP	87.0(F)	30.6(C)	AREA	SQFT	2.97	1.93	SQM	0.276	0.180	MASS FLOW	LB/S	126.7	104.8	KG/S	57.5	47.5
PRES	30.10IN	1.02BAR	P.R.		1.59	2.19		1.59	2.19	THRUST,IDL	LB	5846.7	7205.6	N	26007	32052
REL H	37.0%		TEMP	(R)	1469.0	1999.	(K)	816.1	1110.6	THRUST,MEA	LB		0.0	N		0.0
SDSPD	1146FPS	349M/S	RHO	LB/FT3	0.031	0.024	KG/M3	0.491	0.387	AREA (MOD)	SQFT	0.08	0.05	SQM	0.008	0.005
			VEL	FPS	1485.7	2214.8	M/S	452.8	675.1	W (MODEL)	LB/S	3.5	2.9	KG/S	1.6	1.3

FAA DAY 1/3 OCTAVE BAND ENGINE JET NOISE DATA 27.4 M (90 FT) RADIUS (SCALED ENGINE)

BAND CENTER FREQ (KHZ)	MICROPHONE ANGLES IN DEGREES 60	70	80	90	100	110	120	130	140	150	160	POWER 1E-12W
.050	93.4	92.5	94.2	95.7	97.8	99.8	100.4	104.6	109.1	114.0	118.1	144.5
.063	96.4	95.9	97.1	97.4	100.6	101.9	104.1	108.2	113.3	117.2	119.1	147.2
.080	97.5	96.9	98.1	99.3	101.5	102.0	104.6	108.9	115.5	119.1	120.1	148.8
.100	99.3	98.7	99.9	101.2	103.8	104.0	106.5	111.6	117.0	120.5	121.1	150.3
.125	99.3	99.7	100.8	101.8	104.9	104.6	107.1	111.9	117.2	121.1	120.4	150.6
.160	99.5	100.3	101.4	102.3	106.4	106.4	108.9	112.3	116.9	120.2	120.1	150.3
.200	99.2	101.1	102.2	102.9	106.7	106.4	109.4	112.4	115.6	118.7	119.4	149.4
.250	99.8	100.5	102.0	102.8	106.8	107.0	109.4	112.3	114.5	117.2	118.3	148.6
.315	99.1	100.4	102.2	103.1	107.0	107.0	109.8	111.9	113.2	115.4	116.7	147.7
.400	99.6	100.8	102.4	103.6	107.7	107.7	110.5	111.9	112.8	115.2	116.4	147.7
.500	100.6	101.1	102.4	103.9	108.1	108.4	111.0	111.7	112.9	115.5	116.5	148.0
.630	101.1	101.2	102.9	104.2	108.5	108.9	111.4	111.9	113.2	116.6	116.7	148.6
.800	101.4	101.0	102.4	104.1	108.6	109.3	111.1	111.5	113.8	117.1	115.9	148.6
1.00	101.0	100.9	102.5	104.3	108.9	109.4	111.6	112.1	115.1	117.0	114.9	148.9
1.25	99.6	100.7	102.3	104.2	109.2	109.5	111.4	112.1	115.5	115.8	113.1	148.6
1.60	98.4	100.3	102.2	104.2	108.9	109.7	111.2	112.0	115.2	114.1	111.4	148.1
2.00	98.5	99.6	101.6	103.6	108.3	109.1	110.7	111.5	113.7	112.3	109.5	147.1
2.50	97.4	98.9	100.8	103.1	107.7	108.4	109.8	110.7	112.0	110.9	107.9	146.1
3.15	96.0	97.2	99.4	102.2	105.9	106.9	108.3	108.9	110.0	108.9	105.9	144.4
4.00	94.3	96.3	98.7	100.9	104.9	106.1	106.9	108.0	109.5	107.9	104.6	143.4
5.00	92.7	94.7	97.2	99.5	103.9	104.9	105.5	106.6	108.2	106.5	103.1	142.1
6.30	91.2	93.4	96.0	98.6	102.9	103.7	104.8	105.6	107.3	105.5	101.9	141.2
8.00	89.8	91.3	94.3	96.7	101.2	101.7	103.1	104.5	106.4	105.1	101.3	139.8
10.0	87.6	89.4	92.8	95.0	99.4	100.4	101.9	103.4	106.1	104.8	100.1	138.9
											OAPWL =	161.4
OASPL	112.1	112.8	114.4	116.0	120.2	120.6	122.7	124.4	127.5	130.0	130.2	
PNL	122.7	123.8	125.7	127.7	132.0	132.6	134.3	135.5	137.6	138.0	136.4	
61.0 M (200 FT) SIDELINE												
PNL	113.9	115.8	118.2	120.3	124.4	124.6	125.5	125.6	126.0	123.9	118.8	
112.8 M (370 FT) SIDELINE												
PNL	107.8	109.7	112.1	114.2	118.3	118.5	119.3	119.4	119.7	117.5	112.5	
243.8 M (800 FT) SIDELINE												
PNL	99.2	101.3	103.6	105.7	109.9	109.9	110.7	110.5	110.9	108.6	103.9	
648.6 M (2128 FT) SIDELINE												
PNL	86.2	88.3	90.7	92.7	96.8	96.7	97.4	97.1	97.4	96.4	91.6	

20188F Q1257 VCE PRI./FAN NOZ. NO EJECTOR 15.2049

STAND X206 RIG ID 70530 TEST DATE 10/05/78 SCALE RATIO 6.0/1 RUN NUMBER 20188 CONDITION 08

					PRIMARY	FAN		PRIMARY	FAN			PRIMARY	FAN		PRIMARY	FAN
TEST DAY CONDITIONS																
TEMP	88.0(F)	31.1(C)	AREA	SQFT	2.97	1.93	SQM	0.276	0.180	MASS FLOW	LB/S	127.4	124.9	KG/S	57.8	56.7
PRES	30.08IN	1.02BAR	P.R.		1.60	2.61		1.60	2.61	THRUST,IDL	LB	5916.7	9404.0	N	26319	41831
REL H	37.0%		TEMP	(R)	1476.0	2001.	(K)	820.0	1111.7	THRUST,MEA	LB		0.0	N		0.0
SDSPD	1147FPS	349M/S	RHO	LB/FT3	0.031	0.025	KG/M3	0.489	0.403	AREA (NOD)	SQFT	0.08	0.05	SQM	0.008	0.005
			VEL	FPS	1495.0	2424.0	M/S	455.7	738.8	W (MODEL)	LB/S	3.5	3.5	KG/S	1.6	1.6

FAA DAY 1/3 OCTAVE BAND ENGINE JET NOISE DATA 27.4 M (90 FT) RADIUS (SCALED ENGINE)

BAND CENTER FREQ (KHZ)	NICROPHONE ANGLES IN DEGREES 60	70	80	90	100	110	120	130	140	150	160	POWER 1E-12W
.050	94.4	93.8	95.3	96.9	99.1	100.7	101.9	106.1	110.3	115.6	119.8	146.0
.063	97.7	97.2	98.1	98.6	101.5	102.4	105.2	109.5	114.6	119.0	120.7	148.8
.080	98.8	98.1	99.0	100.3	102.6	102.9	105.9	110.4	117.1	121.1	121.8	150.6
.100	100.2	100.0	101.0	102.3	104.9	104.7	107.6	112.8	118.4	121.9	122.6	151.7
.125	100.5	100.9	102.0	103.0	106.4	105.8	108.5	113.2	118.4	122.7	122.2	152.1
.160	101.1	101.7	102.8	103.7	107.8	107.8	110.5	114.1	118.3	122.1	122.3	152.1
.200	101.0	102.9	103.8	104.7	108.4	107.7	111.0	114.2	117.1	120.8	121.8	151.3
.250	101.5	102.3	103.4	104.6	108.3	108.3	111.3	114.1	116.4	120.0	121.0	150.8
.315	101.1	102.3	104.0	104.8	108.8	108.4	111.5	113.8	115.3	119.0	120.2	150.2
.400	101.8	102.7	104.0	105.5	109.5	109.2	112.4	114.0	115.5	119.3	120.2	150.5
.500	102.6	103.1	104.0	105.7	109.9	109.7	113.1	114.1	116.0	120.0	120.1	151.0
.630	102.8	103.0	104.4	105.8	110.3	110.4	113.4	114.3	117.2	120.7	119.7	151.6
.800	103.1	102.7	104.1	106.2	110.5	110.7	113.8	114.3	118.0	120.6	117.9	151.6
1.00	102.7	102.7	104.2	106.2	110.6	111.1	113.9	114.9	119.2	119.3	116.2	151.6
1.25	101.7	102.5	104.3	106.2	111.2	111.4	113.8	115.4	119.0	117.5	114.4	151.2
1.60	101.7	102.7	104.0	106.0	111.0	111.6	113.4	115.6	117.5	116.3	112.8	150.5
2.00	102.9	103.2	103.9	105.6	110.6	111.0	113.1	115.1	115.9	114.6	111.2	149.6
2.50	101.4	103.2	104.4	105.6	110.0	110.5	112.4	114.3	114.7	113.4	109.7	148.8
3.15	98.8	100.6	103.0	105.3	108.5	109.1	110.8	112.3	112.8	111.7	107.7	147.2
4.00	97.7	99.2	101.6	104.1	107.8	108.2	109.6	111.6	112.3	110.6	106.7	146.3
5.00	96.6	98.3	100.2	102.6	107.5	107.2	108.4	110.4	111.4	109.2	105.2	145.2
6.30	94.6	97.1	99.3	101.6	105.8	106.3	107.9	109.7	110.7	108.3	104.0	144.4
8.00	93.5	94.9	97.5	100.1	104.2	104.5	106.8	108.9	110.0	108.2	103.6	143.4
10.0	90.9	92.9	96.4	98.3	102.6	103.7	105.6	108.2	109.9	108.1	102.7	142.6
											OAPWL =	163.7
OASPL	114.3	115.0	116.4	118.0	122.2	122.3	124.9	127.0	129.9	132.4	132.4	
PNL	125.7	126.9	128.4	130.2	134.2	134.5	136.7	138.7	140.3	140.6	138.7	
61.0 M (200 FT) SIDELINE												
PNL	116.9	118.9	120.8	122.8	126.7	126.5	127.9	128.7	128.7	126.6	121.4	
112.8 M (370 FT) SIDELINE												
PNL	110.8	112.8	114.8	116.6	120.6	120.4	121.7	122.5	122.3	120.1	115.0	
243.8 M (800 FT) SIDELINE												
PNL	102.2	104.3	106.2	108.0	112.0	111.8	113.0	113.6	113.4	111.5	106.4	
648.6 M (2128 FT) SIDELINE												
PNL	89.0	90.8	92.9	94.7	98.9	98.4	99.6	100.0	99.8	99.0	94.0	

STAND X206 RIG ID 70530 TEST DATE 10/04/78 SCALE RATIO 6.0/1 RUN NUMBER 20188 CONDITION 10

					PRIMARY	FAN		PRIMARY	FAN			PRIMARY	FAN		PRIMARY	FAN
TEST DAY CONDITIONS																
TEMP	85.0(F)	29.4(C)	AREA	SQFT	2.97	1.93	SQM	0.276	0.180	MASS FLOW	LB/S	128.5	134.6	KG/S	58.3	61.1
PRES	30.10IN	1.02BAR	P.R.		1.60	2.59		1.60	2.59	THRUST,IDL	LB	5936.7	9261.8	N	26408	41198
REL H	39.0%		TEMP	(R)	1459.0	1686.	(K)	810.6	936.7	THRUST,MEA	LB		0.0	N		0.0
SDSPD	1144FPS	348M/S	RHO	LB/FT3	0.031	0.030	KG/M3	0.495	0.481	AREA (MOD)	SQFT	0.08	0.05	SQM	0.008	0.005
			VEL	FPS	1487.4	2215.0	M/S	453.4	675.1	W (MODEL)	LB/S	3.6	3.7	KG/S	1.6	1.7

FAA DAY 1/3 OCTAVE BAND ENGINE JET NOISE DATA 27.4 M (90 FT) RADIUS (SCALED ENGINE)

BAND CENTER FREQ (KHZ)	MICROPHONE ANGLES IN DEGREES 60	70	80	90	100	110	120	130	140	150	160	POWER 1E-12W
.050	93.9	93.2	95.1	96.8	98.8	101.5	101.3	105.6	110.0	114.9	119.2	145.5
.063	97.5	96.8	97.7	98.1	101.4	103.0	104.9	109.0	114.5	118.4	120.1	148.3
.080	98.3	97.8	99.0	100.1	102.4	103.0	105.5	109.8	116.6	120.3	121.2	149.9
.100	99.9	99.5	100.6	102.3	104.7	104.9	107.4	112.5	118.2	121.6	122.3	151.4
.125	100.2	100.5	101.4	102.6	106.1	105.8	108.0	112.8	118.3	122.1	121.5	151.6
.160	100.6	101.2	102.2	103.3	107.4	107.5	109.8	113.3	118.3	121.5	121.5	151.6
.200	100.3	102.0	103.2	103.9	107.6	107.2	110.2	113.3	117.0	120.1	120.8	150.7
.250	100.8	101.3	102.8	103.8	107.6	107.7	110.3	113.4	115.8	118.6	119.8	149.8
.315	100.4	101.4	103.0	104.0	108.0	107.9	110.7	112.9	114.7	117.2	118.7	149.1
.400	100.8	101.6	103.1	104.6	108.6	108.6	111.3	113.1	114.3	117.0	118.3	149.1
.500	101.6	102.1	103.2	104.7	109.0	109.0	111.6	112.9	114.4	117.3	118.5	149.3
.630	102.1	102.0	103.5	105.1	109.3	109.4	112.1	113.1	114.9	118.3	118.3	149.8
.800	102.2	101.7	103.1	104.8	109.2	109.7	111.8	112.6	115.4	118.5	117.3	149.8
1.00	101.8	101.7	103.0	105.0	109.1	109.8	112.2	113.1	116.5	118.2	116.0	149.9
1.25	101.3	101.7	103.0	105.0	109.7	109.8	112.1	113.0	116.8	116.5	114.0	149.5
1.60	102.1	102.1	103.0	105.0	109.3	110.0	111.9	112.8	116.0	114.9	112.3	148.8
2.00	104.1	103.5	103.4	104.4	108.8	109.5	111.4	112.1	114.6	113.1	110.5	147.9
2.50	102.4	103.8	104.5	104.7	108.4	108.9	110.4	111.7	113.0	112.0	109.1	147.2
3.15	99.4	100.8	103.1	104.8	107.1	107.4	109.1	110.0	110.9	110.2	106.8	145.6
4.00	98.1	99.2	101.4	103.5	106.3	106.8	107.9	109.0	110.5	109.2	105.7	144.6
5.00	96.8	98.3	99.9	101.6	105.6	105.8	106.3	107.5	109.3	107.6	104.2	143.3
6.30	94.7	97.0	99.0	100.9	104.5	104.9	105.9	106.9	108.5	106.9	103.1	142.6
8.00	93.5	94.6	97.2	99.2	103.1	103.1	104.4	105.6	107.8	106.5	102.8	141.4
10.0	90.7	92.7	95.7	97.5	101.3	101.9	103.2	104.8	107.5	106.3	101.6	140.4
												OAPWL = 162.5
OASPL	114.0	114.5	115.7	117.1	121.0	121.3	123.5	125.4	128.8	131.3	131.6	
PNL	126.0	126.9	128.1	129.5	132.9	133.2	135.0	136.5	138.8	139.2	137.7	
61.0 M (200 FT) SIDELINE												
PNL	117.2	116.9	120.5	122.0	125.3	125.2	126.2	126.6	127.1	125.2	120.2	
112.8 M (370 FT) SIDELINE												
PNL	111.0	112.8	114.4	115.9	119.2	119.1	120.1	120.4	120.8	118.7	113.9	
243.8 M (800 FT) SIDELINE												
PNL	102.5	104.2	105.9	107.2	110.7	110.5	111.4	111.5	112.0	109.9	105.3	
648.6 M (2128 FT) SIDELINE												
PNL	89.1	90.6	92.5	93.8	97.5	97.3	98.2	98.1	98.6	97.8	93.1	

20188F Q1364 VCE PRI./FAN NOZ. NO EJECTOR 15.2049

STAND X206 RIG ID 70530 TEST DATE 10/04/78 SCALE RATIO 6.0/1 RUN NUMBER 20188 CONDITION 11

					PRIMARY	FAN		PRIMARY	FAN			PRIMARY	FAN		PRIMARY	FAN
TEST DAY CONDITIONS																
TEMP	87.0(F)	30.6(C)	AREA	SQFT	2.97	1.93	SQM	0.276	0.180	MASS FLOW	LB/S	127.4	115.2	KG/S	57.8	52.3
PRES	30.10IN	1.02BAR	P.R.		1.60	2.22		1.60	2.22	THRUST,IDL	LB	5895.4	7295.6	N	26224	32453
REL H	25.0%		TEMP	(R)	1459.0	1675.	(K)	810.6	930.6	THRUST,NEA	LB		0.0	N		0.0
SDSPD	1146FPS	349M/S	RHO	LB/FT3	0.031	0.029	KG/M3	0.495	0.466	AREA (MOD)	SQFT	0.08	0.05	SQM	0.008	0.005
			VEL	FPS	1489.6	2039.2	M/S	454.0	621.6	W (MODEL)	LB/S	3.5	3.2	KG/S	1.6	1.5

FAA DAY 1/3 OCTAVE BAND ENGINE JET NOISE DATA 27.4 M (90 FT) RADIUS (SCALED ENGINE)

BAND CENTER FREQ (KHZ)	MICROPHONE ANGLES IN DEGREES 60	70	80	90	100	110	120	130	140	150	160	POWER 1E-12W
.050	92.4	91.9	93.4	95.0	96.4	99.5	100.2	104.3	109.0	113.6	117.7	144.1
.063	95.6	95.3	96.9	97.2	98.8	101.5	103.7	108.0	113.3	117.1	118.6	147.0
.080	97.1	97.0	98.1	98.8	99.6	101.7	104.5	109.0	115.5	118.9	119.5	148.6
.100	99.4	98.4	99.1	100.8	101.5	103.6	106.4	111.5	117.1	120.2	120.4	150.0
.125	98.8	99.4	100.2	101.3	102.6	104.3	106.8	111.9	117.3	120.8	119.9	150.3
.160	99.4	100.0	100.9	102.0	104.0	106.2	108.8	112.4	117.4	120.4	119.8	150.4
.200	99.0	101.0	101.8	102.7	104.0	106.0	109.1	112.1	116.3	119.1	119.3	149.6
.250	99.3	99.8	101.2	102.3	104.1	106.4	109.0	111.9	114.9	117.9	118.3	148.7
.315	98.3	99.5	101.2	102.2	104.0	105.4	109.3	111.6	113.3	116.2	117.1	147.6
.400	98.8	99.6	101.2	102.8	104.7	107.1	109.9	111.6	113.0	116.2	116.8	147.7
.500	99.6	100.1	101.3	102.9	104.9	107.5	110.2	111.6	113.0	116.3	116.5	147.7
.630	99.9	100.0	101.6	103.3	105.3	108.0	110.7	111.6	113.2	116.9	116.4	148.1
.800	100.2	99.8	101.3	103.1	105.2	108.1	110.3	111.1	113.6	116.8	115.4	147.9
1.00	99.8	99.9	101.3	103.2	105.4	108.3	110.7	111.5	114.8	116.3	114.0	148.1
1.25	98.5	99.5	101.1	103.2	105.8	108.4	110.6	111.2	114.9	114.9	112.2	147.6
1.60	97.2	99.1	100.9	103.0	105.3	108.3	110.1	110.7	114.2	113.3	110.5	146.8
2.00	97.1	98.1	100.3	102.2	104.6	107.7	109.7	109.9	112.5	111.2	108.5	145.6
2.50	96.3	97.5	99.3	101.5	104.2	106.9	108.5	109.2	110.9	110.0	107.1	144.6
3.15	94.8	95.9	98.1	100.7	102.5	105.3	107.1	107.3	108.7	108.2	105.0	142.9
4.00	93.2	95.1	97.4	99.4	101.3	104.4	105.7	106.3	108.3	107.2	104.1	141.9
5.00	91.9	94.0	96.3	98.5	100.7	103.4	104.4	105.1	107.4	106.0	102.8	140.8
6.30	91.1	93.3	95.8	98.2	100.3	103.0	104.2	104.8	106.7	105.4	102.1	140.4
8.00	91.0	92.2	95.0	97.3	99.7	102.1	103.4	104.4	106.6	105.7	102.2	140.0
10.0	90.1	91.7	94.8	96.8	98.7	101.7	102.9	104.0	106.9	106.0	101.8	139.8
												OAPWL = 161.0
OASPL	111.4	112.0	113.5	115.1	117.1	119.7	122.0	123.9	127.4	130.0	129.9	
PNL	121.8	122.9	124.7	126.6	128.8	131.5	133.4	134.6	137.1	137.7	136.0	
61.0 M (200 FT) SIDELINE												
PNL	113.0	114.9	117.1	119.2	121.3	123.5	124.6	124.6	125.4	123.6	118.6	
112.8 M (370 FT) SIDELINE												
PNL	106.9	108.7	111.0	113.1	115.2	117.4	118.4	118.4	119.1	117.2	112.2	
243.8 M (800 FT) SIDELINE												
PNL	98.3	100.2	102.5	104.6	106.6	108.8	109.8	109.6	110.4	108.5	103.6	
648.6 M (2128 FT) SIDELINE												
PNL	85.3	87.3	89.6	91.7	93.5	95.6	96.6	96.6	97.4	96.5	91.4	

APPENDIX C - ACTUAL OPERATING AND AMBIENT TEST CONDITIONS

Test Pt.	FAN P_{TF}/P_A	T_{TF} K	T_{TF} °R	V_f m/s	V_f f/s	PRIMARY P_{tp}/P_A	T_{TP} K	T_{TP} °R	V_p m/s	V_p f/s	T_A K	T_A °R	RH %
1	2.39	1093	1968	703	2306	1.58	797	1435	449	1472	304	548	37
2	2.39	997	1795	670	2178	1.59	801	1442	450	1475	303	546	38
3	2.39	921	1658	643	2110	1.61	803	1446	454	1489	303	545	39
4	2.40	698	1256	560	1838	1.60	799	1438	451	1481	303	546	25
5	2.40	585	1053	512	1679	1.60	792	1425	441	1474	304	547	26
6	2.20	1089	1961	669	2195	1.59	801	1442	449	1474	304	547	37
7	2.80	1085	1953	753	2471	1.59	803	1446	450	1477	305	549	37
8	2.61	1088	1259	731	2399	1.6	803	1446	451	1480	304	548	37
9	2.80	701	1262	603	1978	1.6	802	1443	451	1479	303	546	25
10	2.60	922	1660	670	2199	1.6	798	1437	450	1478	303	545	39
11	2.22	914	1645	615	2018	1.6	796	1433	449	1474	304	547	25
12	2.06	1085	1953	632	2075	1.6	801	1442	451	1481	303	546	38
13	2.01	705	1269	508	1666	1.61	806	1451	455	1492	303	546	26
14	2.39	1084	1951	700	2295	1.6	1084	1952	525	1723	307	552	29
15	2.40	1083	1949	700	2297	1.6	914	1645	483	1584	307	552	28
16	2.4	1088	1959	702	2302	1.59	579	1042	380	1247	305	549	32
17	2.4	1084	1952	701	2299	2.0	600	1080	466	1529	307	552	29
18	2.4	1087	1957	702	2302	1.9	595	1071	331	1087	306	551	30
19	2.10	892	1606	589	1932	2.08	859	1547	574	1883	306	550	29
20	1.93	931	1676	569	1867	1.93	935	1683	571	1871	306	550	30
21	2.35	902	1624	631	2069	1.79	821	1478	504	1654	306	550	29
22	2.09	1080	1944	646	2120	1.36	718	1292	348	1141	306	550	29
23	2.24	1080	1944	675	2213	1.46	758	1365	397	1302	306	550	29
24	2.49	1084	1951	714	2343	1.52	815	1467	432	1416	306	550	30
25	2.21	1093	1967	708	2619	1.52	813	1464	431	1415	306	550	29
26	2.39	427	769	435	1428	1.58	774	1394	439	1439	304	547	17
27	2.21	1082	1947	795	2607	1.60	797	1435	449	1473	306	550	30
28	2.21	696	1252	634	2079	1.58	797	1434	445	1460	306	551	29
29	2.21	703	1265	637	2089	2.40	801	1441	600	1969	306	551	29
30	1.99	856	1540	557	1828	2.0	851	1531	556	1825	306	551	29
38	2.41	1089	1961	704	2310	1.39	803	1445	383	1257	305	549	17
1E	2.41	1082	1948	702	2302	1.59	802	1443	450	1475	304	548	36
3E	2.41	925	1665	648	2125	1.6	801	1441	450	1478	304	547	37
4E	2.40	688	1239	555	1822	1.6	801	1442	451	1480	304	547	37
10E	2.10	890	1602	589	1932	2.07	860	1548	573	1881	305	549	34
1P	1.60	No Fan Flow				1.60	797	1434	449	1472	303	545	39
14P	1.61	No Fan Flow				1.61	885	1665	542	1779	303	546	28
15P	1.60	No Fan Flow				1.60	825	1665	486	1591	303	546	28
17P	2.01	No Fan Flow				2.01	802	1444	542	1771	303	545	28

E denotes ejector configuration.
P denotes points run with primary only.

APPENDIX D - LIST OF SYMBOLS

A	Area
ASF	Area scale factor
C	Acoustic velocity
C-D	Convergent - divergent
C_D	Discharge coefficient - actual weight flow/ideal weight flow
C_T	Thrust coefficient - actual thrust/idea thrust
D	Diameter
f	Frequency
F	Thrust
g_c	Gravitational constant
IVP	Inverted velocity profile
L	Length
LSF	Linear scale factor
OAPWL	Overall Power Level
OASPL	Overall Sound Pressure Level
P	Pressure
PNL	Perceived noise level
PWL	Power level - dB re 10^{-12} watts
r	Radius
R	Radius or Universal gas constant
Ref	Reference
S	Scale factor
SCAR	Supersonic Cruise Airplane Research
s/l	Sideline

SPL	Sound pressure level re .0002 dynes/cm^2
T	Temperature (Static with no subscript, total with "t" subscript)
V	Velocity
W	Weight flow
Xc	Axial distance from nozzle exit plane

GREEK LETTERS

θ	Angle measured from upstream jet axis
ω	SAE density exponent
γ	Ratio of specific heats
ρ	Mass density
Δ	Difference in noise or aerodynamic performance levels

SUBSCRIPTS

a	ambient
eq	equivalent
ex	exit
f	fan
i	initial region
id	ideal
j	jet
m	merged
o	initial conditions
p	primary

ref	reference
s	static
t	total
8	primary nozzle throat
18	fan duct nozzle throat
9	primary flow exit station
19	fan duct flow exit station

REFERENCES

1. Kozlowski, H., and Packman, A.B., "Aerodynamic and Acoustic Tests of Duct Burning Turbofan Exhaust Nozzles," NASA CR-2628, 1976.

2. Kozlowski, H. and Packman, A.B., "Flight Effects on the Aerodynamic and Acoustic Characteristics of Inverted Velocity Profile Coannular Nozzle," NASA CR-3018, 1978.

3. Larson, R.S., Nelson, D.P., and Stevens, B.S., "Aero/Acoustic Investigation of Inverted Velocity Profile Coannular Exhaust Nozzle Models and Development of Aerodynamic and Acoustic Prediction Procedures", NASA CR-3168, 1979.

4. Stone, J.R., "An Empirical Model for Inverted Velocity Profile Jet Noise Prediction," NASA TM-73838, 1978.

5. Nelson, D.P., and Morris, P.M., "Experimental Aerodynamic and Acoustic Model Testing of the VCE Testbed Coannular Exhaust Nozzle System - Comprehensive Data Report", NASA CR-159711, 1980.

6. VCE Testbed Program Final Design Report, PWA-5546-12, Aug. 1978

7. Society of Automotive Engineers: Aerospace Recommended Practice 876, Gas Turbine Jet Exhaust Noise Prediction, March 1978.

8. Society of Automotive Engineers: Aerospace Recommended Practice 866A, March 15, 1975.

9. Larson, R.S., "Theoretical Jet Exhaust Model for the Duct Burning Turbofan," AIAA Paper No. 77-1264, 1977.

10. Atvars, J., Paynter, G.C., Walker, D.Q., and Wintermeyer, C.F., "Development of Acoustically Lined Ejector Technology for Multitube Jet Noise Suppressor Nozzles by Model and Engine Tests Over a Wide Range of Jet Pressure Ratios and Temperatures," NASA CR-2382, April 1974.

11. Society of Automotive Engineers: Aerospace Recommended Practice 865A, Definitions and Procedures for Computing the Perceived Noise Level of Aircraft Noise, April 1978.